International Scientific-Technical and Production Journal

The Paton WELDING JOURNAL

July 2012 # 7

English translation of the monthly «Avtomaticheskaya Svarka» (Automatic Welding) journal published in Russian since 1948

Founders: *E.O. Paton Electric Welding Institute of the NAS of Ukraine*
International Association «Welding»

Publisher: *International Association «Welding»*

Address:
E.O. Paton Electric Welding Institute,
International Association «Welding»,
11, Bozhenko str., 03680, Kyiv, Ukraine
Tel.: (38044) 200 82 77
Fax: (38044) 200 81 45
E-mail: journal@paton.kiev.ua
URL: www.rucont.ru

State Registration Certificate
KV 4790 of 09.01.2001

Subscriptions:
$324, 12 issues per year,
postage and packaging included.
Back issues available.

CONTENTS

INTER-INFLUENCE OF DEFECTS IN WELDED JOINT ZONE AT DIFFERENT FORCE LOADING

V.I. MAKHNENKO, E.A. VELIKOIVANENKO, A.S. MILENIN, G.F. ROZYNKA and **N.I. PIVTORAK**
E.O. Paton Electric Welding Institute, NASU, Kiev, Ukraine

It is noted that force interaction of group discontinuity defects of material in welded structures is not necessarily reduced to the concept, according to which the adjacent defect impairs the service load resistance or does not affect it at a sufficiently large distance between them. A variant is considered, when interaction of group defects of the type of cracks or wall thinning defects, improves the resistance to service loading.

Keywords: *welded joints, group defect interaction, parallel defects, collinear defects, fracture probability*

Extent of damage of a particular structure under specific service conditions is usually determined by the number of found inadmissible defects. It is natural that the greater the number of such defects, the more damaged the examined structure is believed to be. The existing rules of allowing for inter-influence of defects [1–3, etc.] are usually reduced to combining by the respective rules two or more admissible defects located closest to each other into one independent admissible (inadmissible) defect based on a concept, according to which the neighbouring defect impairs or does not influence the service load resistance of this defect.

Such a concept is quite simple, but on the whole it is too conservative in a number of cases, as it does not allow for the possibility of a third alternative, namely that the neighbouring defect can unload this defect, and thus, improve its performance under specific service conditions.

Allowing for the third alternative at engineering diagnostics of structures requires application of the appropriate calculation procedures, normative documents, etc. but, nonetheless, considering the modern tendencies in development of computer engineering, methods of mathematical modeling, information systems, as well as growing requirements to optimization of the developed critical structures, the good prospects for application of these developments are undoubtful, particularly for prediction of safe operation of welded structures with long service life by the results of the respective engineering diagnostics of their state.

This paper deals with such a possibility for sufficiently characteristic in-service defects of welded structures in the form of cracks and thinning.

Let us start with the simplest examples of interaction of two and three through-thickness parallel cracks of the same dimensions in an unlimited plate, uniformly tensioned along a normal to crack plane (Figures 1 and 2) by stress σ. The characteristic of such defect loading is the stress intensity factor in crack tip K_I. Respective data from [4] for the case of two cracks are given in Figure 1 and in Table 1, and those for three cracks — in Figure 2, depending on distance between cracks d. These data show that d decrease noticeably lowers K_I values, both for two and for three cracks.

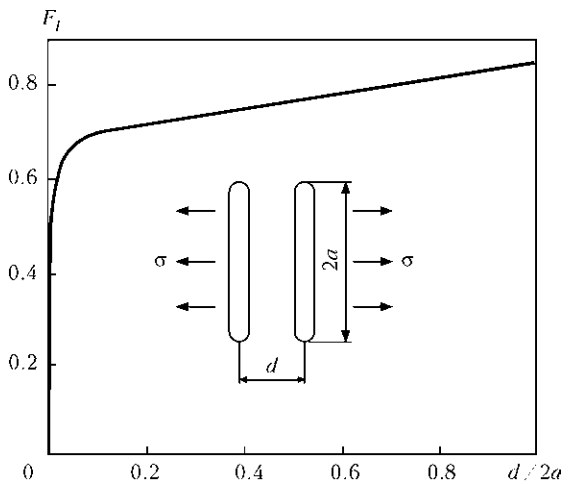

Figure 1. Dependence $F_I = K_I/(\sigma\sqrt{\pi a})$ on $d/2a$ [4]

Table 1. Numerical results [4]

$2a/d$	F_I
0	1.0000*
0.2	0.9855*
0.4	0.9508*
0.6	0.9089*
0.8	0.8727*
1.0	0.8319
1.25	0.8037
2	0.7569
5	0.6962
10	0.6651
100	0.5846

*Plate with central crack.

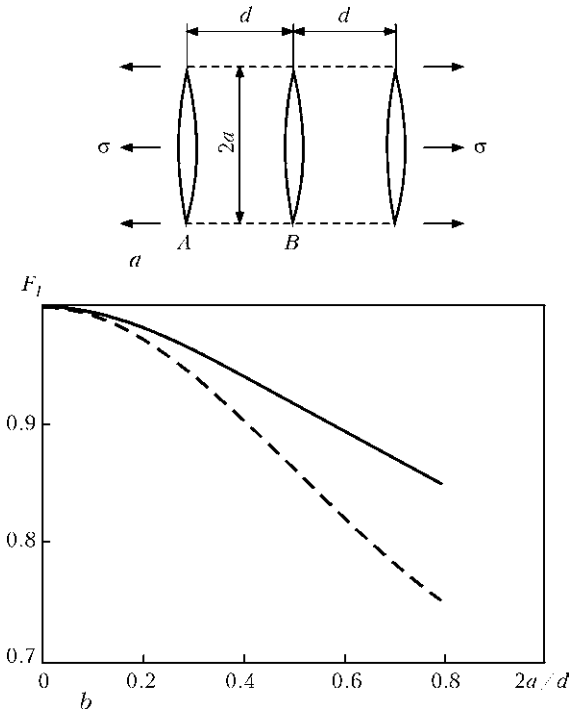

Figure 2. Uniform tension of plane with three parallel cracks of equal length along the normal to crack lines (*a*), and dependence of $F_{I,A}$ (solid curve) and $F_{I,B}$ (hatched) on $2a/d$ (*b*)

Explanation of such a fact follows from the local stress field, arising around the crack tips. Figure 3 gives the typical picture of distribution of stresses σ_{zz} in the zone of through-thickness crack $2a = 20$ mm with normal z in the strip-plate in plane $z = 0$. It is seen that on crack faces $z = 0$, $\sigma_{zz} = 0$, and then, as z rises, stresses σ_{zz} gradually increase up to 300 MPa, for those applied on the boundary $z = 500$ mm. Width of strip is $2L_x = 200$ mm, material is steel with yield point $\sigma_y = 420$ MPa. Thus, near the crack — its free faces — a field of unloading by stresses σ_{zz} forms that will, naturally, affect values K_I, if the second crack is placed into this field that is quite convincingly

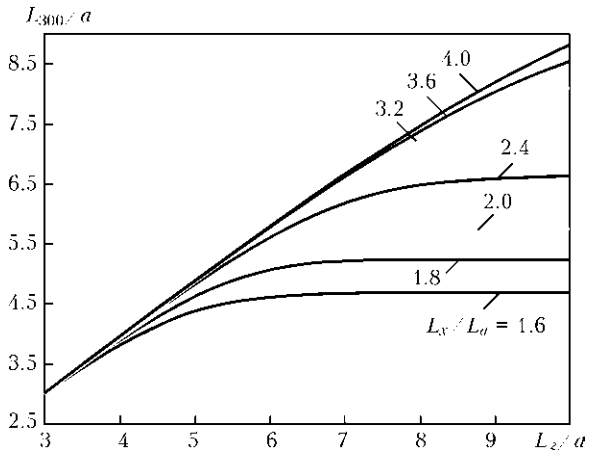

Figure 4. Extent of unloading zone along the axis $x = 0$ for isolated crack in plate of $L_z \times L_x$

demonstrated by the data in Figure 1 and Table 1. As the unloading zone has finite dimensions, at sufficiently large d the interaction between the two cracks becomes negligible.

It is characteristic that the extend of unloading zone L_σ along axis z depends on dimensions of crack $2a$ and overall dimensions of the strip $2L_z \times L_x$, that can be seen from the data in Figure 4. Such examples of interaction of parallel defects-cracks in the case of welded joints are quite numerous in practical diagnostics, for instance, a cruciform joint of elements of sufficiently large thickness t, welded by fillet welds with leg S at incomplete penetration, forming two extended (along the weld) defects of material discontinuity (cracks) of size $2a$ (Figure 5). This joint is quite well-studied both under tension (Figure 5, *a*) and at bending (Figure 5, *b*) [4], that allows these data for $K_{\theta_{max}}$ to be used both at evaluation of brittle strength, and at evaluation of growth of $2a$ value at cyclic loading [3]. In Figure 5 parameter $\varepsilon = l/t_2$, where $l = S$ is the fillet weld leg; t_2 is the thickness of uncut element — distance between parallel defects,

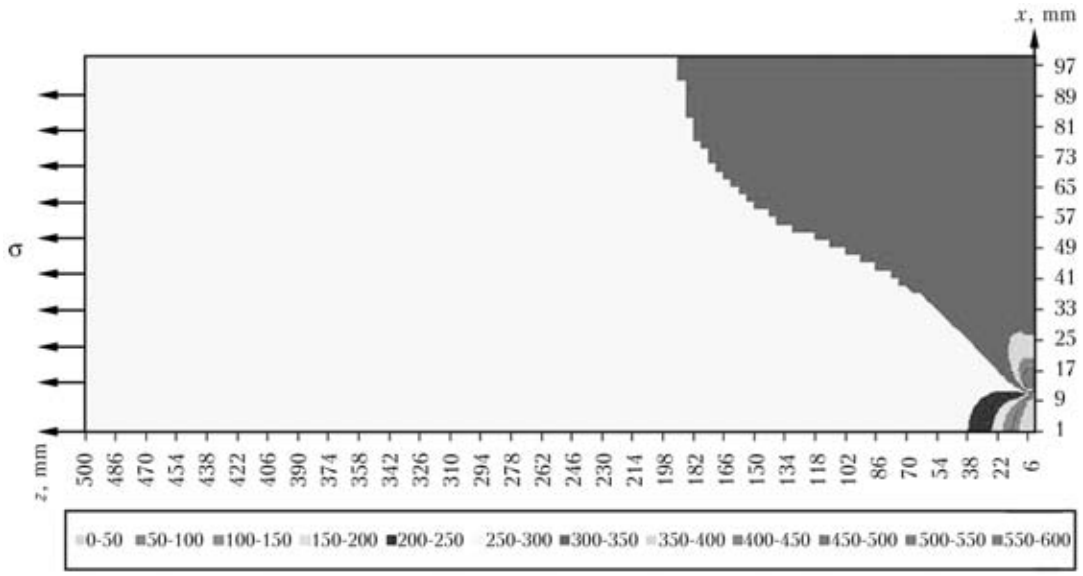

Figure 3. Unloading zone for the case of $a = 10$ mm of isolated crack in plate of $2L_z = 1000$ mm $2L_x = 200$ mm of steel with $\sigma_y = 420$ MPa and $\sigma = 300$ MPa

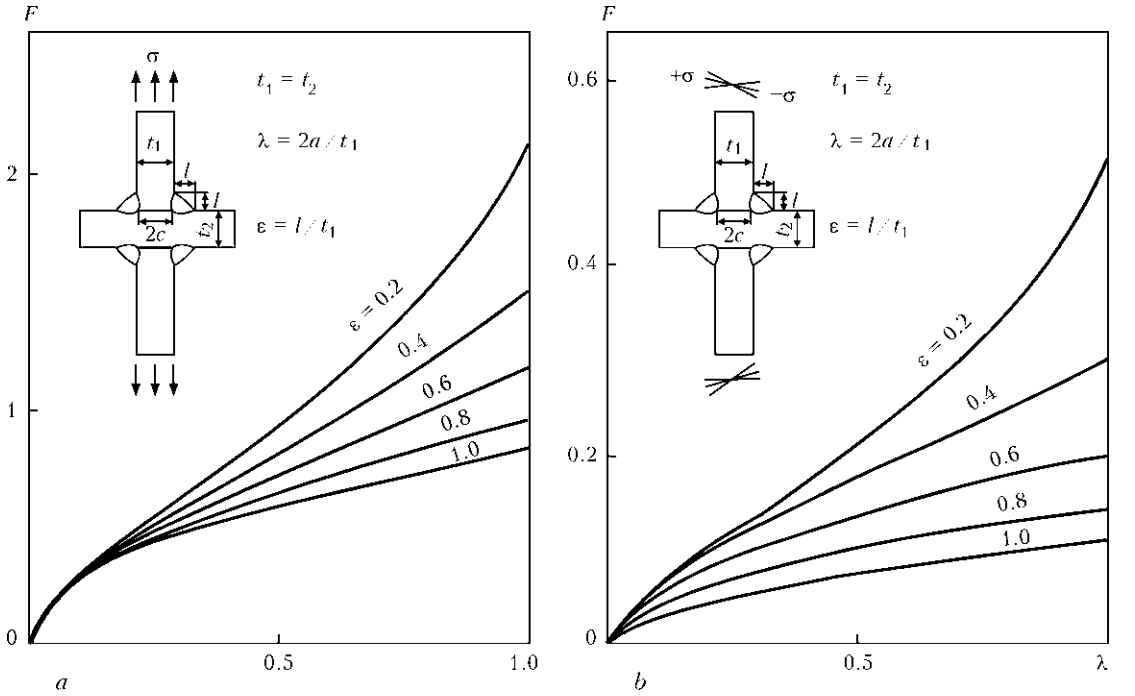

Figure 5. $F(\lambda)$ dependence ($F = K_{\theta_{max}}/\sigma\sqrt{t_1}$, $t_1 = t_2$) at tension (*a*) and bending (*b*) in cruciform joint [4]

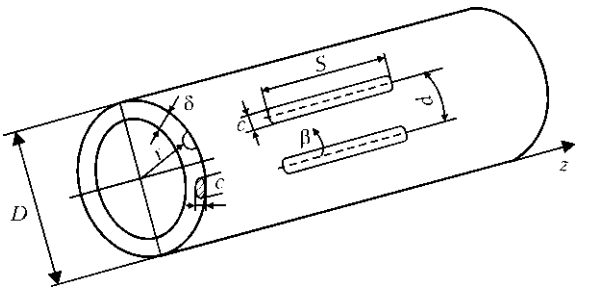

Figure 6. Schematic of cylindrical shell-pipe with longitudinal groove thinning defects

demonstrates t_2 influence on $K_{\theta_{max}}$ value at other conditions being equal, i.e. defect interaction.

Note that the effect of defect parallelism in the respective field of nominal stresses is manifested not only for crack-like defects, but also for thinning defects. For instance, in cylindrical shell-pipe two groove thinning defects along the pipe generatrix, at their parallel location (Figure 6), interacting with each other, in the case of in-pipe pressure P, lower the critical pressure in the pipe, depending on distance between defects d. Results of numerical calculations using the procedure from work [5] are given below. Defects with overall dimensions $s \times c \times a$ (a is the maximum defect depth) are modeled by a semi-ellipsoid on pipe surface, i.e. defect surface is described in the coordinate system r, β, z by the equation

$$\left(\frac{2z}{s}\right)^2 + \left(\frac{2\beta r}{c}\right)^2 + \left(\frac{R-r}{a}2\right)^2 = 1 \quad (2R = D). \tag{1}$$

At internal pressure maximum circumferential stresses $\sigma_{\beta\beta}$ arise in midplanes $\beta = 0$ and $\beta = d/R$. Fracture probability in these planes of area F according to [5] is determined by Weibull dependence

$$p = 1 - \exp\left[-\int_F \left(\frac{\sigma_{\beta\beta}(0, r, z) - A}{B}\right)^4 dF\right] \quad \text{at } \sigma_{\beta\beta}(0, r, z) > A, \tag{2}$$

where A, B are the Weibull distribution parameters experimentally determined for this material. If experimental data from [2] are used, then $A = (\sigma_y + \sigma_t)/2$ can be assumed for a steel pipe, for isolated defect in a pipe with $D = 1420$ mm, $\delta = 28$ mm, $A = 500$ MPa, $\sigma_y = 440$ MPa, respectively.

Respective calculation of the stress-strain state for the above initial data shows that at $P = 9$ MPa in the

Table 2. Results of calculation of failure probability p by (2) for groove thinning defects (see Figure 6) at different distances between defects d and pressures P

Variant #	Pressure P, MPa	One defect	Two defects		
			d = 90 mm	d = 60 mm	d = 48 mm
1	7	0.00075	0	0	0
2	8	0.0068	0.0013	0.0010	0.0010
3	9	0.05	0.0072	0.0057	0.0049
4	10	0.16	0.0290	0.0268	0.0200

case of an isolated defect at s = 66 mm, c = 40 mm, a = 14 mm, $p \approx 0.05$ according to [2] that corresponds to B = 470 MPa. Considering such B value, p values were calculated by (2), which are given in Table 2 at different d and P.

CONCLUSIONS

1. Interaction of defects at force loading of welded structures largely depends on defect geometry and their position relative to the direction of force load application.

2. The most studied is the interaction of material discontinuity defects of the type of cracks and thinning, which are located in one loaded section of the item, so-called collinear defects. There are the respective schematics of combining such defects, depending on overall dimensions of defects and distance between them.

3. Unlike collinear defects, parallel defects of the type of cracks and groove thinning, located in different, but parallel sections of the item, usually unload each other. Therefore, they are less critical when they draw closer to each other, compared to similar collinear defects.

4. At present, owing to development of information technologies and computer engineering means, it is possible to assess the interaction of the found defects in welded structures based on the respective solutions of deformation mechanics for elasto-plastic continua with cracks or thinning defects.

1. *MR-125-01–90*: Calculation of stress intensity factors and section weakening for defects in welded joints. Kiev.
2. (2000) *Fitness-for-service*: American Petroleum Institute Recommended Practice 579.
3. Makhnenko, V.I. (2006) *Safe operation resource of welded joints and assemblies of current structures*. Kiev: Naukova Dumka.
4. (1999) *Reference book on stress intensity factors*. Vol. 1 and 2. Ed. by Yu. Murakavi. Moscow: Mir.
5. Makhnenko, V.I., Velikoivanenko, E.A., Rozynka, G.F. et al. (2010) Improvement of method for estimation of the risk of fracture within the thinning zone on walls of main pipelines. *The Paton Welding J.*, **5**, 10–14.

APPLICATION OF POWDERS OF COBALT AND NICKEL ALLOYS FOR PLASMA SURFACING OF EXHAUST VALVES OF INTERNAL COMBUSTION ENGINES

E.F. PEREPLYOTCHIKOV
E.O. Paton Electric Welding Institute, NASU, Kiev, Ukraine

Properties of alloys based on cobalt and nickel for plasma surfacing of exhaust valves of gasoline and diesel engines of cars and lorries as well as engines of diesel locomotives and ships are considered. Recommendations on application of powders of various compositions for valve surfacing are given.

Keywords: *plasma-powder surfacing, powders of cobalt alloys, powders of nickel alloys, valves of internal combustion engines*

Exhaust valves of internal combustion engines (ICE) suffer from high temperature cycling, power loads as well as corrosion in operation. Operating temperature of valve head of ICE of a car reaches 700 °C and that for a lorry makes 800 °C. Multiple heating and cooling, non-uniform distribution of temperature over a valve section and cyclic power loading result in damage of contact surface of a valve face. Surfacing of the face by alloys with high heat resistance, thermal stability, hot hardness and corrosion resistance is the most effective method for a burn-out and wear-out preventing.

Nickel and cobalt based alloys are used for surfacing of contact surfaces of the faces depending on operating conditions of ICE valves. Cobalt-chromium-tungsten alloys (stellites) Nos. 6 and 12 as well as stellite F and VZK (domestic analog of stellite No.6) (Table 1) are the most widely used for surfacing of the valves among the stellites.

All these alloys differ by high wear resistance, thermal stability and heat resistance at standard and elevated temperatures as well as high corrosion resistance in many aggressive media. Corrosion resistance of the stellites exceeds approximately 10 times resistance of steel used for ICE valves. It is usually evaluated on weight loss in molten plumbic oxide PbO at 910 °C in engine construction.

Characteristic of the stellites is the possibility to preserve sufficient hardness at high temperatures. As can be seen from Figure 1, hardness of alloy of stellite F has the most intensive decrease starting from 500 °C. Properties of solid solution and carbide eutectics as well as relationship of these main constituents determine hardness being an integral characteristic of the stellites. Significant decrease of hardness of F stellite alloy at 700 °C is related with softening of the solid solution enriched with nickel.

Table 1. Chemical composition (wt.%) and alloy hardness applied for surfacing of exhaust valves of ICE [1–4]

Alloy grade	C	Mn	Si	Cr	W	Ni	Fe	B	Co	Others	Hardness *HRC*
110K65Kh28V4 (stellite No.6)	1.1	0.5	1.1	28	4.5	≤ 3	≤ 3	–	Base	–	44
140K60Kh30V8 (stellite No.12)	1.4	≤ 1.0	≤ 2.0	30	8.0	≤ 3	≤ 3	–	Same	–	50
110KKh30VS (VZK)	1.1	–	2.0	30	4.5	≤ 3	≤ 3	–	»	–	42
180KKh25N20V12 (stellite F)	1.8	0.3	1.1	26	12.0	20	≤ 2	–	»	0.5Mo	43
90KKh30N6VSR (PN-AN34)	0.8	–	1.7	30	4.5	6	≤ 3	0.8	»	–	45
EP-616A	0.9	0.4	2.5	26	–	Base	≤ 3	1.5	–	0.2Ti 0.8Al 0.25Cu	40
150N40Kh25V6	1.5	–	0.6	26	6.0	Same	25	–	–	–	35
50NKh25S5R	0.5	–	5.0	25	–	»	8	0.9	–	–	46

F stellite alloy characterizing by reduced cobalt content and increased fraction of tungsten and, in particular, nickel is mostly used for surfacing of the valves of gasoline engines. The alloys of stellite No.6 and VZK are used for surfacing of the valves of diesel engines. Stellite No.12 with higher content of tungsten is rarely applied. However, high cost of cobalt and reduction of its production require it to be replaced by other materials.

Nickel-based alloys gain more and more spread as a substitute of cobalt alloys. Alloys of Ni–Cr–Si–B system as well as nimonic and inconel type alloys find an application in manufacture of the valves in the world practice. An important peculiarity of inconel is the fact that content of up to 20 % of iron provides a small change of its properties and the first deposited layer already has high corrosion resistance.

Two grades of nickel-based alloys, i.e. 150N40Kh25V6 and EP-616A (see Table 1) have been used in CIS countries till recently. Long-term experience of operation of the deposited valves confirms their good service characteristics. 150N40Kh25V6 alloy is mainly used for surfacing of the engine valves of heavy lorries, the sealing faces of which operate at 800 °C. The alloy is ductile and easy to machining. Structure of the alloy is austenite with carbide hardening. Chromium and tungsten carbides provide excellent mechanical wear resistance.

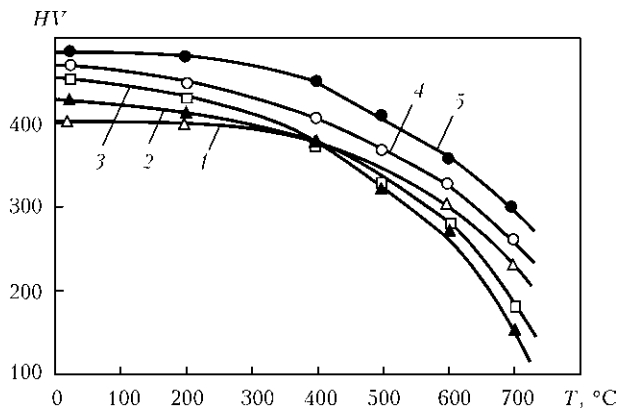

Figure 1. Hot hardness of alloys for surfacing of ICE valves: *1* — 150N40Kh25V6; *2* — EP-616A; *3* — stellite F; *4* — stellite No.6; *5* — 50NKh25S5R

Deposited metal of this type has high hot resistance, i.e. its hardness is approximately the same as in stellite No.6 (see Figure 1) at temperatures higher than 700 °C. Lower sensitivity to presence of iron, which significantly reduces properties of cobalt alloys, is sufficiently important advantage of 150N40Kh25V6 alloy in comparison with the stellites. This alloy does virtually not yield to cobalt-based alloys on the level of corrosion resistance in the melt of plumbic oxide.

Chromium-nickel alloy EP-616A refers to Ni–Cr–Si–B alloy system which is well known under the trade name «Colmonoy». These alloys have low melting temperature 960–1050 °C as well as the properties of self-fluxing brazing alloys. Boron and silicon promote excellent formation of the deposited layer. Tendency to formation of shrinkage porosities is a disadvantage of these alloys. Nickel and chromium borides are present in the structure of the deposited metal of this type together with complex eutectics.

Hardness of nickel alloys varies from *HRC* 20 up to 65. Chromium-nickel alloys with boron and silicon do not yield to the stellite on heat resistance at temperatures of 500–550 °C, however, their hot hardness characterizing by heat resistance to a certain degree is lower at higher temperatures than in the stellites (see Figure 1).

Alloys of Ni–Cr–Si–B system are close to the stellites on ductility and coefficient of linear expansion. As can be seen from Table 2, temperature of melting of nickel-based alloys 150N40Kh26V6 is lower than that of cobalt stellites and EP-616A alloy.

Automatic surfacing of the valves with 150N40Kh25V6 alloy was carried out using plasma arc over a stationary additive in a form of cermet ring.

Table 2. Physical-mechanical properties of alloys based on nickel and cobalt [1, 5, 6]

Alloy grade	Density, g/cm^3	Temperature of melting, °C	Coefficient of linear expansion, $K^{-1}\cdot10^{-6}$	Friction coefficient	Ultimate strength, MPa
110K65Kh28V4 (stellite No.6)	8.42	1290	14.9	0.07–0.13	740
140K60Kh30V8 (stellite No.12)	8.47	1285	14.4	0.07–0.13	530
110KKh30VS (VZK)	8.49	1280	15.5	0.08–0.11	620
180KKh25N20V12 (stellite F)	8.68	1300	13.8	0.07–0.13	660
EP-616A	8.51	1230	15.0	0.07–0.09	536
150N40Kh25V6	8.55	1100	15.1	0.07–0.10	550

The latter is manufactured by means of pressing of the fine-dispersed powders of nickel, chromium, tungsten, graphite and other materials and their further sintering in a vacuum. Industrial production of the cermet rings was stopped on series of organizational reasons in the resent years that made impossible the application of plasma surfacing over the stationary additive in bulk production of the automobile valves.

Plasma method using additive in a form of metal powder opens new possibilities for automatic surfacing of the valves. It is differ by high efficiency at low penetration of a base metal [1]. Efficiency of the plasma-powder surfacing is determined in many respects by quality of additive powder. The latter should have good flowability, low gas-saturation and specified grain-size distribution. The powders with 45–63 μm particle size (for valves of cars) or 80–200 μm particle size (for valves of diesels of locomotives and ships) are used depending on structure of a plasmatron as well as the deposited valves and saddles. They are obtained, as a rule, by spraying of liquid metal using inert gas.

Wider range of the additive materials can be used in plasma-powder surfacing, and this method meets the increased requirements made to valve control gears of ICE to a higher degree due to rising of specific power of the engines and increase of their ecological characteristics.

Cobalt- or nickel-based alloys with high service properties 110KKh30VS (VZK), 90KKh30N6VSR (AN34), 180KKh25N20V12 (stellite F), EP-616A, 50NKh25S5R are used for the plasma-powder surfacing depending on operation requirements, dimension-types of the valves and saddles. 50NKh25S5R is of interest since it exceeds EP-616A (see Table 1) on the level of initial and hot hardness and, besides, it is more sparsely alloyed. This alloy differs by high corrosion resistance, thermal fatigue resistance, and shows good behavior in metal-to-metal friction even at high pressures [1]. Investigations on Shevenar dilatometer in heating to 900 °C at 150–170 °C/h rate provide a representation of structural changes taking place in 50NKh25S5R alloy at working temperatures.

Alloy 50NKh25S5R has no structural transformations as can be seen form Figure 2. Insignificant inflections of the curves at 650 °C are, apparently, connected with a dissolution of carbide and chromium boride particles in the nickel-chromium solution. Alloy 50NKh25S5R is recommended for application in surfacing of the heavy-loaded valves of 5D70 diesel locomotive engines instead of cobalt alloy VZK based on evaluation of the service and welding-processing characteristics.

Quality of the deposited meal and economic indices of the process of plasma-powder surfacing mainly depend on the structural peculiarities of a groove of working face for surfacing. Two types of grooves are used in industrial practice for the plasma-powder surfacing of the valves, i.e. trapezoid and radius ones. Trapezoid groove (Figure 3, *b*) has the specific advantages since allows depositing layers of smaller thickness and, thus, reducing consumption of the additive powder, obtaining minimum machining allowance as well as stabilizing the heat input over the groove width and improv-

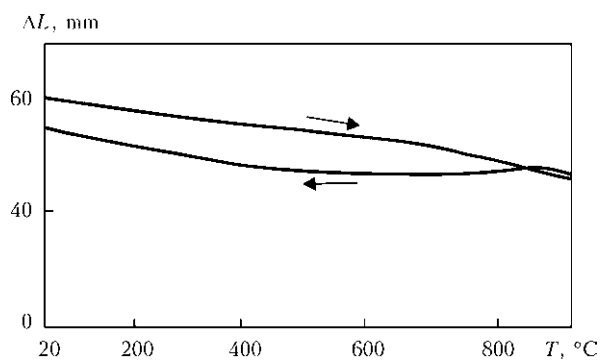

Figure 2. Dilatometric curve of heating–cooling of 50NKh25S5R alloy

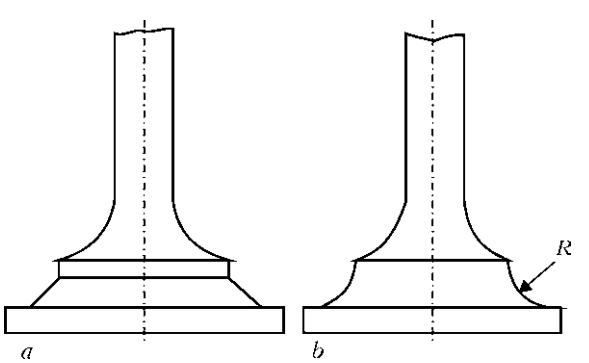

Figure 3. Schemes of trapezoid (*a*) and radius (*b*) groove of valve billets for surfacing

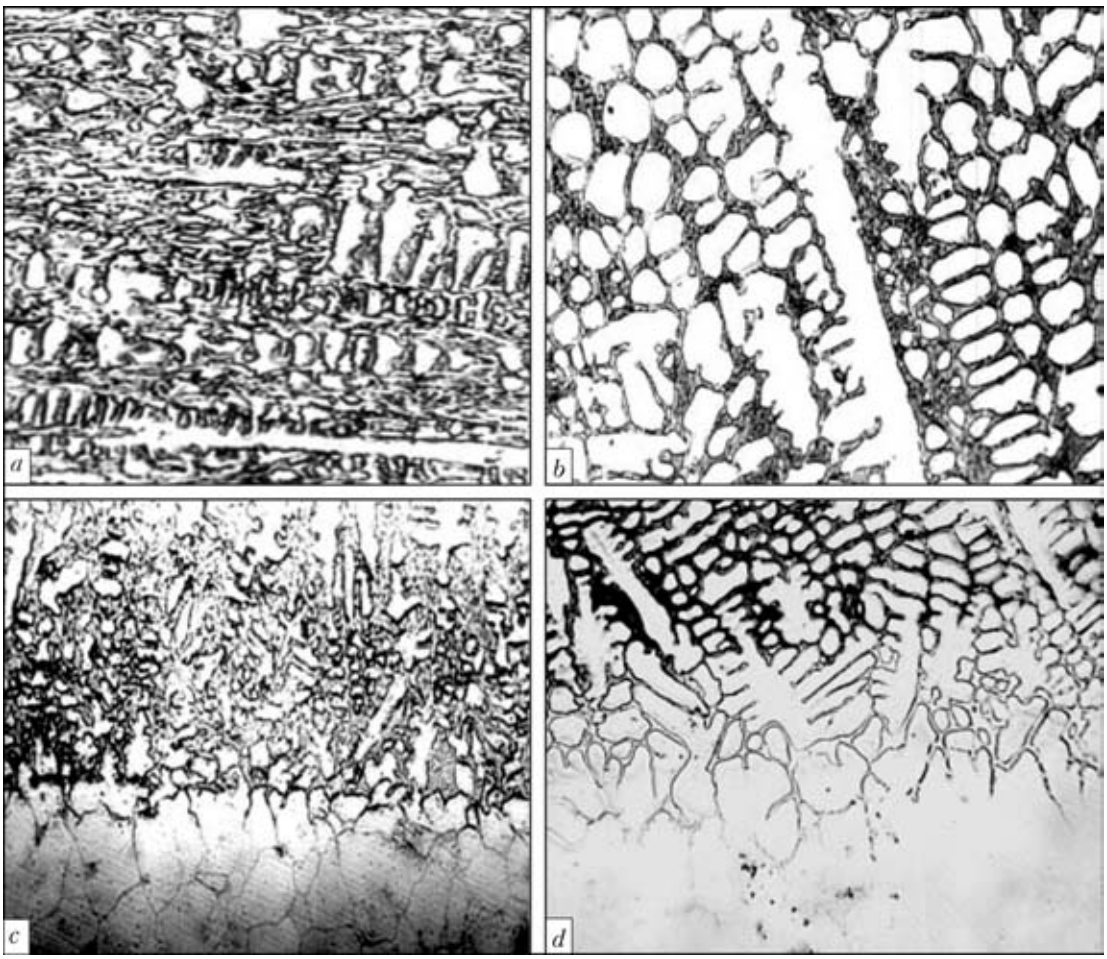

Figure 4. Microstructures (×480) of deposited metal of type of cobalt alloys K60Kh30VS (*a*) and K25Kh25N20V12 (*b*), and zones of their fusion with steel (*c*, *d*) for 55Kh20G9AN4 valves

ing formation of the deposited layer in comparison with radius one (Figure 3, *b*).

Technological experiments showed that optimum angel of bevel of trapezoid groove makes 90°. A valve is set on a water-cooled bearing and smoothness of a surface contacting with the bearing should be not lower than grade 5 roughness for better heat removal.

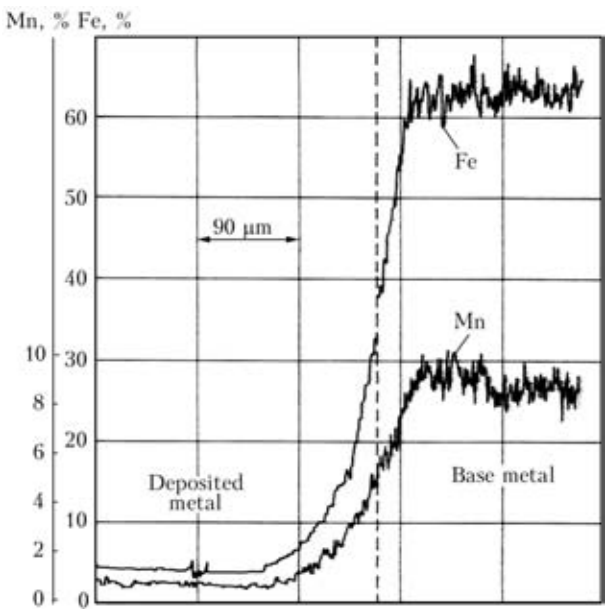

Figure 5. Distribution of iron and manganese in fusion zone of cobalt alloy K25Kh25N20V12 with steel for 55Kh20G9AN4 valves

Surfacing of the small passenger car valves are of particular difficulty. Rigid requirements are made to their quality, safety and service properties. This requires accurate selection of laws of variation of parameters and algorithm of technological process of surfacing in whole.

Selection of the mode parameters is based on a necessity of providing of maximum speed of surfacing at which formation of the deposited layer is not yet violated (15–22 m/h for car valves). Weight rate of a powder feeding should provide necessary dimensions of the deposited layer. Current of the main and pilot arcs was selected in such a way that safe and defect-free joining of the layer being deposited with billet material was provided and, at the same time, dilution of the deposited metal with the base one was minimum (5–7 %).

Values of current of the main and pilot arc, as well as efficiency of feeding of the additive wire, were changed on specific laws selected based on the methodological experiments for providing uniform and minimum penetration of the valve billet, since it is significantly and non-uniformly heated by the arc in the process of surfacing.

Only computer control of the main parameters of the process and high reliability of mechanical part of the equipment can provide required indices of quality

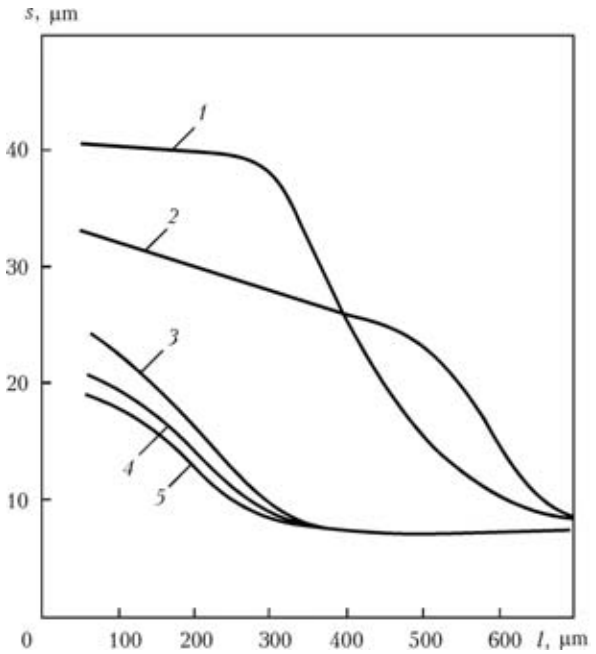

Figure 6. Dependence of grain sizes *s* on distance from fusion boundary *l* at induction (*1*, *2*) and plasma-powder (*3–5*) surfacing of valves with different alloys: *1*, *3* — K60Kh30VS; *2*, *4* — EP-616A; *5* — K25Kh25N20V12

Figure 7. Surface appearance of 5D70 diesel engine valve, deposited using plasma-powder method with 50NKh25S5R alloy, immediately after surfacing (*a*) and after 5000 h of operation (*b*), and macrosection of deposited valve (*c*)

and efficiency of the plasma-powder surfacing of these parts considering that time of surfacing of car valve does not exceed 10 s.

Metallographic investigations showed that structure of the metal deposited on steel for valves 55Kh20G9AN4 using RP-K60Kh30VS and PR-KKh25N20V12 powders consists of a solid solution based on cobalt and eutectic constituent which is a mixture of carbides and solid solution, and there are no defects in their fusion zone (Figure 4, *a–d*). Transition zone between the base and deposited metals makes 100–150 μm in surfacing of the cobalt alloys and that for nickel alloy surfacing is 50–150 μm. Specified hardness of the deposited layer can be virtually achieved in a distance of 0.15–0.20 mm from the fusion zone line. Thus, if you have the deposited layer of 0.5–0.8 mm thickness the necessary serviceability of the valve after machining can be provided due to this that significantly saves consumption of the additive powder. Iron content in the deposited layer does not exceed 5 % (Figure 5).

Width of an overheating zone with coarse austenite grain makes only 0.2–0.3 mm in the plasma-powder surfacing. This is its profitable difference from induction surfacing at which the base metal suffers inevitably from strong overheating with large zone of the coarse austenite grain (Figure 6).

Plasma-powder surfacing is the most efficient, as a rule, in serial production of new valves and saddles of ICE. Surface appearance (Figure 7, *a*) and macrosection of the valve of diesel engine 5D70 deposited with 50NKh25S5R alloy (Figure 7, *c*) indicate good quality of formation of beads in the plasma-powder surfacing. This reduces laboriousness of machining due to allowance reduction. Figure 7, *b* shows the same valve after 5000 h of operation in the engine of diesel locomotive. Inspection showed that contact faces of the valve head have insignificant and uniform wearing and no signs of corrosion and other damages are observed.

Plasma-powder surfacing is sufficiently widely used in repair of the worn valves and saddles of large ship diesels (diameter of sealing surfaces 300–450 mm). Surfacing is performed in one pass with preheating and, sometimes, with concurrent heating. Delayed cooling of the deposited valves is provided after surfacing. Universal units for the plasma-powder surfacing can be used for manufacture and repair surfacing of the valves and saddles of various dimension-types in small-scale production and special units with computer control are to be used in a series production.

Plasma-powder method allows surfacing of all range of the valves. i.e. from valves of the engines of small capacity up to valves of the large ship diesels. This method is sufficiently flexible since allows easily transferring from one valve structure to another, using virtually any alloys independent on their melting temperature, capability to self-fluxing and other properties. Plasma-powder surfacing provides economical consumption of the additive materials (2–3 times lower than in induction surfacing), high quality of deposited metal, minimum heating of the valve and small allowances for machining.

1. Gladky, P.V., Pereplyotchikov, E.F., Ryabtsev, I.A. (2007) *Plasma surfacing*. Kiev: Ekotekhnologiya.
2. Kopylov, D.Yu., Amanov, S.R. (2001) Study of principles of thermal cycle effect on properties of coating with EP-

616A alloy. In: *Science, technique and education in Toliatty city and Volzhsky region*. Pt 2. Tolyatti: TolPI.
3. Amanov, S.R., Kargin, A.V., Kopylov, D.Yu. et al. (2005) Technology of plasma-powder surfacing of exhaust valves of automobile engines VAZ. *Svarochn. Proizvodstvo*, **2**, 33–40.
4. Wu, J.B.C., Redman, J.E. (1994) Hardfacing with cobalt and nickel alloy. *Welding J.*, **9**, 63–68.
5. Malyshevsky, V.A., Muraviov, K.K. (1962) Structure and properties of cobalt stellites. In: *Properties of materials in turbine construction and methods of testing*. Ed. by A.I. Chizhik. Moscow; Leningrad: Mashgiz.
6. Knotek, O., Lugscheider, E., Eschnauer, H. (1975) *Hardlegierungen zum Verschleis. Schutz*. Duesseldorf.

STRUCTURE AND WEAR RESISTANCE OF CHROME-MANGANESE DEPOSITED METAL

V.L. MALINOV and **L.S. MALINOV**
Priazovsky State Technical University, Mariupol, Ukraine

Presented are the results of investigations into structure and wear resistance of low-carbon metal of different structural classes, deposited with flux-cored strips and containing approximately 13 % chromium and different amounts of manganese (from 2 to 12 %). The possibility of increasing wear resistance of the deposited metal by tempering and case hardening after hardfacing was studied. It is shown that achieving the optimal amount of meta-stable austenite, along with martensite, in structure of the deposited metal improves its wear resistance.

Keywords: *arc hardfacing, chrome-manganese deposited metal, structure, martensite, meta-stable austenite, tempering, case hardening, wear resistance*

To repair and strengthen parts operating under conditions of a mechanical wear combined with the corrosion effect at normal and increased temperatures, the industry widely applies hardfacing consumables that provide deposited metal of the type of low-carbon high-chromium steels (≤0.2 % C, ~13 % Cr) of the martensitic-ferritic grade. They are used to repair and strengthen plungers of hydraulic presses and hydraulic cylinders, continuous casting machine rollers, components of power and petrochemical fixtures, etc. [1].

Ferrite is characterised by the lowest fracture resistance, compared to martensite and austenite, which hampers achieving a high wear resistance of the deposited metal. To decrease the content of ferrite and provide mostly the martensitic structure, the deposited metal is alloyed with nickel in an amount of 2–4 %. Examples of such hardfacing consumables are PP-Np-12Kh13N2MFA and PP-Np-12Kh14N3. Along with nickel, formation of ferrite is also suppressed by alloying with less expensive manganese. Properties of the low-carbon deposited metal with approximately 13 % Cr and different contents of manganese have been insufficiently studied as yet. However, the data on structure and properties of this type of chrome-manganese steels can be found in studies [2–4].

Table 1. Chemical composition of deposited metal, %

Hardfacing consumable	C	Cr	Mn	Si	Ti
Sv-12Kh13	0.11	12.6	0.7	0.55	–
PL-OP1	0.12	12.5	2.3	0.73	0.14
PL-OP2	0.15	13.3	4.1	0.62	0.17
PL-OP3	0.13	13.1	6.2	0.71	0.15
PL-OP4	0.16	12.9	7.8	0.65	0.18
PL-OP5	0.17	12.6	12.2	0.66	0.16
Note. Content of S and $P \le 0.03$ wt.%.					

The purpose of this study was to investigate structure of the low-carbon Cr–Mn deposited metal of different structural grades (martensitic, martensitic-austenitic, austenitic-martensitic, austenitic) and determine its wear resistance under different test conditions to define rational compositions of hardfacing consumables for different service conditions. The possibility of improving properties of the deposited metal due to tempering parameters and case hardening was also investigated.

One-lock flux-cored strips with a cross section of 10 × 3 mm and a fill factor of 48–50 % were manufactured for hardfacing of experimental samples. Cold-rolled strip of steel 08kp (rimmed) was used as a steel sheath. Manganese and chromium metals, iron powder and a small amount of ferrotitanium to refine grains and strengthen the deposited metal due to formation of dispersed carbides TiC were added in different quantities to the charge composition. Hardfacing was performed in three layers by the submerged-arc method using flux AN-26 on a 30 mm thick plate of steel VSt3sp (killed). The hardfacing parameters were as follows: current 450–500 A, voltage 30–32 V, and hardfacing speed 25 m/h. Chemical compositions of the metal deposited with wire Sv-12Kh13 and experimental flux-cored strips PL-OP (1–5) are given in Table 1.

As found at the preliminary stage of investigations, in hardfacing without preheating the deposited metal (~13 % Cr and ≥6 % Mn) was free from cracks. No cracks were detected in the metal deposited with wire Sv-12Kh13 either. However, they were detected at 2–4 % Mn. Preheating to a temperature of 250 °C made it possible to avoid cracks in all the cases. Al-

lowing for this fact, preheating was used only when necessary in hardfacing of samples for further investigations.

The effect of the tempering temperature, as well as of case hardening on wear resistance of the deposited metal with different manganese contents was also investigated. Tempering of the hardfaced samples was carried out at temperatures of 450, 550, 650 and 750 °C with holding for 1 h and subsequent cooling in air. Case hardening of the samples was performed in a solid carbonaceous medium at a temperature of 950 °C for 10 h, followed by cooling of the samples in air. After case hardening, some of the samples were subjected to tempering at a temperature of 650 °C.

Relative wear resistance of the deposited metal under conditions of dry friction by the block–roller scheme was evaluated at room temperature (ε_1) and at 500 °C (ε_2). The 70 mm diameter roller used for wear was hardfaced by the TIG welding method using alloy P18 (*HRC* 56). The roller rotation speed was 200 rpm. The sample was pressed to the roller by the 8 kg load. Wear at the increased temperature was evaluated by using a continuous furnace working chamber after preliminary holding of the sample for 15 min.

Relative wear resistance ε_3 was determined by affecting the surface of a flat sample by a grit transported with a flow of compressed air under a pressure in the system equal to 5 atm. Diameter of the nozzle at exit of the jet from a mixer was 16 mm. Duration of the tests of the samples was determined by a grit consumption equal to 20 kg. The relative wear resistance was evaluated from a ratio of the losses of weights of a reference and the sample related to the area of their worn out surfaces, respectively. This test method used to evaluate resistance to fatigue fracture of metal under the repeated force effect is considered in study [5].

One of the main causes of failure of the continuous casting machine rollers is thermal cracking [1]. Resistance to thermal cracking (fire cracking) of the metal deposited with the experimental flux-cored strips was determined from the quantity of heating–cooling cycles to appearance of the cracks that could be seen with unaided eye. The fire crack resistance tests were conducted according to the procedure similar to that suggested in study [6], the difference being that the samples were heated not in a melt of salts, but in a laboratory furnace at a temperature of 550 °C for 15 min, after which they were cooled in water.

Note that in all the cases the reference for evaluation of properties of the deposited metal was metal deposited with wire Sv-12Kh13.

Durometric and metallographic examinations were carried out. Phase composition was determined by the X-ray method using diffractometer DRON-4. Variations in the amount of the magnetic phase in the deposited metal over a range of 5 to 60 % C were estimated by using ferritometer FM-1.

Results of the tests to wear resistance, hardness and content of the ferritic component after hardfacing without tempering, as well as at different temperatures of tempering, are given in Table 2.

Microstructures of the deposited metal with different contents of manganese after hardfacing without tempering are shown in the Figure.

The metal deposited with wire Sv-12Kh13 and containing 0.7 % Mn has a martensitic-ferritic structure (Figure, *a*). Its hardness is *HRC* 36–38. At approximately 2 % Mn, structure of the deposited metal is mostly martensitic. Along with martensite, also a small amount (≤5 %) of high-temperature ferrite may persist in structure. Hardness of the deposited metal is *HRC* 40–42. As the manganese content is increased to 4 %, retained austenite appears in structure of the

Table 2. Effect of manganese and tempering temperature on properties of deposited metal

Hardfacing consumable	Tempering temperature, °C	Hardness *HRC*	Content of ferromagnetic component, %*	Relative wear resistance	
				ε_1	ε_3
Sv-12Kh13	Without tempering	36–38	100	1.0	1.0
	450	34–36	100	1.1	1.0
	550	31–33	100	0.8	0.8
	650	23–25	100	0.6	0.7
	750	34–36	100	0.9	1.1
PL-OP1	Without tempering	40–42	100	1.6	1.2
	450	41–43	100	1.8	1.3
	550	38–40	100	1.4	1.1
	650	36–38	100	0.9	0.9
	750	40–42	100	1.5	1.3
PL-OP2	Without tempering	38–40	80–85	1.8	1.5
	450	40–42	80–85	1.9	1.7
	550	37–39	85–90	1.6	1.4
	650	34–36	90–95	1.2	1.2
	750	39–41	75–80	1.7	1.5
PL-OP3	Without tempering	35–37	65–70	1.6	1.8
	450	36–38	65–70	1.7	2.0
	550	35–37	70–75	1.5	1.7
	650	34–36	75–80	1.4	1.6
	750	36–38	60–65	1.5	1.8
PL-OP4	Without tempering	32–34	25–30	1.4	2.2
	450	30–32	25–30	1.2	2.5
	550	33–35	30–35	1.4	2.3
	650	34–36	35–40	1.6	1.9
	750	32–34	20–25	1.3	2.1
PL-OP5	Without tempering	22–24	5–10	1.2	2.0
	450	20–22	5–10	1.1	1.9
	550	23–25	10–15	1.2	2.1
	650	24–26	15–20	1.4	2.2
	750	22–24	3–5	1.2	2.0

*Content of the carbide phase is less than 1 %, balance — austenite.

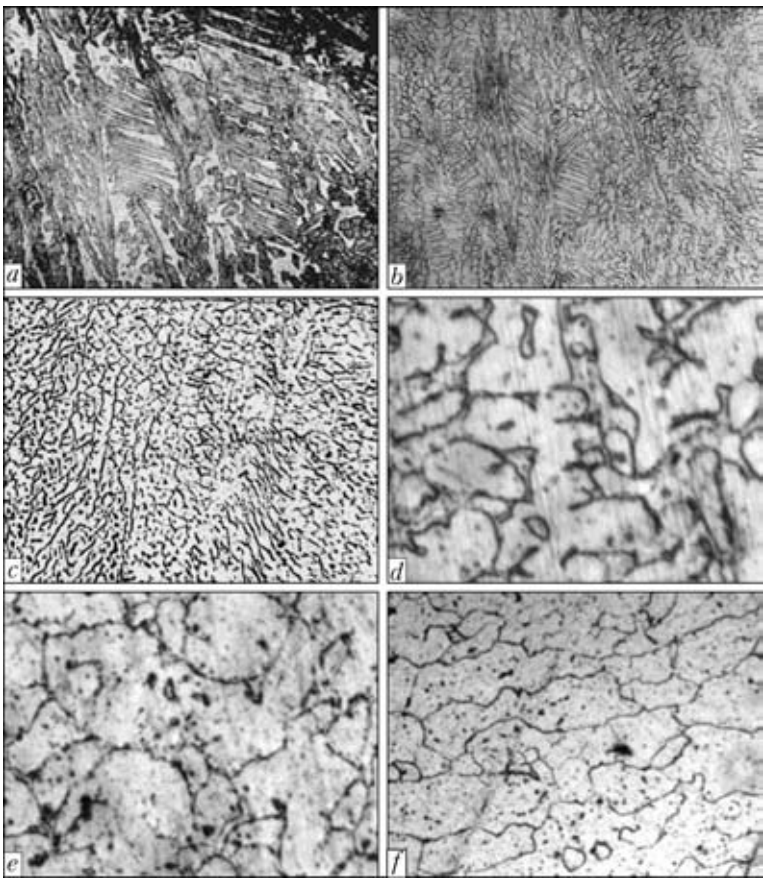

Microstructures (×550) of Cr–Mn deposited metal with different manganese contents: *a* — Sv-12Kh13 (reference); *b* — 2; *c* — 4; *d*, *e* — 8; *f* — 12 % Mn

deposited metal. With further increase in the manganese content of the deposited metal the amount of austenite grows, and hardness of the deposited metal decreases (see Table 2).

Under conditions of dry friction at an ambient temperature, the deposited metal containing 2 % Mn has a 1. 6 times higher relative wear resistance ε_1 than the Sv-12Kh13 deposited metal. The maximal wear resistance (ε_1 = 1.8) is achieved at 4 % Mn, which is caused by solid-solution strengthening of martensite alloyed with manganese, as well as by dynamic deformation martensite transformation (DDMT) of meta-stable retained austenite taking place in wear. The growth of the latter on the wearing surface is 10–17 %. As the manganese content of the deposited metal is increased to 6 %, the amount of retained austenite grows to 30–35 %. This decreases to some extent the relative wear resistance (ε_1 = 1.6). Its lowest level corresponds to 12 % Mn (ε_1 = 1.2), when the deposited metal structure becomes mostly austenitic. This can be explained by the fact that the growth of martensite on the wearing surface, which is 30–35 %, cannot compensate for the almost absolute absence of cooling martensite.

Table 3. Fire crack resistance and wear resistance of deposited metal under dry friction conditions at 550 °C

Hardfacing consumable	Hardness *HRC*	Fire crack resistance	Relative wear resistance ε_2
Sv-12Kh13	30–32	1.0	1.0
PL-OP1	38–40	0.8	1.7
PL-OP2	36–38	0.9	2.0
PL-OP3	33–35	1.1	1.8
PL-OP4	30–32	1.2	1.5
PL-OP5	20–22	1.0	1.3

When wear occurs in the grit flow, with increase of the manganese content from 2 to 8 % the relative wear resistance grows more than 2 times (to ε_3 = = 2.2), compared to the reference, and remains at a high level (ε_3 = 2.0) at 12 % Mn. This is attributable to the fact that deformation of the wearing surface by grit is much higher than in dry friction, this leading to a more intensive development of DDMT. The growth of martensite on the wearing surface of the sample at 8 % Mn in the deposited metal is 45–50 %, and at 12 % Mn — 38–42 %. This causes substantial strengthening of the surface of the deposited metal (hardness in this case grows to *HRC* 45–50) and increase in fracture resistance. A considerable part of energy of the abrasive particles is consumed for DDMT, which is characterised by an intensive development [7].

The data on hardness, relative wear resistance ε_2 and fire crack resistance of the deposited metal at 550 °C depending on its manganese content are given

in Table 3. Hardness at 550 °C decreases with increase of the manganese content. Moreover, decrease in hardness of the deposited metal, compared to its level at an ambient temperature, is fixed for the corresponding manganese contents.

Dependence of relative wear resistance ε_2 of the deposited metal on its manganese content (see Table 3) is similar to that considered above for ε_1 determined at the ambient temperature. However, the values of wear resistance ε_2 for similar compositions of the deposited metal are higher than those of ε_1. Increase in relative wear resistance ε_2 can also be caused by strengthening of martensite alloyed with manganese, as well as by the effect of dynamic ageing of martensite taking place in wear.

The lowest fire crack resistance (see Table 3) is exhibited by the deposited metal containing about 2 % Mn with mostly the martensitic structure. Increase of the manganese content to 8 %, when structure becomes austenitic-martensitic, increases the fire crack resistance, whereas further increase of the manganese content to 12 % causes its decrease. The given regularity is explained by the fact that increase in the content of austenite, which is a more ductile phase than martensite, leads to increase in crack resistance. Decrease in fire crack resistance with increase in the content of austenite above its optimal amount is related to the fact that the γ-phase has an almost twice as high thermal expansion coefficient, compared to the α-phase, this leading to a growth of stresses forming in structure.

The effect of the tempering temperature on properties of the deposited metal was investigated. It was found to depend on the proportion of martensite and austenite in the initial structure after hardfacing. The common pattern of variations in properties is observed for the deposited metal with mostly the martensitic structure at 2–6 % Mn. The highest hardness and relative wear resistance under dry friction conditions, ε_1, and in the grit flow, ε_3, are achieved after tempering at a temperature of 450 °C, this being provided by precipitation hardening and activation of DDMT [4]. With increase of the tempering temperature from 450 to 650 °C, hardness and relative wear resistance ε_1 and ε_3 decrease due to weakening of martensite. As the tempering temperature is further increased to 750 °C, again this causes a rise in hardness and relative wear resistance ε_1 and ε_3. This is a result of heating into the inter-critical temperature range ($A_{c_3} > T > A_{c_1}$) causing redistribution of carbon between the α- and γ-phases, thus leading in cooling to formation of martensite with the increased carbon content from the enriched γ-phase.

For the deposited metal having mostly the austenitic structure, at 8 and 12 % Mn the lowest values of hardness and relative wear resistance in dry friction, ε_1, are fixed after tempering at a temperature of 450 °C. This is caused by increase in stability of austenite due to blocking of the dislocations providing an increase in energy required for DDMT. Raising the tempering temperature to 650 °C increases hardness and relative wear resistance ε_1 up to the maximal values because of precipitation of carbides and activation of DDMT [8]. After tempering at 750 °C, the values of hardness and relative wear resistance ε_1 decrease due to dissolution of part of carbides, thus increasing the amount and stability of austenite.

At 8 and 12 % Mn in the deposited metal the tempering temperature was found to have a differing effect on relative wear resistance in the grit flow, ε_3, which is caused by a differing stability of austenite. Tempering at 450 °C increasing stability of austenite raises relative wear resistance ε_3 in the case when stability of austenite is low (at 8 % Mn). And on the contrary, tempering at 650 °C destabilising austenite increases wear resistance ε_3 in the case when stability of austenite is increased (at 12 % Mn).

The investigations performed showed the expediency of application of the flux-cored strips, which provide the low-carbon Cr–Mn deposited metal with 4–6 % Mn (with martensitic-austenitic structure), for hardfacing of parts operating under dry friction conditions. They are characterised by indices 19, 25, 26 and 34, according to the classification of study [9].

Hardfacing flux-cored strips, which provide the deposited metal containing 8 % Mn and having the austenitic-martensitic structure, are efficient for the use for hardfacing of parts operating under contact-fatigue loading (corresponding to indices 18, 23, 24, 30, 35 [9]). At a not less than 6 % Mn content of the deposited metal it is possible to perform hardfacing without preheating, this being a technological advantage and reducing the power intensity of the process [10].

The deposited metal containing 12 % Mn has the austenitic structure, which provides its good manufacturability (workability by cutting, low sensitivity to cracking) and resistance to the contact-dynamic effect. However, its relative wear resistance under dry friction conditions and crushing resistance are insufficient. Hardfacing with the flux-cored wire providing the 12 % Mn content can be recommended for parts operating under conditions characterised by indices 21 and 27–29 [9].

Increasing the carbon content of the deposited metal improves its relative wear resistance, but hampers machining and often leads to cracking. The technique that makes it possible to handle this contradiction is hardfacing with low-carbon steels followed by their case hardening [11]. This technique can be effectively used for strengthening and repair of parts operating under the conditions characterised by indices 15, 25 and 26, e.g. necks of axles and shafts, contact surfaces of hinged joints, etc. The expediency of case hardening of the deposited metal is proved in study [12].

After case hardening, carbides of the Cr_7C_3 type form in a surface layer of the Cr–Mn deposited metal

Table 4. Properties of deposited metal after case hardening and subsequent tempering

Hardfacing consumable	Treatment	Structure	Hardness *HRC*	Relative wear resistance	
				ε_1	ε_3
Sv-12Kh13	Case hardening	15–17 % A; M + C — balance	45	1.7	1.2
	Same + tempering at 650 °C	10–12 % A; FCM + C — balance	42	1.4	1.1
PL-OP1	Case hardening	20–25 % A; M + C — balance	52	2.5	1.5
	Same + tempering at 650 °C	15–18 % A; FCM + C — balance	48	2.2	1.3
PL-OP2	Case hardening	35–40 % A; M + C — balance	55	4.3	1.9
	Same + tempering at 650 °C	28–30 % A; FCM + C — balance	50	4.0	1.5
PL-OP3	Case hardening	55–60 % A; M + C — balance	44	3.8	2.4
	Same + tempering at 650 °C	45–50 % A; FCM + M′ + C — balance	48	4.2	2.1
PL-OP4	Case hardening	75–80 % A; M + C — balance	38	3.0	2.5
	Same + tempering at 650 °C	65–70 % A; FCM + M′ + C — balance	41	3.4	2.8
PL-OP4	Case hardening	80–85% A; C — balance	35	2.6	2.2
	Same + tempering at 650 °C	75–80 % A; M′ + C — balance	37	2.9	2.5

Note. A — austenite; C — carbide; FCM — ferrite-carbide mixture; M — martensite; M′ — martensite formed in cooling from tempering temperature.

with 13 % Cr. In all the cases the matrix consists of austenite and martensite with different proportions of these phases. As the manganese content is increased, the amount of austenite grows and that of martensite decreases accordingly (Table 4). The carbon content of the surface layer was about 1.6 %, and thickness of the case hardened layer was 1.3–1.5 mm.

High stability of the investigated compositions of the deposited metal subjected to case hardening, with respect to decomposition of overcooled austenite to form the ferrite-carbide mixture, allows refusing from hardening in a liquid coolant, as self-hardening occurs in air cooling. Important in this case is reduction of stresses and residual strains in parts, simplification and environment friendliness of the technological process.

The Cr–Mn deposited metal with 4 % Mn has the highest wear resistance after case hardening under dry friction conditions. In this case about 40–50 % of meta-stable austenite is fixed in the structure, along with martensite and carbides. As the manganese content is further increased, wear resistance of the deposited metal decreases due to increase in the amount and stability of austenite in its structure. Subjecting the deposited metal with maximum 4 % Mn to tempering at 650 °C leads to deterioration of its wear resistance ε_1. This is caused by weakening of martensite and decomposition of retained austenite. And on the contrary, relative wear resistance ε_1 of the deposited metal containing not less than 6 % Mn grows because of activation of DDMT due to precipitation of carbides from austenite. These data are in agreement with the results of study [13].

In testing in the grit flow, the highest relative wear resistance ε_3 was achieved after case hardening of the deposited metal containing 8 % Mn and having 75–80 % of retained austenite in its structure. Tempering at a temperature of 650 °C has a differing effect on wear resistance in the grit flow, ε_3, for the deposited metal with differing manganese contents: at not higher than 6 % Mn it decreases, and at not less than 8 % Mn it increases. This is attributable to the fact that at no more than 6 % Mn tempering at 650 °C leads to weakening of martensite and excessive activation of DDMT, where stability of austenite is low, this leading to decrease in relative wear resistance ε_3. At not less than 8 % Mn, where stability of austenite is increased, on the contrary the activation of DDMT raises relative wear resistance ε_3.

The method suggested for improving wear resistance by hardfacing with the low-carbon Cr–Mn-based metal, followed by case hardening [11], in all the cases provides formation of retained meta-stable austenite in structure, along with martensite and carbides. However, it should be taken into account that the highest wear resistance for a specific type of a test is achieved at the optimal amount and stability of austenite, which can be controlled by tempering.

CONCLUSIONS

1. It is shown that development of hardfacing consumables providing the deposited Cr–Mn metal of different structural grades and having the martensitic, martensitic-austenitic, austenitic-martensitic or austenitic structure, depending on the imposed requirements, holds high promise for extending the life of parts operating under conditions of dry friction and contact-fatigue loading.

2. The amount and stability of austenite with respect to DDMT have a substantial effect on wear

resistance, and should be controlled by tempering parameters, allowing for the specific loading conditions.

3. The efficiency is shown of improving wear resistance by combining hardfacing with the low-carbon Cr–Mn-based metal and subsequent case hardening.

1. Ryabtsev, I.A. (2004) *Hardfacing of machine parts and mechanisms*. Kiev: Ekotekhnologiya.
2. Malinov, L.S., Chejlyakh, A.P. (1981) Chrome-manganese steels of transition grade. *Izvestiya Vuzov. Chyorn. Metallurgiya*, **4**, 101–103.
3. Malinov, L.S., Chejlyakh, A.P. (1983) Effect of manganese and heat treatment on structure and properties of steels Fe–0,1 % C–14 % Cr. *Ibid.*, **6**, 83–87.
4. Malinov, L.S., Malinov, V.L. (2009) *Resource-saving sparsely alloyed alloys and hardening technologies providing the effect of self-hardening*. Mariupol: Renata.
5. Malinov, V.L. (2011) Effect of manganese on structure and wear resistance of deposited metal of the low-carbon steel type. *The Paton Welding J.*, **8**, 12–16.
6. Tylkin, M.A. (1965) *Strength and wear resistance of metallurgical equipment parts*. Moscow: Metallurgiya.
7. Popov, V.S., Brykov, I.N. (1996) *Wear resistance of steels and alloys*. Zaporozhie: IPK Zaporozhie.
8. Malinov, L.S., Konop-Lyashko, V.I. (1982) Effect of ageing on development of martensitic transformation in deformation of meta-stable austenitic steels. *Izvestiya AN SSSR. Metally*, **3**, 130–133.
9. Gladky, P.V., Kondratiev, I.A., Yumatova, V.I. et al. (1991) *Hardfacing flux-cored strips and wires*: Refer. Book. Kiev: Tekhnika.
10. Malinov, V.L. *Charge of flux-cored strip*. Pat. 94862 Ukraine. Int. Cl. C2 B23K 35/28. Fil. 07.06.2010. Publ. 11.06.2011.
11. Malinov, L.S., Malinov, V.L. *Method of hardening*. Pat. 63462 Ukraine. Int. Cl. C 21 D1/2. Fil. 22.04.2003. Publ. 15.01.2004.
12. Pikalov, S.V. (2009) About possibilities of repair of automobile parts by gas-shielded surfacing with subsequent case hardening. In: *Proc. of 1st Int. Sci.-Techn. Conf. on Current Automobile Materials and Technologies*, 216–223. Kursk: STU.
13. Malinov, L.S., Chejlyakh, A.P., Malinova, E.L. (1991) Effect of case hardening and subsequent heat treatment on structure, phase composition and abrasive wear resistance of Fe–Cr–Mn steels. *Izvestiya AN SSSR. Metally*, **1**, 120–123.

PECULIARITIES OF STRUCTURE AND MECHANICAL HETEROGENEITY IN EB-WELDED JOINTS OF 1201-T ALLOY

V.R. SKALSKY[1], **L.R. BOTVINA**[2] and **I.N. LYASOTA**[1]

[1]H.V. Karpenko Physico-Mechanical Institute, NASU, Lvov, Ukraine

[2]A.A. Baikov Institute of Metallurgy and Materials Science, RAS, Moscow, Russia

The peculiarities of microstructure and distribution of microhardness of weld and heat-affected zone metal of welded joints of 1201-T alloy, produced using electron beam welding at different values of heat input, were studied. Using plotted temperature fields the running of phase transformations occurred in welding was analyzed. It was established that due to change of cooling rate across the thickness of plates the microstructure of near-weld zone in upper and lower parts of welded joint were considerably different. The increase of heat input of welding facilitates recrystallization processes which leads to increase of heat-affected zone.

Keywords: *electron beam welding, aluminium alloy, heat-affected zone, weakening, temperature field, structure and mechanical heterogeneity, microstructure*

Due to high strength and resistance to cryogenic and corrosion embrittlement the aluminium alloys of Al–Cu–Mn system are widely applied in aircraft industry [1, 2]. For joining critical elements of structures the electron beam welding (EBW) is applied as far as this method provides high quality of weld metal in one-pass welding large thicknesses [3]. The characteristic property of thermal cycle of welding is rapid heating of metal and also its cooling. The short periods of this process provide special kinetics of structural transformations which results in weakening and heterogeneity of welded joints (WJ) [4–12]. It is the most clearly revealed in welding of thick plates and caused by decay of solid solution of copper in aluminium and partial coagulation of strengthening phases due to uniform heating of weld and adjacent zones of base metal [4].

Elements of structures of aluminium alloys containing WJ are operating under conditions of alternating dynamic loads, deep vacuum and cryogenic temperatures, which frequently results in initiation and propagation of micro- and macrofracture in them. The process of microcrack propagation depends directly on the structure and mechanical characteristics of metal. Therefore, to perform efficient diagnostics of WJ of structure elements manufactured of mentioned aluminium alloy including methods of acoustic emission [5–7], it is important also to investigate the microstructure of HAZ metal.

The purpose of the work is to study peculiarities of structure and mechanical heterogeneity of WJ of thick plates of heat-hardened 1201-T alloy, produced using EBW.

It is known that level of weakening and structure changes in HAZ metal of WJ of heat-hardened aluminium alloys is determined by welding cycle and structure of base metal [8–10]. It was also established [11] that a weld is weakened to the level characteristic for metal in annealed state (for 1201 alloy to *HRB* 70). This phenomenon is predetermined by both the processes of dissolution of strengthening phases as well as their further precipitation during cooling.

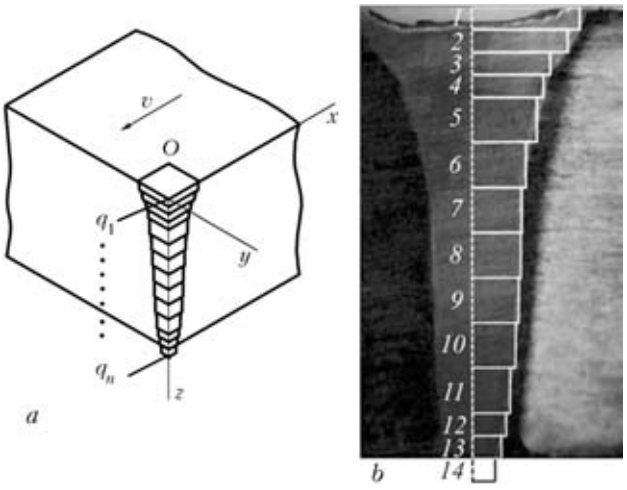

Figure 1. Scheme of modeling of splitting moving linear power sources across the thickness of plates (*a*), and macrosection of WJ of 1201-T alloy (*b*)

In works [9, 11, 12] the influence of welding method on the width of weakening zone of WJ of aluminium alloys was studied. It was shown that this area is narrower in EBW as compared to that of argon arc welding, thus influencing mechanical properties of these WJ and general strength of the structure [13]. To increase properties of WJ they are subjected to heat treatment, which for dispersion-strengthened alloys (including 1201 alloy) consists in tempering and further artificial ageing [14]. The influence of post-weld heat treatment on the structure and mechanical characteristics of WJ were investigated in works [9–11, 14–17]. It was established that such heat treatment allows increasing hardness of 1021 alloy weld metal only by 10 %. Thus, the repeated artificial ageing practically does not change the strength characteristics of these WJ.

The investigations of structural transformations in HAZ metal of 2219 alloy showed that the zone of high temperature dissolution of strengthening phases is formed independently of initial structure of base metal [18]. It is explained by the fact that heating of HAZ metal in vicinity of fusion boundary exceeds the temperature of hardening. Under these conditions the dissolution of precipitates occurs, and the further rapid cooling facilitates the formation of main strengthening particles. The low-temperature dissolution of strengthening phases, except of thermal cycle of welding, depends on initial structure of base metal. Its level at low temperatures (523–573 K) is determined by the size of precipitates, type of crystalline lattice and coherency relatively to the matrix. The dissolution of coherent particles occurs more intensively than non-coherent ones, i.e. Guinier–Preston zones are dissolved more rapidly than θ-phase. Between the areas of high- and low-temperature dissolution of strengtheners more equilibrium phases can be formed accompanying by annealing of alloy.

To investigate WJ of 20 and 25 mm thickness produced using through EBW without filler metal the following conditions were used: welding speed v_w = = 70 m/h; beam current I_b = 120 (180) A; acceleration voltage U_{acc} = 60 (55) kV; heat input q/v = 337.3 (463.7) kJ/m. The plates to be welded were manufactured of heat-hardened aluminium 1201-T alloy.

It is known [11] that dynamics of structural transformations in each point of HAZ depends on maximum temperature of their heating and time of remaining in the corresponding temperature range. Therefore for better analysis of metallurgy processes running in EBW of thick plates of aluminium alloys, it is necessary to calculate the temperature field and thermal cycles in HAZ metal of WJ.

To plot temperature fields the methods were applied described in [19]. Its principle consisted in fact that in EBW the channel of penetration is considered as totality of linear heat sources q_i (i = 1, ..., n) of general power q, moving at the speed of welding in the middle of plates (Figure 1, *a*). Therefore, the sum of temperature fields of separate linear sources deter-

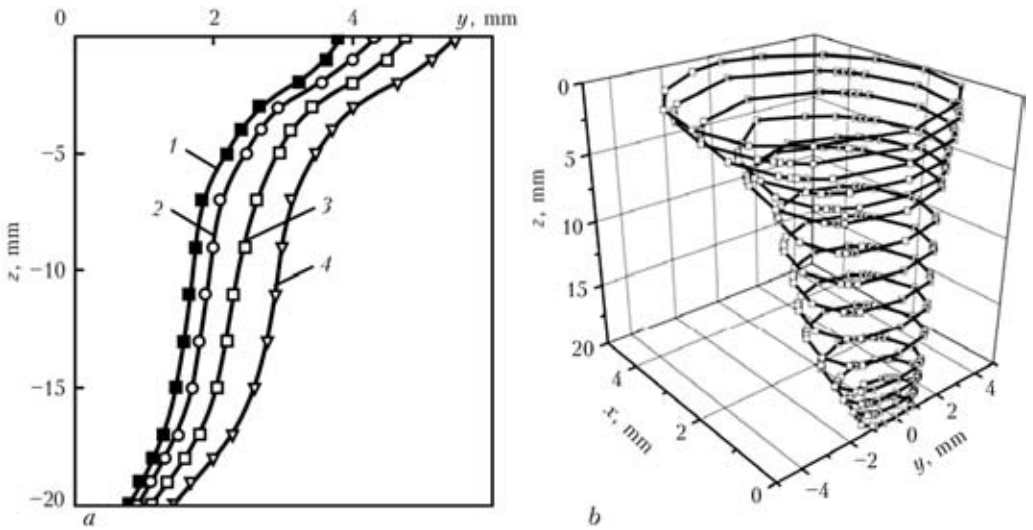

Figure 2. Isotherms in the plane *yOz* (*a*) (*1* — 853; *2* — 773; *3* — 673; *4* — 573 K), and isothermic surface at T = 673 K (*b*) in EBW of plates 20 mm thick

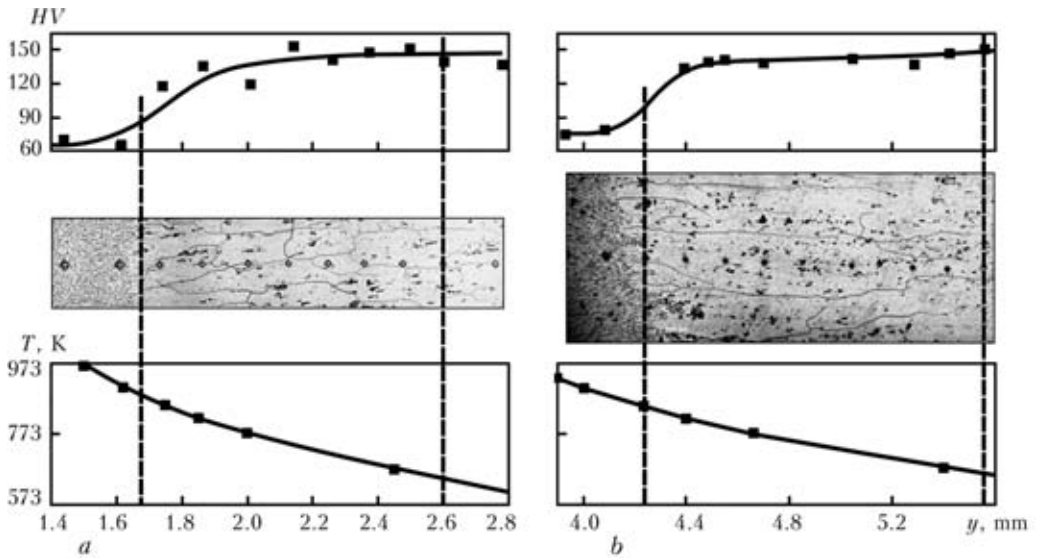

Figure 3. Distribution of microhardness and microstructure of HAZ metal of WJ at q/v = 337.3 (*a*) and 463.7 (*b*) kJ/m at removing from the weld axis

mines the general field. Such optimal amount of power sources is offered to provide minimal thickness of splitting layer within the range of 1–5 mm. The distribution of temperatures from such a source was determined according to the model of N.N. Rykalin [20]. For accurate calculation of geometry of a fusion boundary in the areas, where considerable nonlinearity of its form is observed, this area was split into more finer layers (Figure 1, *b*). The advantage of this method in welding of thick-wall structure elements is consideration of uniformity of distribution of energy of heat source across the section of a joint.

The hardness of WJ metal was measured using microhardness meter PMT-3. The loading on indenter was 0.54 Pa.

The results of calculations presented in Figure 2 show that fields are non-uniform according to all three spatial coordinates, which, in its turn, is the reason of non-uniform heating of HAZ points along the WJ section. The characteristic concentricity of isothermal field (Figure 2, *b*) is predetermined by physical properties of aluminium alloys, in particular, their high heat conductivity, significantly influencing the processes of heat distribution in welding [21].

Figure 3 shows that changes in HAZ metal occur already at the temperature of 723 K. The clear etching of structure components is observed caused by partial coagulation of strengthening phases which precipitated in the bulk of grains and along their boundaries.

The characteristic peculiarities of thermal influence in EBW is rapid heating of metal up to maximum temperatures and slower rate of its further cooling (Figure 4). In welding of artificially aged alloy in the period of its rapid heating the coagulation processes do not manage to run over, and during further cooling starting from the temperature of 823 K and lower high-temperature decay of solid solution occurs which is followed by formation of strengthener. The originates of θ-phase are, first of all, formed along the grain boundaries [4], as far as these areas contain impurities of different type, and also in the body of a grain. Their development occurs due to coming of atoms of copper from the surrounding solution. Thus, the grain boundaries are getting thicker at their removing from base metal to fusion line and light near-boundary areas of aluminium solution, depleted with copper, arise, that, in its turn, facilitates decrease in metal hardness.

Depending on the time of remaining of metal in the temperature range of 573–823 K the conditions for complete decay of solid solution, coagulation of precipitated phase Al_2Cu and recrystallization processes are formed. Figure 4 shows thermal cycles of spots located in different zones of WJ. Due to decrease of q/v across the thickness of WJ the instant rate of cooling is increased from the beginning of counting out to the direction of z axis. It is evidenced by the changes of inclination of curves *1–3* in Figure 4 at the stage of cooling. In connection with different time of remaining in temperature range mentioned above the level of recrystallization and precipitation of strengthening phase is differed. The analysis of microstructure (Figure 5) shows that grains of HAZ metal of upper

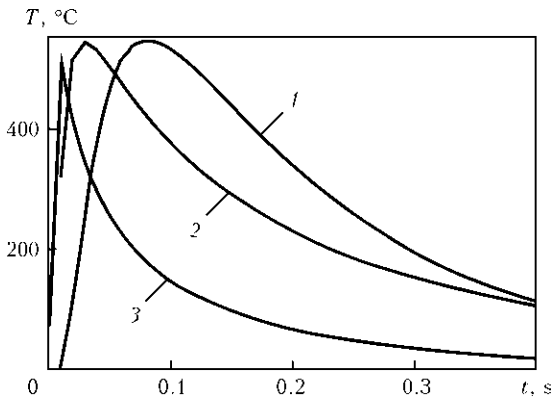

Figure 4. Thermal cycles of points located in different zones of WJ: *1* — y = 3.76 mm, z = 0; *2* — y = 1.84 mm, z = 10 mm; *3* — y = 0.83 mm, z = 20 mm

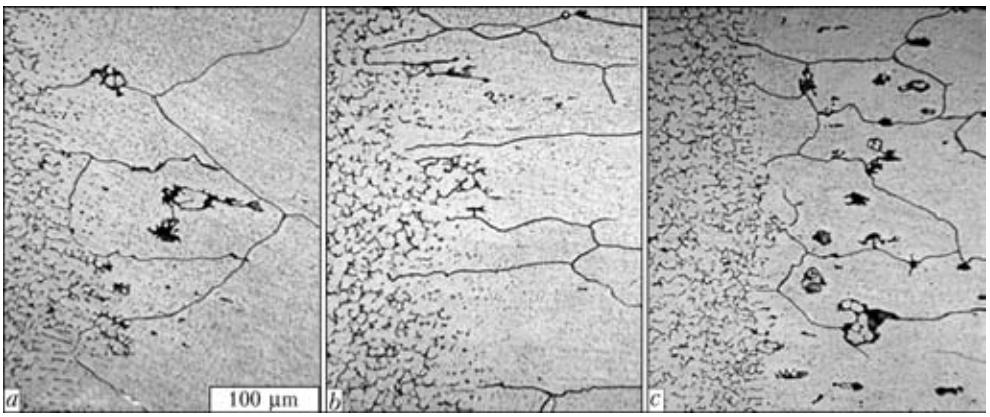

Figure 5. Microstructures of upper (*a*), central (*b* — ×150) and lower (*c* — ×150) areas of fusion zone of aluminium 1201-T alloy WJ at q/v = 337.3 kJ/m

part of WJ (Figure 5, *a*) are considerably larger than those of central and lower one (Figure 5, *b* and *c*, correspondingly). The grains of upper part of fusion boundary are also strengthened by fine precipitates of Al_2Cu phase, however in a lower one they are depleted as far as θ-phase are mainly distributed along their boundaries. The increase of heat input of welding facilitates intensifying of these processes which correspondingly leads to increase of HAZ (see Figure 3).

Thus, the course of dissolution and repeated formation of solid solution, its decay and coagulation of separate particles form mechanical characteristics of near-weld zone. The fusion of grains at the fusion boundary and formation of constant brittle eutectic interlayers along their boundaries facilitate embrittlement of alloy, and recrystallization and growth of grains decrease strength and crack resistance of WJ [11, 22, 23]. Therefore, it is important to consider these phenomena during diagnostics and investigation of processes of initiation of fracture of structures containing such WJ.

It should be noted in conclusion that investigation of microstructure and hardness of WJ of heat-hardened aluminium 1201-T alloy, produced using EBW, showed that the given material tends to considerable decay of solid solution and weakening of weld and HAZ metal. As a result of changes in cooling rate across the thickness of plates, the microstructure of near-weld zone of upper and lower part of WJ is different. The increase of heat input of welding facilitates the processes of recrystallization and leads to increase of sizes of HAZ: at q/v = 337.3 kJ/m the width of this area is 0.9 mm, and at q/v = 463.7 kJ it is of 1.4 mm, the extension of grains reaches on average 0.5–0.9 mm. As a result all these phenomena can negatively influence the mechanical properties of these joints.

1. Ishchenko, A.Ya. (2004) Specifics in application of aluminium high-strength alloys for welded structures. *The Paton Welding J.*, **9**, 15–25.
2. Ishchenko, A.Ya. (2007) Welding of aluminium alloys (directions of research conducted at PWI). *Ibid.*, **11**, 6–9.
3. Paton, B.E., Bondarev, A.A. (2004) State-of-the-art and advanced technologies of electron beam welding of structures. *Ibid.*, **11**, 20–27.
4. Nikiforov, G.D. (1972) *Metallurgy of fusion welding of aluminium alloys*. Moscow: Mashinostroenie.
5. Skalsky, V.R., Sergienko, O.M., Golaski, L. (1999) Generation of acoustic emission by cracks propagated in welded joints. *Tekhn. Diagnostika i Nerazrush. Kontrol*, **4**, 23–31.
6. Skalsky, V.R., Andrejkiv, O.E. (2006) *Assessment of volume damage of materials by acoustic emission method*. Lviv: I. Franko Lviv NU.
7. Skalsky, V.R. (2001) Procedure of assessment of defect formation in alloys D16-T and 1201-T by acoustic emission method. *Mashynoznavstvo*, **3**, 13–18.
8. Rabkin, D.M. (1986) *Metallurgy of fusion welding of aluminium and its alloys*. Kiev: Naukova Dumka.
9. Rabkin, D.M., Lozovskaya, A.V., Sklabinskaya, I.E. (1992) *Metals science of aluminium and its alloys*. Kiev: Naukova Dumka.
10. Ishchenko, A.Ya., Lozovskaya, A.V. (1980) Kinetics of transformations in welding of heat-hardened aluminium alloy 1201. *Avtomatich. Svarka*, **1**, 29–32.
11. Lozovskaya, A.V., Chajka, A.A., Bondarev, A.A. et al. (2001) Softening of high-strength aluminium alloys in different fusion welding processes. *The Paton Welding J.*, **3**, 13–17.
12. Bondarev, A.A., Lozovskaya, A.V., Ishchenko, A.Ya. et al. (1974) Specifics of electron beam welding of alloy 1201. *Avtomatich. Svarka*, **2**, 20–22.
13. Malarvizhi, S., Alasubramanian, V. (2011) Effect of welding processes on AA2219 aluminium alloy joint properties. *Transact. of Nonferrous Metals Soc. of China*, 21(**5**), 962–973.
14. Frolov, V.V. (2003) *Arc welding of aluminium*. Kharkov: Tekhnologiya.
15. Malarvizhi, S., Alasubramanian, V. (2010) Effects of welding processes and post-weld aging treatment on fatigue behavior of AA2219 aluminium alloy joints. *J. Mat. Eng. and Performance*, 20(**3**), 359–367.
16. Tosto, S., Nenci, F., Hu, J. (1996) Microstructure and properties of electron beam welded and post-welded 2219 aluminum alloy. *Mat. Sci. and Technol.*, **12**, 323–328.
17. Alapati, R., Dwivedi, D.K. (2009) Microstructure and hardness of Al–Cu alloy (A2218) welded joints produced by GTAW. *The Paton Welding J.*, **4**, 21–26.
18. Ishchenko, A.Ya., Lozovskaya, A.V., Sklabinskaya, I.E. (2001) Physical simulation of heat processes in HAZ metal during welding aluminium-lithium alloys. *Ibid.*, **9**, 4–7.
19. Skalsky, V.R., Lyasota, I.M. (2010) Estimation of the heat-affected zone for the electron-beam welding of plates. *Mat. Sci.*, 46(**1**), 115–123.
20. Rykalin, N.N. (1951) *Calculations of thermal processes in welding*. Moscow: Mashinostroenie.
21. Dilthey, U. (2005) Schweisstechnische Fertigungsverfahren 2. *Verhalten der Werkstoffe beim Schweissen*. Vol. XXII. Springer.
22. Bondarev, A.A., Golikov, V.N., Anisimov, Yu.I. (1987) Resistance to brittle fracture of electron beam welded joints of aluminium alloy 1201. *Avtomatich. Svarka*, **3**, 6–7.
23. Labur, T.M., Ishchenko, A.Ya., Taranova, T.G. (1991) Resistance to fracture of welded joints of high-strength aluminium alloys 1151 and 1201. *Ibid.*, **6**, 39–41.

IMPROVEMENT OF FATIGUE RESISTANCE OF WELDED JOINTS WITH ACCUMULATED DAMAGE UNDER MULTISTAGE AND BLOCK LOADING

V.V. KNYSH, S.A. SOLOVEJ and **A.Z. KUZMENKO**
E.O. Paton Electric Welding Institute, NASU, Kiev, Ukraine

The paper gives results of fatigue tests of tee welded joints on steel 09G2S strengthened by the technology of high-frequency mechanical peening after accumulation of 50 % of fatigue damage under the impact of multistage and block loading with differing parameters before and after strengthening. It is established that utilisation of this technology allows increasing the level of stresses initially applied to such joints and extending their residual fatigue life.

Keywords: *accumulation of fatigue damage, high-frequency mechanical peening, cyclic fatigue life, fatigue, welded joint*

Engineering structures are usually affected during operation by complex loading conditions, where the sequence of values of amplitudes and average stresses in a cycle changes in a random way [1]. Studies [2–4] give data of experimental investigations on using high-frequency mechanical peening (HFMP) to increase load-carrying capacity of welded elements of the operating metal structures, which are strengthened after accumulation of a specified level of fatigue damage to initiation of crack. It is shown that after strengthening of the joints by the HFMP technology the levels of service loads can be substantially increased together with ensuring the specified fatigue life. Investigations in this area were carried out only under regular loading. In this connection, proving the efficiency of strengthening of the welded joints in structural elements by the HFMP technology in order to increase the load-carrying capacity of the operating structures under the effect of irregular loading is a task of current importance.

The purpose of this study was to experimentally prove the efficiency of using the HFMP technology for strengthening of tee welded joints in operating metal structures to increase their load-carrying capacity under conditions of different-parameters multistage and block loading before and after peening.

Experimental investigations were carried out with specimens of the T-joints on steel 09G2S (σ_y = = 370 MPa, σ_t = 540 MPa). Billets for the specimens of this steel were cut out from rolled plates, so that the long side was oriented along rolling. Transverse stiffeners were joined by the fillet welds on both sides by manual arc welding using electrodes UONI-13/55. The shape and geometrical sizes of a specimen are shown in Figure 1. The given thickness of the specimen was due to a wide application of the 12 mm thick rolled plates in welded structures, and width of the gauge part of the specimen was chosen on the basis of capacity of the testing equipment. In strengthening of the joints by the HFMP technology the narrow weld to base metal transition zone was subjected to plastic surface deformation. Fatigue tests of the specimens were carried out by using testing machine URS 20 with uniaxial alternating tension at cycle asymmetry $R_\sigma = 0$. All specimens were tested to complete fracture.

The efficiency of using the HFMP technology to improve fatigue resistance characteristics of the welded joints with accumulated fatigue damage under the effect of different multistage and block loadings before and after strengthening was evaluated by comparing the experimental data of fatigue tests of the welded joints in the as-welded state and strengthened after the specified quantity of alternating loading cycles. The experimental data of tests of the investigated welded joints in the as-welded state under multistage and block loading were generated earlier in studies [5, 6].

Fatigue tests of the T-joints on steel 09G2S strengthened after the specified quantity of cycles of alternating stresses were carried out on 18 specimens,

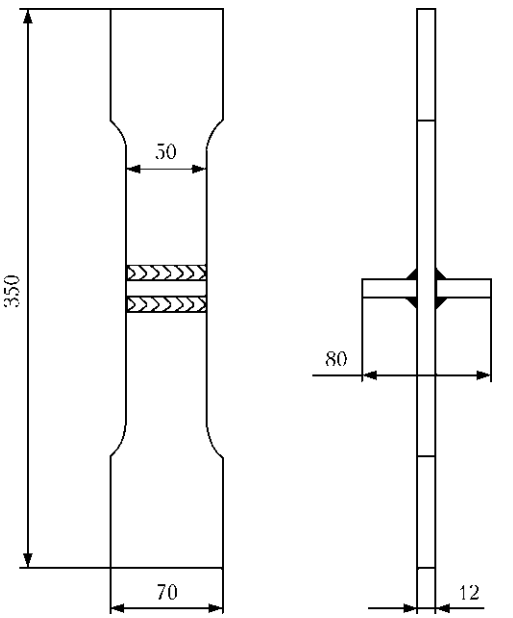

Figure 1. Shape and sizes of the T-joint specimen of steel 09G2S

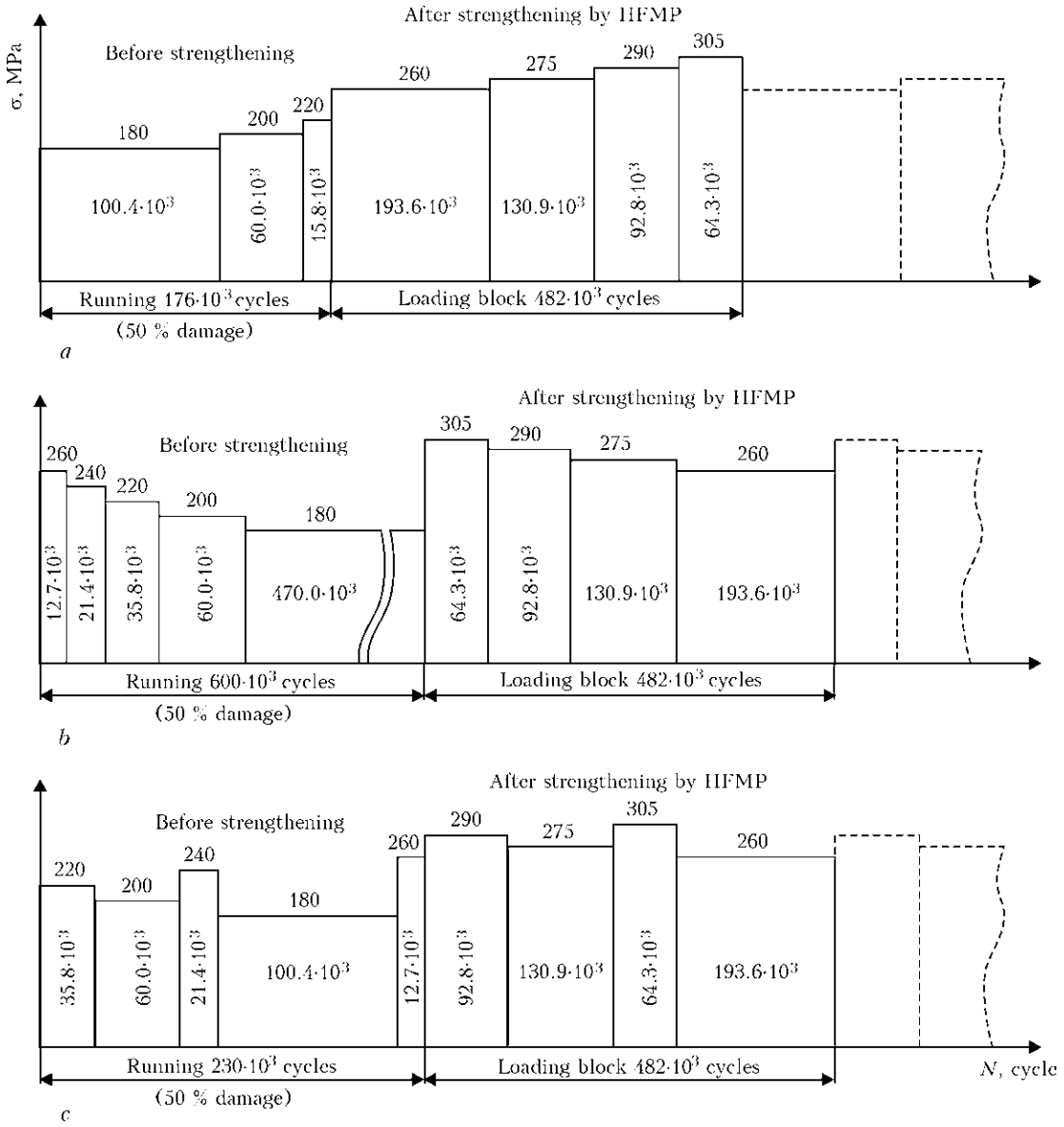

Figure 2. Diagram of loading of the T-joint specimens of steel 09G2S before and after strengthening under multistage loading with increasing (*a*), decreasing (*b*) and quasi-random (*c*) sequences of application of load

9 specimens under each multistage and block loading, respectively, with increasing, decreasing and quasi-random sequences of application of load in a block. Three specimens were tested with each sequence of application of load under the conditions of multistage loading, and three specimens — under the conditions of block loading.

With multistage and block loading of the joints in the as-welded state the sequence of application of load was set by the similar five levels (stages) of the applied maximal stresses in a cycle, but with a different degree of accumulation of damage (quantity of stress alternation cycles) at each level. The increasing sequence of application of load in a block was set by the initial maximal stresses in a cycle equal to 180 MPa at the first stage of loading with their subsequent increase to 260 MPa (the fifth stage of loading) at a pitch of 20 MPa. The decreasing sequence of application of load in a block was set by the initial level of maximal stresses in a cycle equal to 260 MPa with their subsequent decrease to 180 MPa also at a pitch of 20 MPa. The quasi-random sequence of application of load in a block was set by another five sequential levels of maximal cycle stresses in a block: 220, 200, 240, 180 and 260 MPa.

Strengthening of the welded joints by the HFMP technology was carried out after the joints had accumulated 50 % fatigue damage. The quantity of stress alternation cycles before strengthening at each loading stage under the conditions of multistage and block loading was set proceeding from the earlier established ultimate values of the sum of relative fatigue lives (fracture criteria) for the tee welded joints on steel 09G2S in the as-welded state under similar loadings [5, 6]. Under multistage alternating loading, for all sequences of application of loads the total damage of the joints equal to 50 % was set by decreasing two times the values of the running cycles, given in study

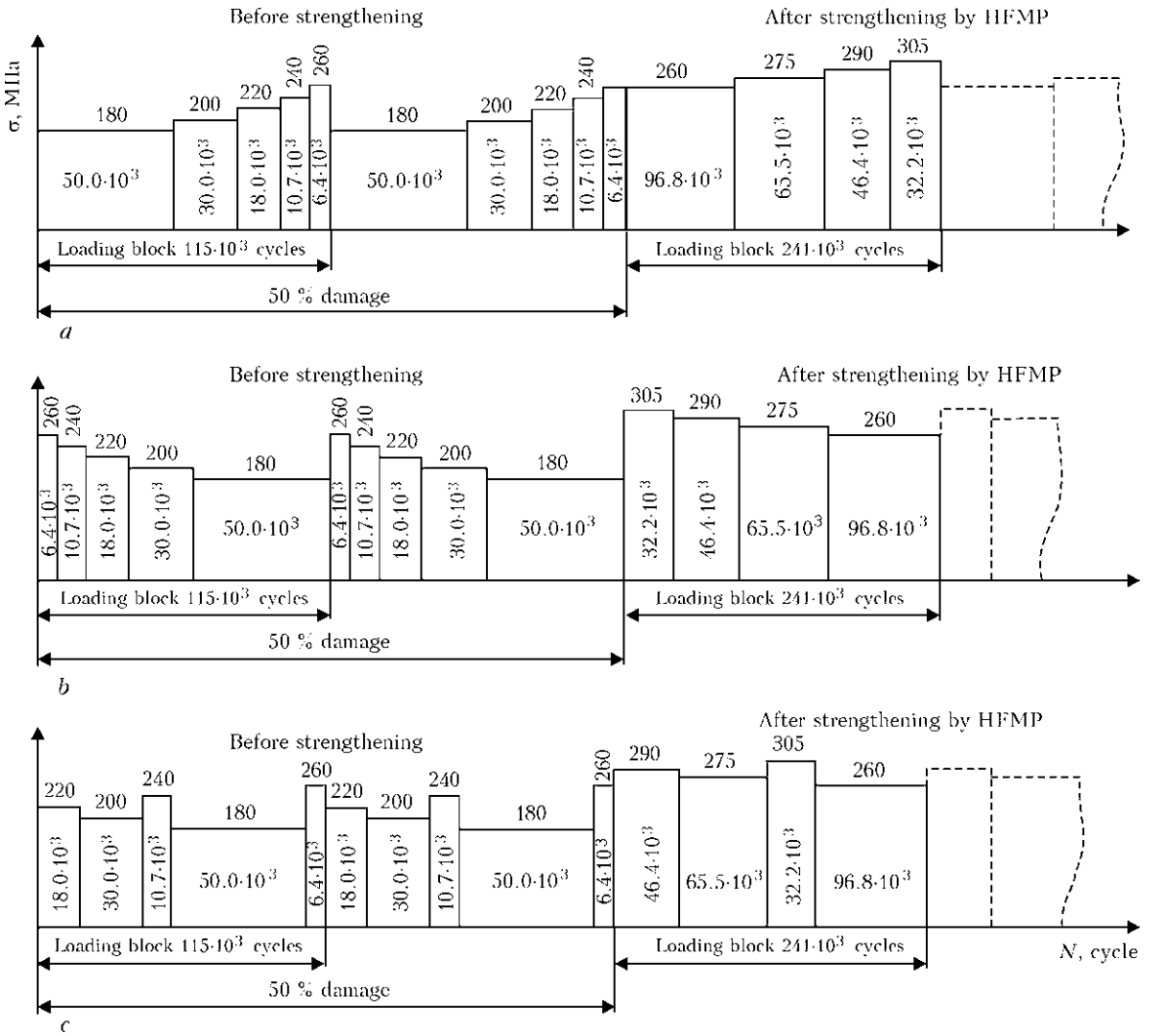

Figure 3. Diagram of loading of the T-joint specimens of steel 09G2S before and after strengthening in block loading with increasing (*a*), decreasing (*b*) and quasi-random (*c*) sequences of application of load in each block

[5], at each stage of loading to fracture of the specimens (Figure 2). The growing sequence of application of load was set by three loading stages, and the decreasing and quasi-random ones — by five loading stages. Under block loading, for all sequences of application of load in a block the total damage of the joints equal to 50 % was set by decreasing 2 times the quantity of the loading blocks to fracture of the welded specimens, compared to that given in study [6], the quantity of cycles in a block being left unchanged (Figure 3). All sequences of application of loads under block loading were set by five loading stages.

After strengthening by the HFMP technology, the sequence of application of load in a block (increasing, decreasing and quasi-random) under the multistage and block loading conditions remained unchanged. The loading block proper was set now not by five loading stages, as before strengthening, but by four stages increased with respect to the initial ones. The increased levels of the applied maximal stresses in a cycle corresponded to the levels of fatigue limits of the strengthened joints (because of HFMP the fatigue limit of the welded joints under consideration grew by 56 %, and the fatigue life increased up to 10 times) [5].

After HFMP strengthening of the tee welded joints with 50 % damage the increasing sequence of application of load in a block was set by the maximal stresses in a cycle equal to 260 MPa at the first loading stage with their subsequent increase to 305 MPa (the fourth loading stage) at a pitch of 15 MPa. The decreasing sequence of application of load in a block was set by the initial level of the maximal stresses in a cycle equal to 305 MPa with their subsequent decrease to 260 MPa also at a pitch of 15 MPa. The quasi-random sequence of application of load in a block was set by the following four sequential levels of the maximal cycle stresses in a block: 290, 275, 305 and 260 MPa. The quantity of the stress alternation cycles at each stage of loading of a specimen under the multistage loading conditions corresponded to 12.5 %, and that under the block loading conditions — to 6.25 % of fatigue life of the specimen strengthened in the as-welded state [5]. This approach provided the total damage per four loading stages (loading block) under multistage loading equal to

Results of fatigue tests of specimens of the tee welded joints

Type of loading	Sequence of application of load	N_{50}, thousand cycles	N_{50}^{str}, thousand cycles	N_{50}^{str}/N_{50}, %	Fracture
Multistage	Increasing	176.2	641.5	364	Stage 1, block 2
		176.2	930.6	528	Stage 4, block 2
		176.2	1274.1	723	Stage 2, block 3
	Decreasing	599.9	1656.0	276	Stage 3, block 4
		599.9	2075.6	346	Stage 2, block 5
		599.9	2378.1	396	Stage 4, block 5
	Quasi-random	230.3	1202.4	522	Stage 3, block 3
		230.3	1847.6	802	Stage 4, block 4
		230.3	2079.1	903	Stage 2, block 5
Block	Increasing	230.2	1909.6	830	Stage 4, block 8
		230.2	2297.2	998	Stage 2, block 10
		230.2	2409.0	1046	Specimen did not fracture
	Decreasing	230.2	1552.6	674	Stage 3, block 7
		230.2	1761.8	765	Stage 2, block 8
		230.2	2409.0	1046	Specimen did not fracture
	Quasi-random	230.2	1401.5	609	Stage 4, block 6
		230.2	2171.9	943	Stage 1, block 10
		230.2	2409.0	1046	Specimen did not fracture

Note. N_{50} — fatigue life of specimen in the non-strengthened state corresponding to 50 % accumulated fatigue damage under preset loading [5, 6]; N_{50}^{str} — fatigue life of specimen strengthened after accumulation of 50 % damage in the as-welded state under preset loading.

50 %, and under block loading — equal to 25 % of that of the specimen strengthened in the as-welded state.

Criterion for the completion of tests under the multistage and block loading conditions was complete fracture of the specimens. If under multistage loading the welded specimen strengthened after accumulation of 50 % damage in the as-welded state did not fracture after the set four loading stages (in one loading block) increased with respect to the initial ones, this loading block was repeated. Therefore, after strengthening, instead of multistage loading, the welded specimens were tested actually to complete fracture under the block loading conditions. The length of a block (quantity of the stress alternation cycles in one block) remained unchanged and equal to $481.6 \cdot 10^3$ cycles (see Figure 2).

Results of fatigue tests of specimens of the tee welded joints on steel 09G2S strengthened by the HFMP technology after accumulation of 50 % damage under the effect of differing multistage and block loadings are given in the Table by indicating the quantity of the running cycles before and after strengthening.

The experimentally established values of fatigue life under multistage loading of the tee welded joints strengthened by the HFMP technology after accumulation of 50 % damage (see the Table) show that these joints have a residual fatigue life ranging from 276 to 903 % of that of the non-strengthened joints. The values of the residual fatigue life obtained in testing the specimens under multistage loading with the increasing sequence of application of load are 364–723 %, with the decreasing sequence — 276–396 %, and with the quasi-random sequence — 522–903 % of those of the non-strengthened joints under the similar sequences of application of load. As follows from the results obtained, strengthening of the tee welded joints on steel 09G2S by the HFMP technology after accumulation of 50 % damage under the multistage loading conditions allows increasing the levels of the initially applied maximal stresses in a block to the stress levels corresponding to the values of high-cycle fatigue limits of the strengthened joints, and provide a guaranteed extension of their residual fatigue life.

Under block loading, for all sequences of application of load after running for two loading blocks in the as-welded state (50 % damage) and subsequent strengthening the specimens were subjected to the increased stress levels with the respect to the initial ones (see Figure 3). The specimens were tested to their complete fracture or running for 10 loading blocks in the strengthened state (see the Table). It was experimentally proved that after strengthening by the HFMP technology the scatter of the residual fatigue life values was within 609–1046 % of that of the non-strengthened specimens. The residual fatigue life values obtained in testing the specimens under

block loading with the increasing sequence of application of load were within 830–1046 %, with the decreasing sequence — within 674–1046 %, and with the quasi-random sequence — within 609–1046 % of those of the non-strengthened welded joints under similar sequences of application of loads.

Therefore, it was experimentally proved that under multistage and block loading (see the Table) strengthening of the tee welded joints after accumulation of 50 % damage by the HFMP technology allows not only substantially increasing the levels of the applied stresses, but also extending their residual fatigue life from 3 to 10 times. Under block loading, the scatter of experimental values of cyclic fatigue life of the welded joints was within a narrower range (1,401,400–2,409,000 cycles) than under multistage loading (641,500–2,378,100), and did not depend on the sequence of application of load in a block.

1. Troshchenko, V.T., Sosnovsky, L.A. (1987) *Fatigue resistance of metals and alloys*: Refer. Book. Pt 1. Kiev: Naukova Dumka.
2. Knysh, V.V., Kuzmenko, A.Z., Vojtenko, O.V. (2006) Increasing fatigue resistance of welded joints by high-frequency mechanical peening. *The Paton Welding J.*, **1**, 30–33.
3. Garf, E.F., Litvinenko, A.E., Smirnov, A.Kh. (2001) Assessment of fatigue life of tubular connections subjected to ultrasonic peening treatment. *Ibid.*, **2**, 12–15.
4. Knysh, V.V., Solovej, S.A., Kuzmenko, A.Z. (2011) Influence of preliminary cyclic loading on effectiveness of welded joint strengthening by high-frequency peening. *Ibid.*, **10**, 36–39.
5. Knysh, V.V., Solovej, S.A., Kuzmenko, A.Z. (2008) Accumulation of fatigue damage in tee welded joints of 09G2S steel in the initial condition and after strengthening by high-frequency mechanical peening. *Ibid.*, **10**, 10–15.
6. Knysh, V.V., Kuzmenko, O.Z., Solovej, S.O. (2009) Accumulation of fatigue damage in tee welded joints in as-welded state and after strengthening by high-frequency mechanical peening under block loading. *Mashynoznavstvo*, **9**, 27–31.

EFFECT OF HEAT TREATMENT ON SENSITIVITY OF THE HAZ METAL ON TITANIUM-STABILISED AUSTENITIC STEEL TO LOCAL FRACTURE

Yu.V. POLETAEV
Volgodonsk Institute (Branch) of South Russian State Technical University
(Novocherkassk Polytechnic Institute), Volgodonsk, Russia

The mechanism of embrittlement of the HAZ metal of welded joints on steel 12Kh18N12T was revealed. This mechanism was found to be associated with development of the processes of direct and relative softening of grain boundaries in welding and at high-temperature low-frequency low-cycle loading. The efficiency of austenising to improve local fracture resistance of the welded joint HAZ metal was experimentally proved.

Keywords: *arc welding, welded joint, austenitic steel 12Kh18N12T, heat-affected zone, structural and chemical microheterogeneity, evaluation of weldability, optical and electron microscopy, heat treatment — austenising, low-frequency low-cycle loading, local fracture*

No common opinion exists now about the efficiency of austenising as a reliable technological method for prevention of local fracture. Studies [1–3] show that austenising does not always give positive results, while deviation from the set parameters of heat treatment may lead to decrease in load-carrying capacity of welded joints. Therefore, a priori application of the known recommendations without proper evaluation of their effect on structure and properties of the HAZ metal of a specific welded joint may cause deterioration of operational reliability.

The purpose of this study was to reveal the mechanism of embrittlement of the HAZ metal on austenitic steel 12Kh18N12T under the technological and service thermal-deformation effects, and propose the efficient technological method for improving local fracture resistance of the welded joints under low-frequency low-cycle loading. The study was performed on lengths of 12Kh18N12T steel steam pipes with a diameter of 230 mm and thickness of 30 mm cut out after being in operation for 70,000 h to perform overhaul of a run of the steam pipe of boiler 2 in the turbine section of Cherepetskaya power plant. As known from the operation experience, this material is sensitive to local fracture. Therefore, it is expedient to use it as a test one. This material complies with requirements of the regulatory documents in its chemical composition (wt.%: 0.13 C, 1.21 Mn, 0.55 Si, 18.7 Cr, 12.4 Ni, 0.51 Ti) and mechanical properties.

Welded joints were made by the technology accepted to perform erection work on steam pipelines [4]. An annular asymmetric single-bevel groove was made in the pipes. One half of the groove was welded up by using 4 mm diameter electrodes of the TsT-15 grade, and the other — by using electrodes of the TsT-26 grade. The welded joints on steel 12Kh18N12T were tested in the as-welded state and after austenising at T = 1373 K with holding for 1 h and cooling in air.

The as-welded joints featured high heterogeneity of mechanical properties, K_σ, between the weld metal ($\sigma_{0.2WM}$) and base metal ($\sigma_{0.2BM}$): $K_\sigma = \sigma_{0.2WM} / \sigma_{0.2BM}$. Dimensionless criterion K_σ characterises the degree of three-dimensionality of the stressed state. At temperature T = 873 K, all the as-

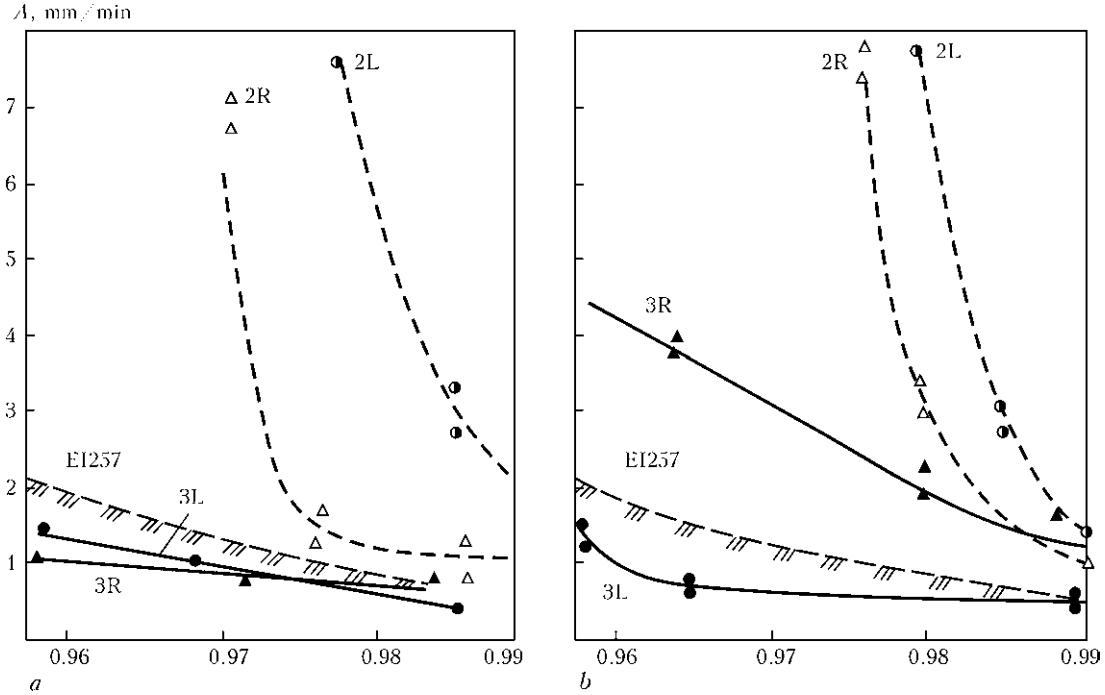

Figure 1. Resistance of steels 12Kh18N12T and EI257 to formation of hot sub-solidus cracks in HAZ metal in a state after operation (*a*), overheating and austenising at 1373 K(*b*): 2R, 2L, 3R, 3L — metal of the pipes adjoining the welds of joints 26L and 3A on their right and left sides (values of relative temperature θ are marked on the axis of abscissa)

welded joints had $K_\sigma > 0.9–1.0$. After austenising the heterogeneity markedly decreased, and the value of K_σ became close to the optimal one.

The sensitivity to formation of hot sub-solidus cracks in the HAZ metal under the simulated thermal-deformation welding cycle was evaluated by the procedure of TsNIITMASH by using $A–\theta$ dependencies [5].

The obtained $A–\theta$ dependencies for the steel, which are located in a region of compositions that are insensitive to hot cracking, are indicative of its satisfactory weldability (Figure 1). Hot processing (re-forging) and heat treatment also added to increase in hot ductility of the steel and its resistance to intergranular fracture during welding.

Steel 12Kh18N12T contains substantial concentrations of carbon and elements that exhibit a differing ability to form carbides in the condensed state [6].

Strong monocarbide TiC with a wide range of homogeneity, C/Ti = 0.53–0.95, forms in the Ti–C system. Complete fixation of carbide to form titanium carbides in steel 12Kh18N12T is provided at TiC > > 10 [7]. This ratio is approximately equal to four for the investigated heat of steel 12Kh18N12T. Therefore, the presence of non-fixed carbides creates conditions for formation of new particles of the $Cr_{23}C_6$ type strengthening phase in the steel. Owing to the presence of titanium acting as a stabilising element, a high density of fine carbides of the MeC type is provided in grains, and precipitates of carbides of the $Me_{23}C_6$ type are observed along the grain boundaries (Figure 2). As shown by calculations of electron diffraction patterns of these precipitates, carbides of the MeC type have the TiC or probably Ti(C, N) composition, and carbides of the $Me_{23}C_6$ type — the $Cr_{23}C_6$ composition. The closer the second-phase precipitates to the weld, the higher is their quantity along the grain boundaries and in the bulk of grains. Therefore, the most substantial changes take place in a region that directly adjoins the fusion line. These are partial dissolution of fine carbides, growth of grains, and precipitation of carbides of the dendritic shape at new boundaries, which increases with distance to the fusion line. In this case, of a decisive importance are heating above the carbide dissolution temperature and growth of grains accompanied by migration of boundaries. Presumably, while migrating, the boundaries seem to collect some free atoms of carbon and their clusters they run across, and to retain them in the form of segregations with a concentration sufficient to form carbides.

As diffusion of all impurities, including the substitutional ones, is accelerated at high temperatures of welding heating, it is probable that the boundaries collect and retain these elements as well. Formation of such segregations can be favoured by a sink of vacancies and dislocations to the grain boundaries, as well as by adsorption of horophilic elements by the mechanism of ascending diffusion [1].

Therefore, direct softening of the grain boundaries due to precipitation of the dendritic-shape $Me_{23}C_6$ type carbides on them, and their relative softening as a result of the process of titanium carbide precipitation hardening of the austenitic matrix of the HAZ metal on steel 12Kh18N12T after welding heating may be the main cause of an increased sensitivity to local (intergranular) fracture in high-temperature operation.

The sensitivity of the welded joints to formation and development of local fracture was evaluated under

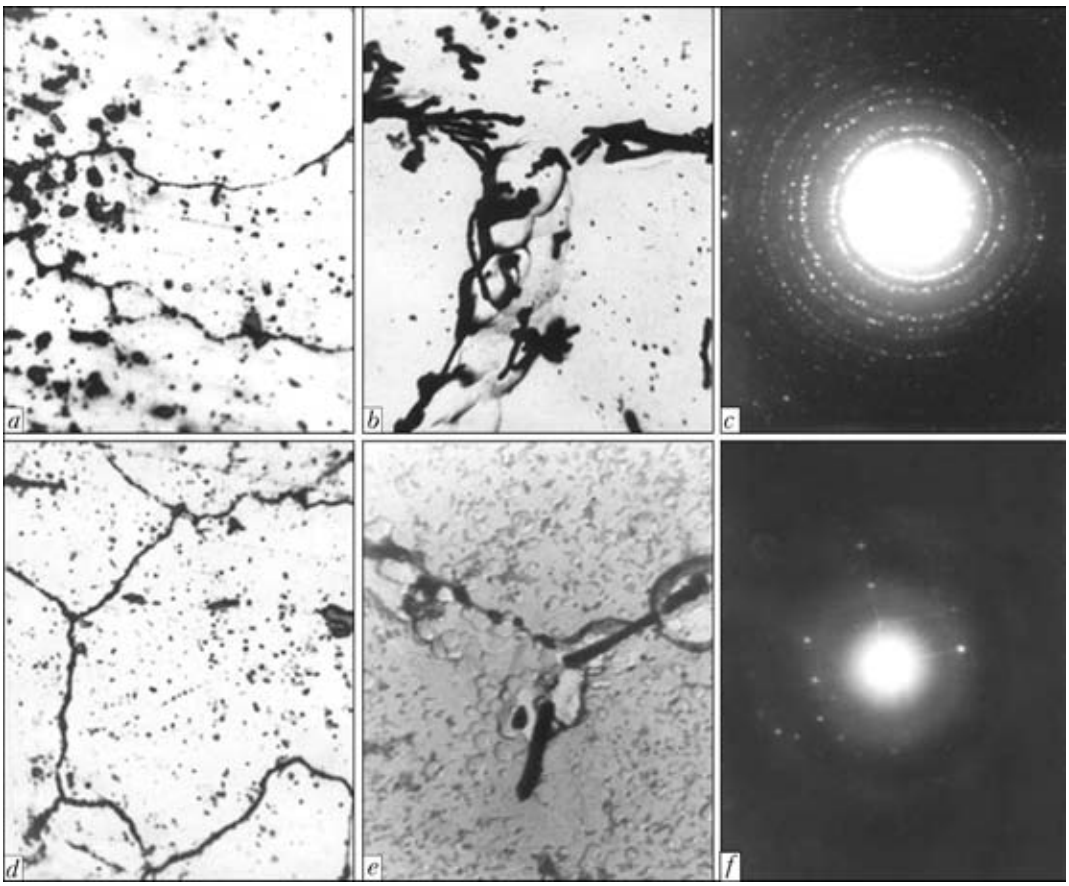

Figure 2. Microstructures of HAZ metal on steel 12Kh18N12T at different distances from the weld and at different magnifications (*a*, *d* — ×700; *b*, *e* — ×5000): *a*, *b* — fusion line; *d*, *e* — 0.1 mm from the fusion line; *c*, *f* — electron diffraction patterns of the carbide phase of TiC and $Cr_{23}C_6$ compositions, respectively

conditions of high-temperature low-frequency low-cycle loading according to the procedure described in [8]. Prismatic specimens with transverse welds, having one edge notch of a differing sharpness made along the fusion line, were tested. The specimens were tested under high-temperature low-cycle loading (trapezoidal cycle) by pure bending at a temperature of 823 K. The chosen time of a tension half-cycle was $\tau_1 = 24$ h, and that of a compression half-cycle was 10 min, which provided low frequency $v = 4.2 \cdot 10^{-2}$ cycle/h.

As might be expected, the shortest life to local fracture was characteristic of the HAZ metal of the as-welded joints (Figure 3). The use of electrodes of the TsT-26 grade, providing a more ductile weld metal and a lower heterogeneity of mechanical properties between the weld and HAZ, led to a small (about 20 %) extension of life of the non-notched specimens. Performing only austenising promoted a marked increase in resistance of the HAZ metal to initiation and propagation of local fracture (Figure 4).

Intensive strengthening and increase in effective stress σ_{eff} in each cycle occurred at strain amplitude $\varepsilon_a = 0.5$ %. In steel 12Kh18N12T, strengthening continued up to formation of a macrocrack in the notch bottom. Formation of the macrocrack about 1 mm long at N_f led to a drop of σ_{eff} in steel 12Kh18N12T. Austenising caused a considerable change in the kinetics of fracture of the welded joints. Three characteristic regions can be distinguished in fracture diagrams. Increase in σ_{eff} in a range of 4–10 cycles from the moment of crack formation ($N_f = 4$ cycles) is fixed in the first region. Here the crack propagates at a relatively low, constant initial speed. In the second

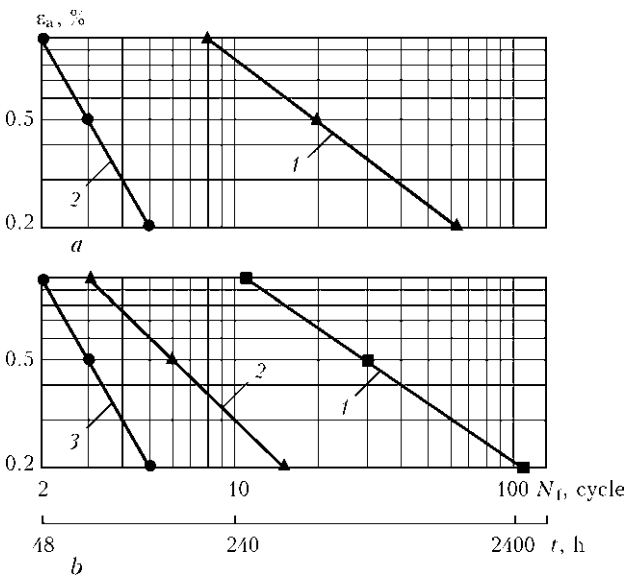

Figure 3. Effect of notch sharpness (theoretical stress concentration factor) on long-time low-cycle strength of welded joints on steel 12Kh18N12T in the as-welded state (*a*) and after austenising (*b*) at $T = 823$ K and $v = 4.2 \cdot 10^{-2}$ cycle/h: *1* — without notch; *2* — Mesnager type notch (3.0); *3* — Charpy type notch (5.3); t — total test time

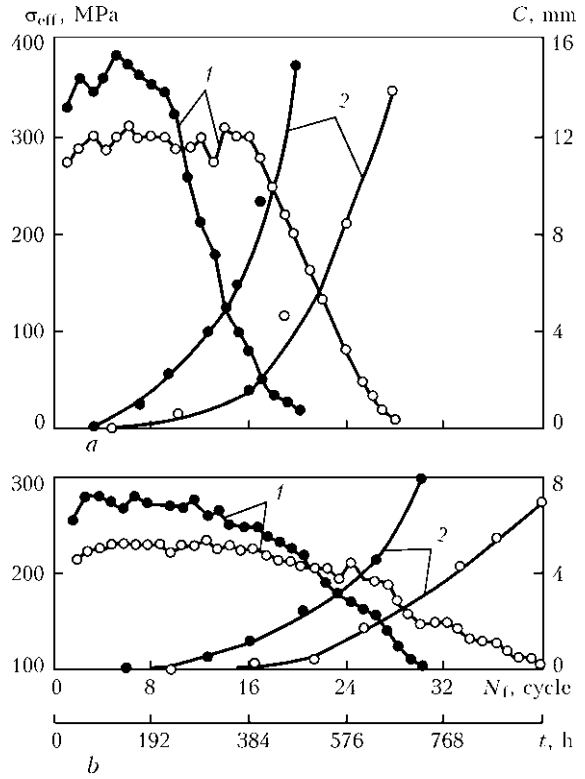

Figure 4. Fracture diagrams of welded joints on steel 12Kh18N12T at ε_a = 0.5 (*a*) and 0.2 (*b*) %: *1* — $\sigma_{eff} = f(N_f)$; *2* — $C = \varphi(N)$; dark circles — as-welded state; light circles — after austenising

region, periodic decrease and increase in σ_{eff} takes place. A stepwise crack growth leads to a drop in σ_{eff}, and its deceleration — to increase in σ_{eff} because of a work hardening taking place under repeated loading.

In welded joints on steel 12Kh18N12T in the as-welded state, the macrocrack forms at N_f = 3 cycles, while an intensive decrease in σ_{eff} related to a high crack growth rate in a specimen takes place after the fifth loading cycle. During 17 cycles from the moment of its initiation, the crack grew to a depth of about 1.5 mm. No loss of the load-carrying capacity of the specimen was fixed. Acceleration of the local fracture was observed in this region. In the third region, in a range of 16–28 cycles an intensive decrease in stresses σ_{eff} occurs in each cycle, this evidencing a loss of the load-carrying capacity of the specimen. This region corresponds to a propagation of crack at a higher acceleration. From the moment of its initiation, during 24 loading cycles the depth of the crack became equal to about 14 mm.

One should note a number of important points in the process of fracture of the welded joints at ε_a = = 0.5 %. For the as-welded joints on steel 12Kh18N12T the loss of the load-carrying capacity occurs at a crack depth of about 1 mm. It takes only two loading cycles to reach this point. After austenising, the loss of the load-carrying capacity of specimens takes place at a crack depth of about 2 mm, which in this case requires 12 cycles. Moreover, both in the as-welded state and after austenising the cracks grow almost at the same acceleration in the regions of intensive, constant decrease in σ_{eff}.

Therefore, austenising extends the stage of subcritical fracture, but exerts no positive effect in the overcritical range, i.e. in a region of the loss of the load-carrying capacity.

Initial damage of the HAZ metal after welding, as well as further changes in its structural-phase state in the low-frequency low-cycle loading process determine the kinetics of local fracture of the welded joints. Austenitic steels usually feature a structurally unstable state, and under the combined effect of high temperature and plastic deformation the dispersed phases may precipitate in them by the $\gamma \rightarrow \alpha$ plus carbide phase scheme. Precipitation of carbides leads to increase in strength and decrease in ductility, while their coagulation changes properties in the reverse direction. The strength of steel greatly depends on the shape, character and size of carbide particles. While strengthening the matrix, fine titanium carbides lead to localisation of strains and fracture in the near-boundary regions of grains. Individual coarse carbides of the $Me_{23}C_6$ type, which precipitate mainly along the grain boundaries, may retard the propagation of cracks during the plastic deformation process [1, 9]. The intensity of carbide formation depends on the level of stresses σ_{eff}, time of loading, temperature and other factors of low-cycle loading, and affects the kinetics of local fracture.

Strengthening, i.e. increase in σ_{eff} in cycles, is fixed at the first stage of low-cycle loading. Growth of the

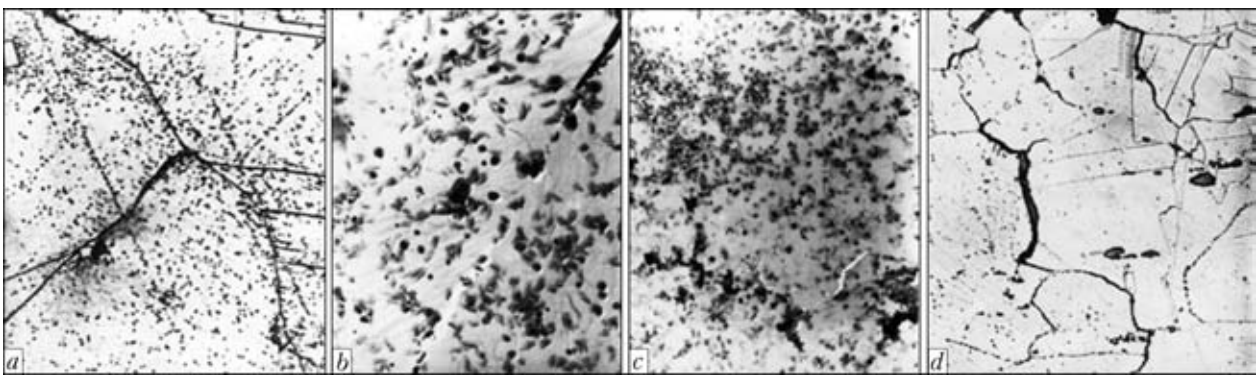

Figure 5. Microstructures of HAZ metal after the low-frequency low-cycle loading tests (ε_a = 0.5 %, τ_l = 24 h and T = 823 K): *a* — formation of discontinuity at a junction of three grains (×1000); *b*, *c* — precipitation of carbide phase in structure of TiC (×5000); *d* — network of wedge-shaped cracks (×300)

deformation resistance is related primarily to precipitation of fine carbides that effectively block the dislocations at which they initiate. The titanium carbides form fine precipitates mostly at extended dislocations, i.e. at thin disks of stacking faults [9, 10]. These precipitates are very stable and, together with the defects forming as a result of intersection of dislocations, form the rows of walls impassable for the dislocations, which can be regarded as a superimposed network of boundaries that hamper sliding [11]. This character of precipitation of the carbide phase led to a substantial strengthening of the matrix. This added to decrease in quantity of the mobile dislocations capable of causing plastic deformation and thus decreasing local stresses σ_l. As a result, the rate of relaxation of σ_l (creep) was markedly decreased, and the intergranular slip process developed, thus providing localisation of deformation at the embrittled grain boundaries. It is this fact that explains why no traces of rough internal sliding were fixed in steel 12Kh18N12T, and the deformation occurred by the mechanism of fine sliding, the traces of which can be detected by electron microscopy (Figure 5).

The key factor that determines conditions of propagation of wedge-shaped intergranular cracks is relaxation microplasticity in the bulk of grains near the ternary junctions. Further development of the carbide formation processes in the bulk of grains and along their boundaries leads to formation of intergranular wedge-shaped cracks.

Investigation of phase composition of the HAZ metal of the welded joints on steel 12Kh18N12T after the tests showed that the steel contained carbides TiC and $Cr_{23}C_6$. The effect of temperature and elasto-plastic deformation with long-time holding led to the process of dissolution, precipitation and coagulation of the carbide particles, the kinetics of which determined the stability of structure and properties of the steel.

The total content of carbide precipitates increased several times with growth of ε_a and quantity of the loading cycles. Thus, the HAZ metal in the state after austenising contained approximately 0.10–0.15 wt.% of the carbide phase; after the tests at ε_a = 0.2 %, τ_1 = = 24 h and T = 823 K (N = 120 cycles) the weight of the carbide precipitates was 1.10–1.25 % of that of the dissolved steel; and after the tests at ε_a = 0.5 %, τ_1 = 24 h and T = 823 K (N = 30 cycles) the weight the carbide precipitates was 2.9–3.3 % of that of the dissolved steel.

Therefore, the favourable influence of austenising related to decrease in the initial structural and chemical heterogeneity of HAZ, which formed during welding, provides the effect of temporary increase in resistance of the welded joints on steel 12Kh18N12T to local fracture.

CONCLUSIONS

1. While promoting the intensive development of the processes of direct (due to precipitation of chromium carbides of the dendritic type) and relative softening of the grain boundaries (due to precipitation hardening of the matrix by TiC carbides), the thermal-deformation welding cycle was found to cause a high initial damage of structure and sensitivity to formation and development of local fracture of the HAZ metal on steel 12Kh18N12T.

2. Austenising is an efficient technological method for improving the local fracture resistance under low-frequency low-cycle loading, as it provides decrease in the initial structural and chemical heterogeneity.

3. Cyclic plastic deformation was proved to intensify the processes of direct and relative softening of the grain boundaries and stimulate decrease in resistance of the HAZ metal to development of local fracture of the welded joints on steel 12Kh18N12T under high-temperature (823 K) low-frequency low-cycle loading. It is because of this fact that austenising provides the effect of temporary increase in local fracture resistance of the welded joints on steel 12Kh18N12T, this being in agreement with data of practical observations.

1. Zemzin, V.N., Shron, R.Z. (1978) *Heat treatment and properties of welded joints*. Leningrad: Mashinostroenie.
2. Zemzin, V.N., Zhitnikov, N.P. (1972) Conditions of cracking in near-weld zone of joints during heat treatment. *Avtomatich. Svarka*, **2**, 1–5.
3. Yarkovoj, V.S., Muromtsev, B.I., Komissarov, V.G. (1969) Long-term strength of parent metal and welded joints of steels 08Kh18N9 and 07Kh16N9M2. *Ibid*., **6**, 38–40.
4. Khromchenko, F.A. (1982) *Reliability of welded joints on boiler pipes and steam pipelines*. Moscow: Energoizdat.
5. Tarnovsky, A.I., Poletaev, Yu.V., Feklistov, S.I. (1983) Applications of A–θ dependencies for evaluation of susceptibility of austenitic class steels and alloys to formation of hot near-weld cracks in welding. In: *Novel in welding technology of nuclear power plant equipment*: Trudy TsNIITMash, **179**, 82–84.
6. Kulikov, I.S. (1988) *Thermodynamics of carbides and nitrides*: Refer. Book. Chelyabinsk: Metallurgiya.
7. Livshits, L.S. (1979) *Metals science for welders (welding of steels)*. Moscow: Mashinostroenie.
8. Poletaev, Yu.V. (2010) *Long-term low-cycle strength of welded joints and choice of austenite-stable steels*. Novocherkassk: LIK.
9. Lozinsky, M.G., Romanov, A.N., Malov, V.V. (1977) Study of austenitic steel structure at different forms of elastic-plastic high-temperature deformation cycles. In: *Structural factors of low-cycle fracture of metals*. Moscow: Nauka.
10. Lyuttsau, V.G. (1977) Current concepts of a structural mechanism of deformation ageing and its role in fracture propagation at low-cycle fatigue. *Ibid*., 5–21.
11. Mints, I.I., Berezina, T.G. (1972) Stability of dislocation structure of cold-worked steels Kh18N12T and Kh16N9M2 in conditions of high-temperature ageing. *Fizika Metallov i Metallovedenie*, 34(**3**), 615–620.

AUTOMATED SYSTEM FOR DIAGNOSTICS AND REPAIR OF REACTOR CONTAINMENT SHELL AT BILIBINSKAYA NPP

R. ROSERT[1], **A.V. SHUTIKOV**[2], **M.E. FEDOSOVSKY**[2], **E.I. LUKIN**[2] and **M.V. KARASEV**[2]
[1]Altleiningen, Germany
[2]CJSC «Engineering and Technological Service», St.-Petersburg, Russia

There exists a multitude of cases of breakdown of parts, components or complete systems because of untimely detection of their failure. Shown is the possibility of complex repair solutions in safety-critical cases, including difficult-of-access zones of industrial plants in Russia. These are complex automated and partially remotely controlled systems made in Russia and applied in the field of gas and power engineering.

Keywords: *reconditioning by welding and surfacing, gas industry and power engineering, object diagnostics, versatile robotic complexes*

There exists a multitude of cases of failure of parts, components and whole systems, because of untimely detection or difficult access to damage sources. A system, allowing performance of diagnostics of the possible weak locations and ensuring replacement or repair of the defective component, can help recondition the object. Tubular structures or vessels are often regarded as difficult-of-access objects. Access can be difficult or impossible at hazardous radiation doses, high temperatures or presence of toxic gases. Over the recent years automated and robotic diagnostic systems have been developed for such purposes. These systems are serviced by an operator using the respective remote control, and eliminate the risk for his health.

Diagnostic systems for gas and power engineering. In these industries application of complex engineering robotic systems is promising. These systems are characterized by the following capabilities: displacement over any surface, also in a forced position and in cramped space; use of any measurement systems for diagnostics; mounting the tools for repair performance, in particular, for cleaning and welding; performance of erection operations; work performance under the conditions of increased temperature and radiation.

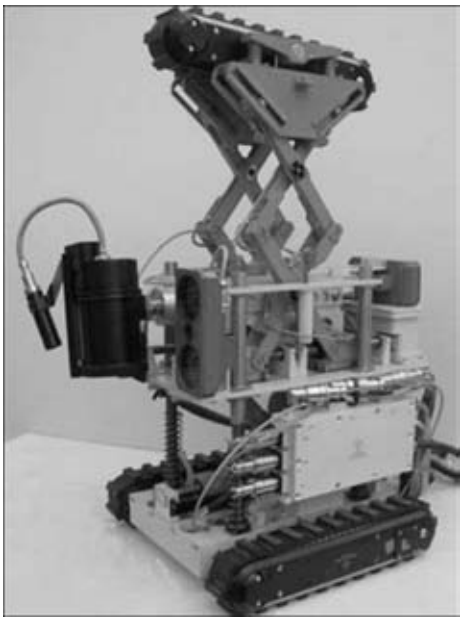

Figure 1. Diagnostic robot with electromagneto-acoustic sensor

These new remotely-controlled systems are ever wider applied for diagnostics and repair in difficult-of-access and critical in terms of safety locations. Various systems are developed for different cases. Complex remotely-controlled systems are already in place for diagnostics of the technical condition of internal surfaces of pumping and compressor stations. As a rule, such stations have straight pipes and pipes bent in many planes.

Figure 1 shows a robot capable of flexibly moving inside a pipe network, both in the horizontal and vertical direction. Using caterpillar belts mounted at an angle of 120° to each other and capable of moving relative to each other, this robot allows controlling piping with the nominal inner diameter from 700 up to 1400 mm. Maximum displacement zone is 500 m.

Owing to various explosion-safe measurement systems mounted on the robot, it is possible to obtain information about the state of the pipe inner surface, position and kind of welds based on visual inspection; possible undercuts, internal defects, as well as cracks and contamination — as a result of ultrasonic testing; surface corrosion and measurement of wall thickness or erosion depth; data on technical condition of piping, in order to determine the need for repair or replacement of pipe sections.

This system was used in 2004–2010 to examine 130 km of tube and tube plates. As a result, more than 500 various hazardous defective locations were detected and repaired. Each of them could lead to gas explosion. List of work performed in the period from

List of work performed in the period from 2008 to 2010 using the explosion-safe measurement system

Work list	2008	2009	2010
Number of inspected compressor stations;	16	9	21
Length of examined pipes, m	2411	1098	1593
Inspection scope:			
visual and measurement of welds, pcs	2411	1098	1593
ultrasonic testing of all pipes, m	23893	21516	25488
Found defects, pcs:			
in weld	205	89	249
in pipe body	671	656	1466
Repair of pipe body urgently required	273	72	75

2008 to 2010 using explosion-safe system is shown in the Table.

In St.-Petersburg training in operation of this system was organized in a test stand with built-in pipes with various defects, where features of system operation under the actual conditions can be followed (Figure 2).

Figure 3 gives pipe defects often found in practice. Improvement of automatic diagnostic system is envisaged, so as to achieve the efficiency of minimum 80 run. m/h on a length of up to 1000 km, obtaining an image in 3D format.

Application of such a diagnostic system allows considerable saving of costs, compared to the method, when the damaged pipe sections are uncovered with all the respective work stages. Experience accumulated at development of a complex remotely-controlled diagnostic system for gas industry and power generation, can be used at development of automated systems for NPP diagnostics and restoration.

Development of the technology of diagnostics and repair of NPP equipment using welding. During the scheduled inspection of reactor 1 at Bilibinskaya NPP, Russia (Figure 4) defects were found in the so-called biological shield, enclosed into external and internal steel shell.

Figure 2. Test stand with artificial and natural defects

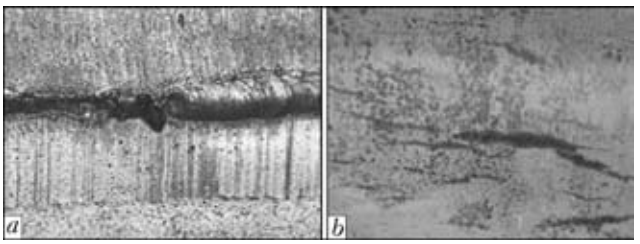

Figure 3. Kinds of defects: *a* — joining defects in the weld root (pipe D = 1000 mm, s = 16 mm); *b* — crack-like defect of 1.5–4.0 mm length (pipe D = 10000 mm, s = 14 mm)

As we are talking about space critical in terms of safety, difficult-of-access and presenting the radiation hazard, a robotic technology was developed, allowing performance of repair work on the steel shell from the inner side of biological shield. Power of Bilibinskaya NPP is 48 MW. This is the smallest NPP in the world working in permafrost zone. It has four boiling-water graphite channel reactors [1]. Shutdown of Bilibino-1 reactor, put into operation in 1974, is scheduled for 2019. Inner shell of biological shield is made from unalloyed steel S 255 (St.3) 20 mm thick. The defined objective was to examine the inner wall of the shielding vessel for defects, classify and eliminate them. Process of flux-cored wire gas-shielded welding was selected at performance of repair first of all because this process lends itself easily to automation. Repaired locations were to guarantee leak-tightness. In connection with the need to weld up defective locations in forced positions in space, seamless rutile flux-cored wire with rapidly-solidifying slag was used.

All the applied systems, instruments and filler materials needed clearance by the respective bodies of nuclear power engineering of the Russian Federation. Comprehensive preparation was performed before the start of repair. Repair included surface diagnostics for possible defects; determination of the kind of defects; preparation of defective locations for subsequent building up by cladding; and performance of cladding.

Full-scale test stands were manufactured for trial experiments, allowing retrofitting of individual work stages and determining all the needed control parameters (Figure 5).

Figure 4. Appearance of reactor 1 of Bilibinskaya NPP [2]

Figure 5. Test stand from steel S 223 of 20 mm thickness

To measure the thickness of steel wall metal layer, damaged by corrosion, an electro-magnetoacoustic sensor was used which functions without the couplant. Special well-illuminated chambers were used for visual inspection.

For the working zone a specialized remotely-controlled robot was designed (Figure 6), which carries the measuring and work tools. Robot, consisting of approximately 1000 individual parts, can move vertically or horizontally, recognize and overcome various obstacles, for instance, reinforcement in the wall.

Figure 6. Appearance of robot with electromagneto-acoustic sensor (*a*), tool for abrasive cleaning (*b*) and welding torch (*c*)

The task of ensuring the wire feed turned out to be the most difficult one. First, the flux-cored wire had to be transported for an up to 20 m distance, and, secondly, stable arcing had to be guaranteed. All together 400 samples were welded and tested at the Departamental Institute of Nuclear Industry.

As a result, the following optimal parameters of welding mode were proposed: wire feed rate of 2.7–3.5 m/min; welding current of 110–130 A; welding voltage of 21 V; welding speed of 4 cm/min; oscillation amplitude of 50 mm for upward fillet weld, and 20 mm in the downhand position; shielding gas being M1 (Ag + 25 % CO_2); weld reinforcement of 2–4 mm; deposition rate of 1.5–2.0 kg/h.

In connection with welding cable (diameter of 16 mm), specific for conducting the welding process, the arc could only run for 1.5–2.0 min, after which cooling was required. Figure 7 schematically shows the working situation at repair of steel wall by cladding.

After preparatory operations, concerning mainly, the sequence of repair performance, the system was applied for the first time at Bilibino. First the internal steel wall was examined. Analysis of the found defects showed certain deviations from values specified by the customer when defining the repair task. It was found that layers of up to 5 mm thickness came off as a result of corrosion, instead of maximum 2 mm. Distance from biological shield to reactor case is just 408 instead of 420 mm. Height of steps between individual sections of steel plates on the inner wall was 10 instead of 18 mm. In addition, tubes for thermocouples, not indicated in the documentation, were found in the robot lock zone. All the mentioned differences required mandatory adaptation of the used equipment. For this reason the robot, shown in Figure 6, *b* with a tool for abrasive cleaning, was additionally created. Speed of

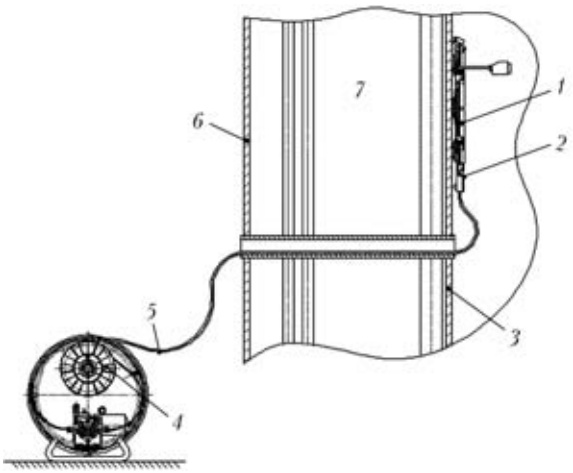

Figure 7. Diagram of welding on the inner wall of biological shield: *1* — repair robot; *2* — device for uniform wire feed; *3*, *6* — inner and outer steel wall, respectively; *4* — wire feed mechanism; *5* — wire feed channel; *7* — biological shield from concrete

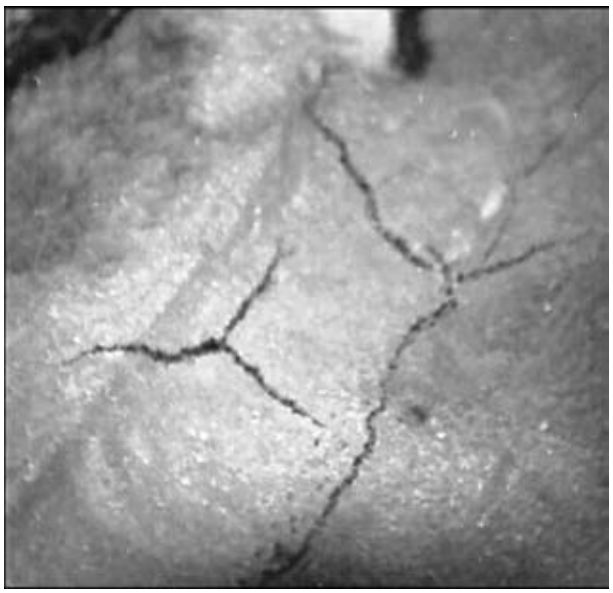

Figure 8. Appearance of defect 11 — crack network in the connecting weld between two sections (×2)

Figure 9. Defects eliminated by cladding on inner steel shell (marked section of the surface, where the network of cracks was rewelded, is shown in Figure 8)

surface cleaning by this system increased greatly. In addition, it was now possible to clean the surface after welding, from slag and remains of wire, stuck to it at ignition, thus increasing the air-tightness of the deposited sections. At the first cleaning of the surface of biological shield inner wall (2.5 m^2) the system found 21 defect. As at any technology application the diagnostic system without abrasive cleaning failed to detect ten surface defects, the advantage of an improved cleaning system is obvious. Cracks found in the weld between two sections of the inner steel wall (Figure 8) can be eliminated by cladding. As the defect was not completely eliminated after deposition of the first cladding layer, the process had to be repeated. Here, a new concept of abrasive cleaning of the surface was used.

Surfaces of the damaged area after welding, shown in Figure 9, were repaired by cladding.

In October 2010 the department of ROSATOM Concern, responsible for operation of the system at Bilibino, performed acceptance of repair work and commissioned the reactor.

CONCLUSIONS

1. A versatile robotic small-sized unit was developed, which can move in a forced position in a closed space at exposure to radioactive radiation. This system can be applied for diagnostics, wall thickness measurement, visual inspection, welding or surfacing, in order to ensure tight joints, performing work on cleaning the surface from slag, corrosion damage or paint.

2. The developed system is used to perform cleaning of the surface of inner steel wall of biological shield of 2.5 m^2 area. Here 10 or more cracks were found, which were repairable.

3. Technology of repairing cracks and sealing the defective locations by single- or multilayer cladding was developed.

4. Experience acquired at repair will be the basis for performance of further work on ensuring the safety of Bilibinskaya NPP, as well as other NPP of ROSATOM Concern.

1. *http*://atomas.ru/rosatom/safety-gp.html
2. *http*://atomas.ru/rosatom/bilibino.html

EVALUATION OF QUALITY OF TECHNOLOGICAL PROCESSES OF SURFACING OF PARTS OF RAILWAY ROLLING STOCK

V.V. ARTEMCHUK
V. Lazaryan Dnepropetrovsk National University of Railway Transport, Dnepropetrovsk, Ukraine

The factors influencing the quality of technological process of surfacing are considered. The results of analysis of the causes leading to appearance of defects and deviations from the required mechanical properties are presented. It is shown that one of the most important factors influencing the reliability of technological process of surfacing is its electrical mode, parameters of which depend not only on those established by surfacing operator, but also on the quality of supplied power. Influence of mode parameters on reliability of the process of multilayer surfacing is considered.

Keywords: *arc surfacing, parts of rail transport, quality of surfacing, reliability of technological process of surfacing, restoration*

The improvement in quality of technological processes of manufacture of different parts is actual and important problem for all spheres of industry. The deviations from the preset parameters of technological process beyond the admissible limits result in rejection of a part. This problem is especially urgent in repair production where it is not always possible to provide high quality of restored parts due to its complicated specifics.

The repair production includes a number of technologies, one of which is direct process of parts restoration. Nowadays surfacing technology is one of the most challenging technologies in restoration.

A great deal of works was devoted to investigation of surfacing processes, many of which concern the analysis of reasons for defects occurrence and give recommendations for their elimination [1–7]. However, in our opinion, no sufficient attention is paid to evaluation of influence of different components of technological process of surfacing on quality of part being surfaced as a whole.

The purpose of this work is evaluation of influence of separate stages of technological process of surfacing on quality of railway rolling stock parts being surfaced.

The optimal technological process of surfacing should provide the preset properties and quality of deposited layers, the defects in them should not exceed the limits restricted by regulation documents. The main factors influencing these characteristics of surfacing process (Figure 1) are quality of preliminary preparation of surfacing materials and surfaces of parts to be deposited; chemical composition of base and deposited metals; their weldability, physical-chemical properties and structure and also their changes during surfacing; surfacing modes; preliminary heating and heat treatment after surfacing; finishing treatment of as-surfaced parts.

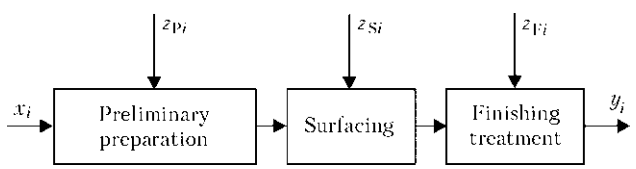

Figure 1. Structural scheme of surfacing process (x_i, y_i — input and output factors, respectively; z_{Pi}, z_{Si}, z_{Fi} — factors of preliminary preparation, surfacing and finishing treatment)

Let us consider the characteristics defining quality of surfaced parts more in detail. Hardness, wear resistance and fatigue strength are of special interest. The mentioned characteristics are selected, basing on the following considerations: mainly wear resistance and fatigue strength define service life of parts, and hardness is related to other mechanical properties and is very easily defined under industrial conditions. During optimal selection of surfacing materials these characteristics should meet the requirements of technical documentation. Otherwise they immediately pass to the category of inadmissible ones.

In accordance with GOST 30242–97 the defects of welding are divided into the following groups: cracks, pores (cavities), lacks of fusion and lacks of penetration, hard inclusions, violations of weld shape, etc.

It is a complicated task to obtain the perfect deposited layer without defects, however, it is necessary to minimize a number and sizes of defects, and also distinguish the admissible defects. As practice shows, in many cases defects arise due to deviations from the preset conditions of surfacing process. To determine the quality of surfacing process, let us systemize the reasons causing above-mentioned defects. According to [1–6] the main reasons, leading to defects in surfacing, are low-quality preparation of materials and surface of the part to be restored; incorrectly matched combinations of materials; violation of surfacing technology; improperly selected surfacing conditions.

The mentioned reasons of defects arising are mainly connected with skills and experience of designers, technologists and surfacing operators.

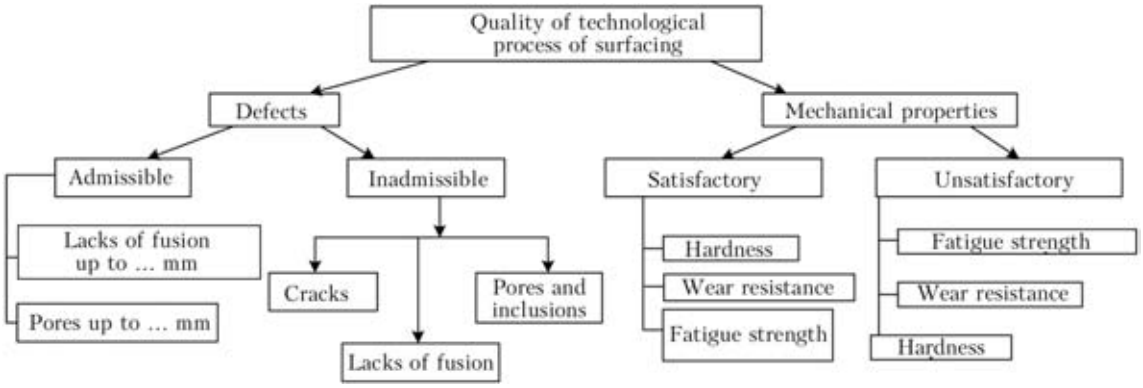

Figure 2. Structural scheme of evaluation of quality and reliability of technological process of surfacing

The electric conditions of surfacing have determinant influence on structure and properties of deposited layer and also defects occurrence. In the structural scheme, presented in Figure 2, no sizes of defects are mentioned in their admissible block, as far as they depend on conditions of service of the definite part and are specified in corresponding technical documentation. The basic reasons in the generalized form, leading to inadmissible defects, are formulated as follows: «unsatisfactory preparation of part surface», including characteristics of quality of cleaning and mechanical treatment during preparation of part surface for surfacing; «unsatisfactory preliminary heating before surfacing», i.e. insufficient or lack of heating of a part when such operation is required; «deviation from rational conditions of part surfacing», i.e. violation of conditions as to voltage, current and surfacing speed, reliability of supply of flux or shielding gases, keeping of surfacing run, electrode stickout, and also its shifting from zenith (the latter is observed in automatic surfacing of cylindrical parts).

In compliance with presented structural scheme of evaluation of quality of technological process of surfacing (Figure 2) and selected system of corresponding characteristics, the acquisition of data on quality of parts, deposited at the electric locomotive repair plant, locomotive depots with the volume of regular repair RR3 and car shops during one year was carried out. The parts of automatic coupler equipment, pivot unit of cargo cars, hinged units, cylindrical parts of the type «shaft» of braking linkage, leaf-spring suspension, etc. were subjected to analysis. In the volume of these observations the database for the further statistic analysis was created.

Mathematically, let us describe the object under investigation by the set of characteristics $\Omega = \{x_1, x_2, \ldots, x_N\}$, representing their information as a matrix of experimental values X:

$$X = \begin{bmatrix} x_{11} & x_{12} & \ldots & x_{1N} \\ x_{21} & x_{22} & \ldots & x_{2N} \\ \ldots & \ldots & \ldots & \ldots \\ x_{M1} & x_{M2} & \ldots & x_{MN} \end{bmatrix},$$

where M is the number of lines corresponding to number of observations for the definite period of time; N is the number of columns corresponding to the number of characteristics; x_{ij} is the value of j-characteristic in the i-th observation (further we assume that $M > N$).

Let us study the basic moments of initial data analysis as far as this stage of modeling considerably influences further accuracy of quality evaluation of technological process.

In the processing of experimental data the certain difficulties were encountered, predetermined by different dimensions of selected characteristics, absence of some data, presence of suspicious values of characteristics being observed. The significant stage of analysis is verification of data for presence of «splashes» with their further processing. The censoring of data (elimination of splashes effect) is performed using either removal of these points from data, or application of methods of evaluation of parameters, sustainable to rough deviations (for example, method of the least modules).

Distribution of causes of occurrence of defects and deviations in mechanical properties in semi-automatic surfacing with flux-cored wire in CO_2

Causes of occurrence of defects and deviations in mechanical properties	Share, %	Variation factor, %
1. Unsatisfactory preparation of surfacing material and part to be surfaced	32	23
2. Unsatisfactory preheating or its absence	6	8
3. Deviation from conditions of cooling or heat treatment after surfacing	5	15
4. Deviation from rational conditions of surfacing	31	19
5. Non-quality cleaning from slag in multilayer surfacing	8	10
6. Deviation from rational conditions of finishing treatment of as-surfaced part	18	18

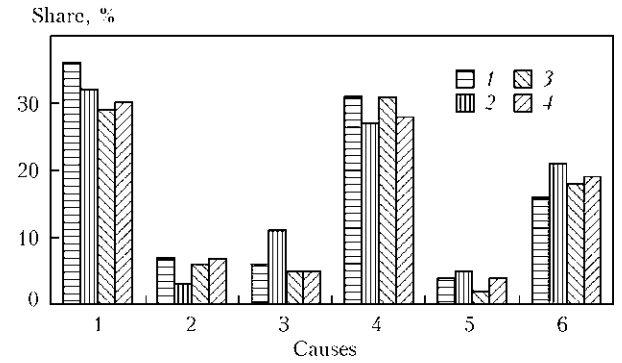

Figure 3. Distribution of causes (1–6 acc. to the Table) of occurrence of defects and deviations in mechanical properties depending on method of surfacing: *1* — semi-automatic surfacing in CO_2; *2* — automatic submerged arc surfacing; *3* — semi-automatic surfacing with flux-cored wires; *4* — manual arc surfacing

In capacity of censoring procedures, the following ones are used [8]:

• visualization of data, when regularities completely non obvious among many values, are established using graphic representation of information;

• analysis of some numerical characteristics of values being investigated. For example, presence of splashes can be evidenced from comparison of such values as a mean value and mode, if these characteristics are significantly different for the selected indication (as far as it is known that the mean selected value is sensitive to splashes, and modal value of the investigated indication is characterized by the property of robustness);

• rule of «3σ», if the hypotheses about normal distribution of values x_i are confirmed, is

$$P\{\varepsilon_i < 3\sigma_i\} = 0.9973,$$

where $\varepsilon_i = x_i - \bar{x}_i$; $\bar{x}_i$ is the mean selected x_i.

It is obvious that the simplest method of data censoring is visualization, however at large amount of data, like in our case, it is impossible to apply it. The procedure of censoring with application of normal law is also low-efficient, as it requires unjustified time losses, moreover, the considered characteristics can have another law of distribution. Therefore, among mentioned procedures of splashes elimination the most acceptable was that, connected with analysis of numerical data and comparison of the mean selected value with the mode for each characteristic of quality.

After fulfillment of the above-mentioned procedures we obtain distribution of causes of arising defects and deviations of mechanical properties from the expected ones. The Table gives distribution of causes of defects occurrence in semi-automatic surfacing using flux-cored wire in CO_2, and Figure 3 shows the same during main methods of arc surfacing.

As was expected, the statistic analysis confirmed that the most stable and high quality of restored parts is provided by automatic submerged arc surfacing. The worst characteristics on probability of arising defects of different type refer to manual arc surfacing with rod electrodes. The intermediate position is occupied by semi-automatic surfacing in shielding gases and open-arc surfacing with self-shielding flux-cored wires.

For all methods of surfacing the most significant characteristics influencing its quality are preliminary preparation of parts to be surfaced and surfacing materials, and also conditions of surfacing.

Influence of these factors is almost equal. Very significant is also influence of machining of surfaced parts on quality. It can be possibly connected with the fact that mechanical treatment of deposited surfaces is performed often in depot using manual grinding tool.

For all methods of arc surfacing, used in railway repair manufacturing, the mentioned causes of defects occurrence are dominating, though they have some different fractions of effect. Thus, to increase the quality and reliability of the surfacing process, they themselves should be subjected to the primary study and elimination.

CONCLUSIONS

1. The statistic analysis shows that automatic surfacing guarantees the higher quality characteristics of repaired parts then semi-automatic shielded-gas surfacing and open-arc surfacing with self-shielding wires, whereas lower characteristics are provided by manual surfacing with rod electrodes.

2. The ranging of causes, leading to the occurrence of defects and deterioration of quality of surfaced part, shows that the effect of non-quality preparation of parts to surfacing and surfacing materials, as well as deviations from surfacing conditions have the most essential effect on these characteristics.

1. Frumin, I.I. (1961) *Automatic electric arc surfacing*. Kharkov: Metallurgizdat.
2. Ryabtsev, I.A. (2004) *Surfacing of machine and mechanism parts*. Kiev: Ekotekhnologiya.
3. (2006) *Machine building. Technology of welding, brazing and cutting*. Vol. 3. Ed. by B.E. Paton. Moscow: Mashinostroenie.
4. (1974) *Technology of electric fusion welding of metals and alloys*. Ed. by B.E. Paton. Moscow: Mashinostroenie.
5. Deev, G.F., Patskevich, I.R. (1984) *Defects of welds*. Kiev: Naukova Dumka.
6. Vlasov, V.M., Nechaev, L.M., Fomicheva, N.B. et al. (2004) Effect of defects formed during surfacing process on mechanical characteristics of metal. *Sovrem. Naukoyomkie Tekhnologii*, **1**, 9–11.
7. Molodyk, N.V., Zenkin, A.S. (1989) *Repair of machine parts*: Refer. Book. Moscow: Mashinostroenie.
8. Kramer, G. (1975) *Mathematical methods of statistics*. Moscow: Mir.

THREE-PHASE INVERTER POWER SOURCE WITH DIRECT CONVERSION AND INCREASED POWER FACTOR

V.V. BURLAKA and **S.V. GULAKOV**
Priazovsky State Technical University, Mariupol, Ukraine

Topology of a converter with high-frequency transformer decoupling and three-phase input without intermediate rectification of input voltage is proposed. Application of direct conversion principle allows reducing the number of elements in the inverter power circuit, thus increasing its efficiency. In addition, application of a special algorithm of switch control allows achievement of input power factor close to a unity.

Keywords: *arc welding, inverter power source, power factor, modelling, direct conversion*

Modern tendencies of development of welding power sources determine increased requirements to such characteristics as conversion efficiency, power per a unit of volume, power factor (PF), quality and dynamics of stabilization of output parameters (current or voltage). Power sources with high-frequency conversion meet such a set of requirements to the greatest degree.

The majority of modern inverter power sources are made by double conversion schematic [1]: mains voltage is rectified by noncontrolled, controlled or active rectifier, smoothed, and then applied to DC-DC converter, made by the single-step [2], half-bridge or bridge circuit.

The disadvantages of such sources include the nonsinusoidal nature of input current (sources with PF active corrector are an exception, where 2–3 % lower efficiency is the price to pay for the low harmonic factor of input currents), presence of high-voltage high-capacity electrolytic capacitor in DC circuit, that creates problems of its initial charge at the source switching on and increases the overall dimensions and weight of the source.

In study [3] a variant of single-phase welding source is proposed, in which the function of input voltage rectification is eliminated (four-transistor AC voltage chopper and low-frequency (50 Hz) transformer with low scattering are applied). The source shows good results on efficiency and PF, but application of low-frequency transformer leads to deterioration of weight and dimensional characteristics of the devices using such a regulation principle. In addition, if it is necessary to perform DC welding, energy storage has to be used in single-phase sources in any case. It ensures arcing at the moments of mains voltage going through zero. This can be filter capacitor or output choke. Work [3] also outlines the long-term goal of development of three-phase sources with isolating high-frequency transformer and direct conversion.

This work suggests circuit implementation of a device, using current achievements in the field of circuit engineering of matrix direct frequency converters [4] with high-frequency transformer decoupling.

The source (Figure 1) consists of input *LC*-filter (*L1–L3*, *C1–C3*), six bilateral controlled switches *S1–S6*, high-frequency isolating transformer *T1*, output bridge rectifier *VD1*, *VD2* and smoothing choke *L4* [5]. The circuit is a matrix converter with three-phase input and two-phase output.

At converter operation primary winding of transformer *T1* is alternatively connected with a high frequency to mains phases, with just one switch from *S1–S3* group and one from *S4–S6* group being open at each moment of time to prevent interphase short-circuit. Capacitors *C1–C3* smooth pulsed voltage surges at the moments of switch switching. Sequence of switching and off-duty ratio are selected so that during the switching period average voltage in *T1* primary winding was equal to zero:

$$\int_0^{T_{sw}} u_{T1} dt = 0, \qquad (1)$$

where u_{T1} is the voltage on *T1* primary winding; T_{sw} is the switching period.

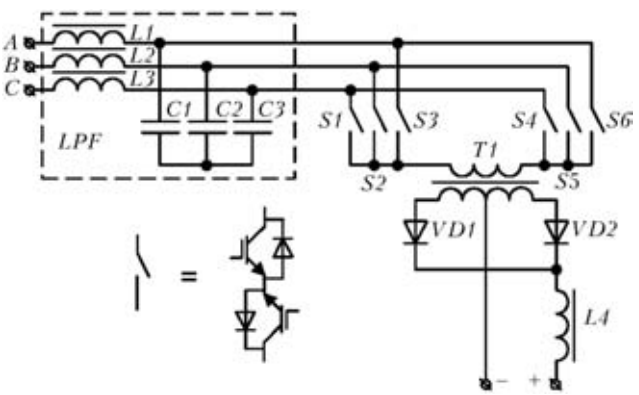

Figure 1. Schematic of source power circuit (for designations see the text)

This condition is necessary to prevent biasing and saturation of *T1* magnet core. Here, the voltage at bridge rectifier output is equal to $|u_{T1}/K_{T1}|$, where K_{T1} is the *T1* transformation ratio. We will determine average (over switching period) output voltage allowing for output filter *L4*:

$$U = \frac{1}{T_{sw}} \int_0^{T_{sw}} \left| \frac{u_{T1}}{K_{T1}} \right| dt. \quad (2)$$

Thus, changing the sequence of *T1* connection to mains phases (while observing condition (1)) allows control of output voltage and, what is quite important, input current shape.

Let us denote the time of transformer connection to *A*, *B*, *C* phases as t_a, t_b, t_c, and off-duty ratios relative to *A*, *B*, *C* phases as $D_a = t_a/T_{sw}$, $D_b = t_b/T_{sw}$, $D_c = t_c/T_{sw}$, respectively. Then for input currents of the considered converter we can write:

$$\begin{aligned} i_a &= I_l D_a \text{ sign } (u_a), \\ i_b &= I_l D_b \text{ sign } (u_b), \\ i_c &= I_l D_c \text{ sign } (u_c), \end{aligned} \quad (3)$$

where I_l is the load current reduced to primary side; u_a, u_b, u_c are the phase voltages of the circuit.

To ensure PF close to a unity, it is necessary for input current in each phase to be proportional to the respective phase voltage. This can be achieved by selection of off-duty ratio as follows:

$$D_a = \gamma|u_a|, \quad D_b = \gamma|u_b|, \quad D_c = \gamma|u_c|, \quad (4)$$

where γ is the coefficient determining the output voltage.

Average voltage on transformer primary winding during time T_{sw} is defined as

$$U_{T1} = u_a D_a + u_b D_b + u_c D_c, \quad (5)$$

this voltage sign being determined by numbers of switched-on switches. Substituting (4) into (5), we get:

$$U_{T1} = \gamma(u_a^2 + u_b^2 + u_c^2) = 1.5\gamma U_{ph}^2, \quad (6)$$

where U_{ph} is the amplitude of mains phase voltage.

Thus, at observation of condition (4) it is possible to achieve source PF close to a unity. Moreover, another important conclusion follows from (6): ripple at mains frequency is absent at source output. This allows considerably increasing the quality of converter voltage and lowering the requirements to output filter.

We have conducted modelling of the proposed source in Mathcad environment. Modelling parameters are as follows: *L1* = *L2* = *L3* = 330 μH, *C1* = = *C2* = *C3* = 4.7 μF, switching frequency of 20 kHz, $\gamma = 1/U_{ph}$. Results show that fundamental harmonics (50 Hz) and harmonics with frequencies, which are a multiple of switching frequency (20 kHz), are present in the input current of switch matrix. After filtering with application of second order input filter, components with frequencies close to the filter resonance frequency appear in the spectrum. In the given example this is 4.04 kHz. The total coefficient of input current harmonics is equal to 4.4 %. Electric diagram of power components of the source, corresponding to Figure 1, is shown in Figure 2. It has the obvious drawback of a large number of power switches equal to 12, and of complexity of their control. To simplify the control circuit and reduce the number of power switches, it is rational to apply the method of conditional division of the source power components into the rectifier and the converter. Such a procedure is often used for analysis of the process in matrix frequency converters.

In the optimized circuit, given in Figure 3, the three-phase input is made as a non-reversible rectifier with current output, transformer «excitation» is performed by bridge *VT4*–*VT7*, while added elements *VT8*, *C4* are used for limiting the transistor voltage during no-current pauses between switching.

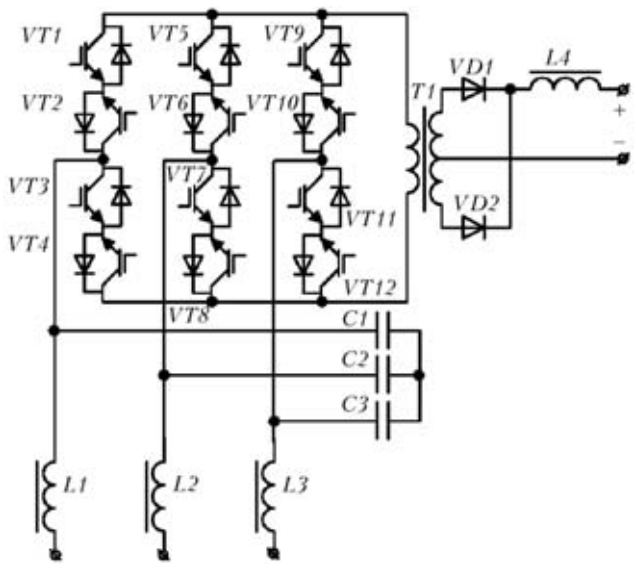

Figure 2. Elementary diagram of power components (acc. to Figure 1)

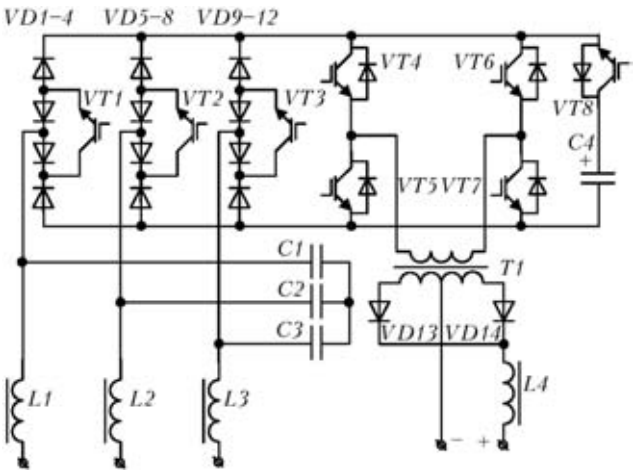

Figure 3. Optimized circuit of power components

To check the theoretical results, a test low-power mock-up of the source was assembled by the circuit shown in Figure 3. Oscillographing of its consumed current, phase supply voltage and PF measurement showed the low level of nonlinear distortions of the current curve and high PF — more than 0.95. These experimental results fully confirm the serviceability of circuit designs, and correctness of theoretical principles presented in the work.

Schematic in Figure 3 can be implemented using mass-produced power units for frequency converters, accommodating power transistors and control and protection circuits in one case. So, elements *VT1–VT3* and *VD1–VD12* can be replaced by three specialized power modules VUI3012N1 (IXYS), and bridge *VT4–VT7* can be of MKI50-12E7 or MKI100-12F8 type. MEK600-04DA assembly can be used as *VD13* and *VD14* diodes. Application of the above power units will enable achieving up to 15 kW power in the load at power supply from the mains with 380–460 V line voltage.

If it is necessary to increase power, higher-power components can be used in the power circuit. However, increase of output current can be also achieved by parallel joining of several sources and respective synchronizing of their control systems. Summing of output currents of several converters is often more cost-effective, than construction of one powerful source. So, three inverters, made by the circuit in Figure 3, can provide output current of up to 1000–1200 A at working voltage of 30–36 V, thus allowing their application in automatic welding technologies. Detuning of switching frequencies of individual sources within narrow limits will allow lowering spectral density of emitted electromagnetic noise.

Control signals can be formatted using specialized DSP processors (for instance, ADSP21xx of Analog Devices) or single-crystal microcontrollers (for instance, AVR ATMega or ARM Cortex STM32).

1. Korotynsky, A.E. (2002) State-of-the-art, tendencies and prospects of development of high-frequency welding converters (Review). *The Paton Welding J.*, **7**, 44–49.
2. Rudyk, S.D., Turchaninov, V.E., Florentsev, S.N. (1999) Power single-step converter of dc voltage with «soft» commutation of power switch. *Elektrotekhnika*, **4**, 55–58.
3. Rudyk, S.D., Turchaninov, V.E., Florentsev, S.N. (1998) Advanced welding current sources. *Ibid.*, **7**, 8–13.
4. Itoh, J., Iida, T., Matsumura, D. (2007) High efficiency high-frequency link converter with AC/AC direct converter technology. *IEEJ Transact. on Electrical and Electron. Eng. D*, 127(**8**), 822–828.
5. Burlaka, V.V., Gulakov, S.V. *Three-phase rectifier of welding current with direct conversion*. Pat. 92420 Ukraine. Int. Cl. H02H 7/09. Fil. 17.07.2009. Publ. 25.10.2010.

INFLUENCE OF VIOLATIONS OF WELDING GUN AXIAL SYMMETRY ON FOCAL SPOT POSITION

O.K. NAZARENKO and **V.A. MATVEJCHUK**
E.O. Paton Electric Welding Institute, NASU, Kiev, Ukraine

In addition to the known requirements to stability of heating spot position on an item specified in international standard ISO 14744-6, violations of adjustment of electron beam welding gun and procedure of their elimination are considered.

Keywords: *electron beam welding, EB gun, triode emission system, electromagnetic focusing system, violations of axial symmetry, beam crossover, focal spot, instability of dimensions and position, welding gun adjustment*

International standard ISO 14744-6 [1] contains strict limitations of instability of focal spot position — they should not exceed ±0.1 mm in the plane located at 300 mm distance from welding gun edge. This requirement cannot be satisfied in many cases, and two serious difficulties arise in practical application of EBW:

• if before welding the operator combines low-power (probing) electron beam with the butt of edges being welded, then at beam current increase up to the nominal value the focal spot can shift, in particular normal to the butt plane. There is the risk of beam deviation from the butt plane, particularly in its root part. Therefore, experienced operator before welding on a run-off tab (close to the weld) performs the so-called piercing with a stationary beam of nominal power. If the root part of the piecing falls on the extension of butt plane, welding can be performed;

• change of focusing current can also lead to shifting of the focal spot towards the butt. Moreover, as in this case the electron beam falls on the item at an angle, different from 90°, the arising tangential component of the recoil reaction of metal vapours disturbs the symmetry of cast metal upper part. At the same time, focal spot diameter is increased and distorted, thus reducing the penetration depth.

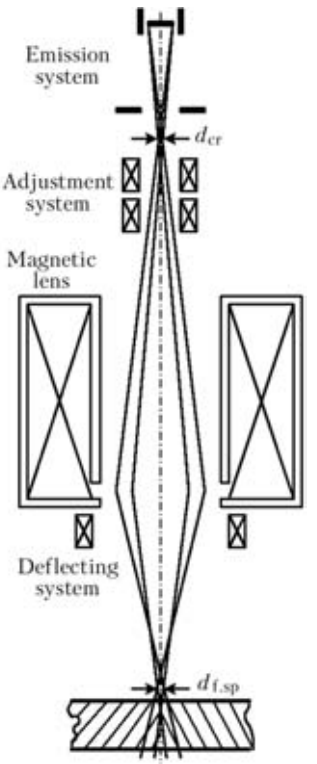

Figure 1. Schematic of welding gun electron-optical system: d_{cr} — beam crossover diameter; $d_{f.sp}$ — focal spot diameter

The cause for the mentioned difficulties is accounted for by violations of adjustment or errors (in keeping with the terminology of light and electron optics) of welding gun axial symmetry, because of inaccuracies of its fabrication and assembly, and local magnetization of gun components and item. These errors are eliminated by adjusted displacement of focusing electromagnetic lens or using two deflecting systems mounted above it and having the role of adjustment system (Figure 1). Only at combination of the axes of emission system and magnetic lens, and this should be in the entire range of welding currents, the focal spot position on item surface does not change during gun operation.

Welding gun emission system, which includes the cathode, control electrode and anode, forms the converging electron beam, the minimum cross-section of which — the crossover — is reflected using a magnetic focusing lens in the item plane as the focal spot (see Figure 1). Term «adjustment» means achievement of gun axial symmetry, i.e. symmetry of electric and magnetic field rotation.

Adjustment errors (in other words, first order aberrations or axial astigmatism) are manifested, first of all, in that the electron-optical system, even at a small angle of beam convergence/divergence, does not create a point image of the crossover. Central beam electrons, the initial speeds of which lie in different meridional planes, experience different action of the refracting medium, and do not cross the axis in one point. Crossover central point is reflected in item plane in the form of a dash, transverse dimensions of the focal spot grow, and its position in item plane is disturbed.

A lot of publications are devoted to problems of violation of axial symmetry of low-current electron-optical systems of electron microscopes, TV instruments, electron accelerators (for instance, [2]). Now, this paper is devoted to errors of axial symmetry of welding gun electron-optical system, forming the electron beam in a wide range of powers from 1 up to 100 kW, mechanism of their influence on weld formation, earlier not discussed in publications.

Mechanism of disturbance of focal spot position on the item at the change of focusing and beam currents. Unlike the glass lens, the magnetic lens not only rotates the image (focal spot) relative to the item (crossover) through 180°, but additionally rotates it through certain angle ψ. At focusing, the electron beam moves in a plane, rotating about a magnetic axis, i.e. by a spiral trajectory [3].

If the electron beam is focused by a system with axial symmetry, the existence of this rotation does not affect the dimensions or position of the spot. However, if as a result of axial symmetry errors, the crossover is shifted relative to the magnetic lens axis, it is exactly beam rotation that affects the focal spot position (Figure 2).

Angle of rotation ψ depends on magnetic field intensity in the focusing lens, its configuration $H(z)$ and accelerating voltage U_{acc}:

$$\psi \approx \frac{0.148}{\sqrt{U_{acc}\,[\mathrm{V}]}} \int_{-\infty}^{\infty} H(z)dz. \qquad (1)$$

For instance, for magnetic lens with turn number $N = 1500$ at magnetization current $I_m = 0.66$ A and $U_{acc} = 60$ kV, beam rotation is equal to

$$\psi = 10.7 \frac{NI_m\,[\mathrm{A}]}{\sqrt{U_{acc}\,[\mathrm{V}]}} \approx 43°. \qquad (2)$$

Variation of focusing current or its direction leads to a change of the angle of rotation ψ and radial shifting of focal spot on the item, respectively. Value of this shifting is maximum in the case of the change of focusing current direction and is also equal to 43°, but in the opposite direction. Thus, at switching of magnetization current polarity, the shift between two melting points will be equal to almost 90°.

Violation of focal spot position at the change of focal current is manifested to the maximum degree at parallel shifting of the axes of emission and focusing systems of the welding gun. In Figure 3 axis $A–A'$ of the emission system is shifted to distance δ relative to axis $O–O'$ of magnetic lens and crosses the item plane in point A, and not in point O. Beam crossover is reflected by the focusing lens in points F_1 or F_2 (depending on magnetic field direction), lying on the circumference, which is circumscribed around the magnetic lens axis, circumference radius depending on lens magnification and δ value.

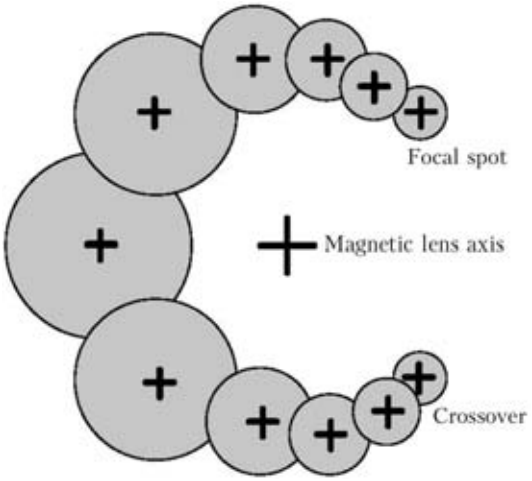

Figure 2. Projection of beam trajectory on item plane at crossover shifting relative to magnetic lens axis

In welding the polarity of power supply of the magnetic lens is certainly not switched, but focusing current can be programmed during the process, thus leading to focal spot shifting along the circumference, on which is falls. At cosmetic smoothing of the weld by deepening of the focal spot, for instance, by 100 mm, that is achieved at lowering of focal lens current by 0.050 A, angle ψ, according to expression (2), will be decreased by 3°, and at circumference radius of 5 mm beam shifting will exceed 0.1 mm and will affect both the alignment accuracy, and cast zone formation (Figure 4).

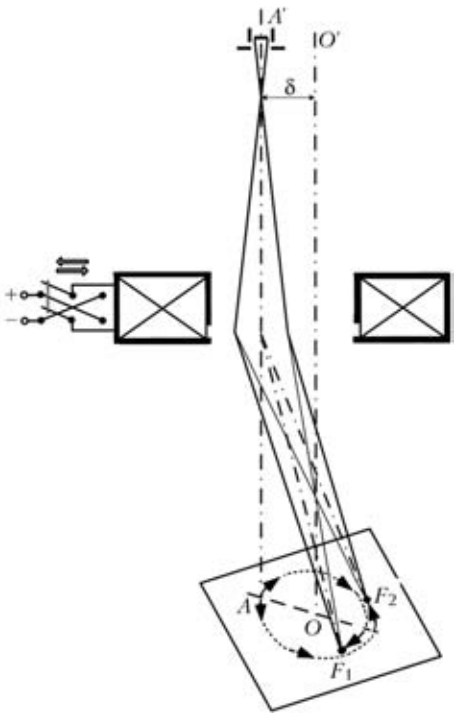

Figure 3. Schematic of influence of parallel shifting of gun emission system and magnetic lens axes on focal spot position in item plane (scale of gun reflection and beam trajectories is not observed to ensure good visual presentation; for designations see the text)

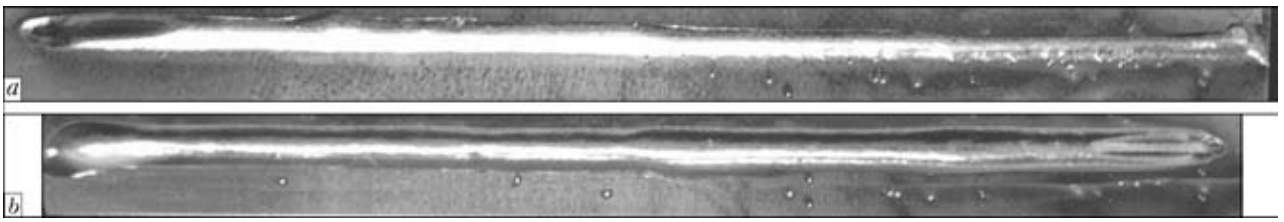

Figure 4. Asymmetrical (*a*) and symmetrical (*b*) change of weld width depending on the value of focusing lens current in a well and poorly adjusted gun, respectively

It should be noted that as follows from Figure 3 and expression (2), in the case of parallel shifting of the axes of emission system and focusing lens, the change of beam current does not affect the focal spot position in item plane.

Figure 5 shows a situation, arising at inclination of the axis of gun emission system relative to magnetic lens axis. The axis of emission system A–A' is inclined at angle θ relative to magnetic lens axis and crosses the item plane in point A, and not in point O. However, as at small beam current 1–2 mA (i.e. in probing mode), beam minimal cross-section — crossover — is located near the cathode in point *1* practically on magnetic lens axis, the crossover is reflected in item plane in point O, lying in butt plane. Now, at nominal beam current, its crossover *2* is significantly — by tens of millimeters — displaced from the previous position and turns out to be shifted to distance Δ relative to magnetic lens axis. Focusing coil reflects the crossover as focal spot in point F of the item, where the electron beam will fall, while rotating around axis O–O'. It is seen that in welding the focal spot will be shifted relatively to butt plane. At the same time, focal spot diameter is increased and distorted, thus lowering the penetration depth.

In practice, certainly, shifting and inclination of emission system axis relative to focusing coil can occur simultaneously, that makes gun adjustment still more complicated.

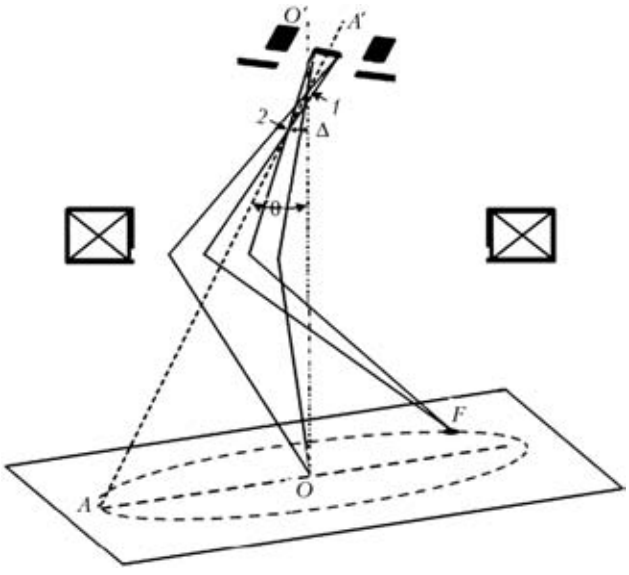

Figure 5. Schematic of influence of inclination of gun emission system axis relative to magnetic lens axis on focal spot shifting in item plane (scale of gun reflection and beam trajectories is not observed to ensure good visual presentation; for designations see the text)

Procedure of elimination of errors of welding gun axial symmetry. Before applying the system of gun electromagnetic adjustment at detection of instability of the focal spot, it is recommended to determine the gun component, responsible for this instability, and try to eliminate it by mechanical processing of parts and their demagnetization.

The most efficient is the following sequence of actions:

1. Checking the axial symmetry of electrodes of the emission system proper. Shifting of ion crater relative to cathode center (Figure 6) is an unambiguous indication of violation of axial symmetry of emission system electrodes and the need for their mechanical retrofitting.

2. Checking the alignment of the geometrical and electron-optical axes of the emission system:

- using the beam in probe mode make two surface-melted spots on the plate by switching the direction of focusing coil current;
- turn the case of the emission system relative to the initial position through an angle of 90–180°, and again make two surface-melted spots on the plate.

If the case rotation did not influence the distance between the surface-melted spots, or their spatial orientation, it is an indication of alignment of the geometrical and electron-optical axes of the emission system.

3. Checking the alignment of the geometrical and magnetic axes of the focusing system:

Figure 6. Shifting of ion crater relative to cathode center

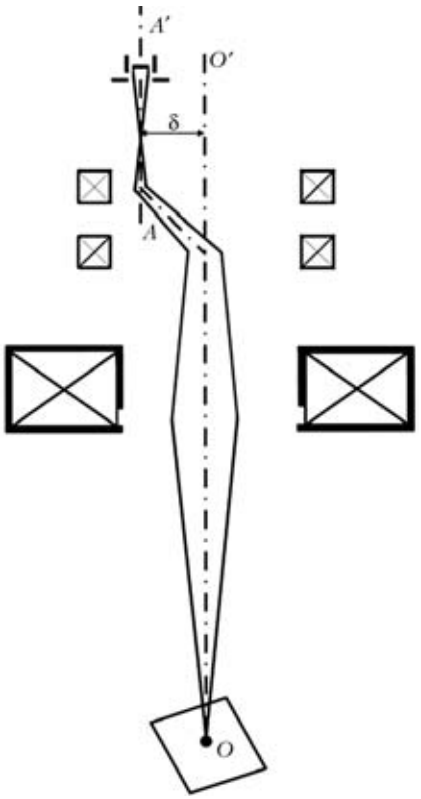

Figure 7. Principle of straightening of axes of emission system and focusing lens using two deflecting systems

• use the beam to produce in the probe mode two surface-melted spots on a plate by switching the direction of focusing coil current;

• turn the focusing lens case relative to the initial position through an angle of 90–180° and again obtain two surface-melted spots on the plate for two directions of focusing lens current.

If rotation of focusing lens case has not affected the distance between the surface-melted spots or their spatial orientation, this is indicative of alignment of the geometrical and magnetic axes of focusing lens.

4. If after fulfillment of the above operations it was not possible to eliminate shifting of the focal spot at the change of beam current or focusing current, the axes of the emission and magnetic systems should be superposed. In the case of parallel shifting of the above axes, as follows from Figure 3, change of beam current will not affect the focal spot position. Asymmetry of the welding beam only will cause shifting and asymmetry of the cast zone at the change of focusing current. Now, if the emission system axis is inclined relative to magnetic axis, then, as follows from Figure 5, change of beam current will cause a noticeable shifting of the focal spot.

At this final stage alignment of the axes of emission and focusing systems is performed using two electromagnetic deflecting systems (Figure 7). Application of one or two algorithms of the alignment process is possible: either step-by-step drawing together of two surface-melted spots on the item, made at nominal and minimal beam current, or displacement of any of these surface-melted spots to calculation point *O* of magnetic lens axis.

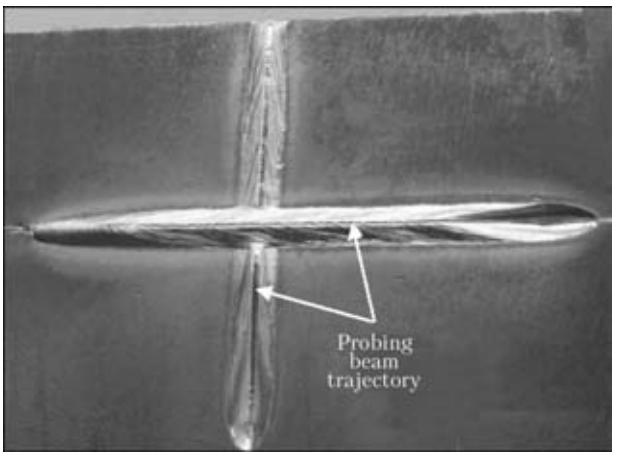

Figure 8. Accurate alignment of probing beam trajectory with the middle of welds made in orthogonal directions

Result of this operation is coincidence of the trajectory of probing beam with the middle of the cast zone, produced at beam nominal current in two mutually normal planes (Figure 8).

CONCLUSIONS

1. The main indication of satisfactory axial symmetry of electron-optical system of the welding gun is coincidence of probing pulse trajectory with the middle of cast zone produced at nominal beam current in orthogonal directions.

2. Procedure of variation of focusing beam current can be used as a convenient express method of preliminary checking of the quality of gun adjustment, as a rule, in the mode of low beam currents.

3. Indications of satisfactory axial symmetry of gun emission system proper are absence of shifting of ion crater relative to the cathode center and constant position of the focal spot on the item at turning of the emission block around its axis through an angle of 90–180°.

4. Axial symmetry of focusing lens is confirmed by unchanged position of the focal spot on the item at turning of the lens around its axis through an angle of 90–180°.

5. A final stage of gun adjustment is straightening of the axes of emission system and focusing lens using two deflecting systems sequentially located below the anode.

1. (2000) *ISO 14744-6*: Welding — acceptance inspection of electron beam welding machines. Pt 6: Measurement of stability of spot position.
2. Glazer, V. (1957) *Fundamentals of electron optics*. Moscow: Gostekhteorizdat.
3. Kelman, V.M., Yavor, C.Ya. (1950) *Electron optics*. Moscow; Leningrad: AN SSSR.

SESSION OF SCIENTIFIC COUNCIL ON NEW MATERIALS AT COMMITTEE ON NATURAL SCIENCES OF INTERNATIONAL ASSOCIATION OF ACADEMIES OF SCIENCES

The 17th session of Scientific Council on New Materials at Committee on Natural Sciences of the International Association of Academies of Sciences (IAAS) on a subject «Structural and functional materials for medicine» took place in Kiev at the E.O. Paton Electric Welding Institute in May 24–25, 2012.

More than 100 scientists and specialists in the field of materials science from academies of sciences, institutes of higher education and enterprises of Belarus, Kazakhstan, Russia and Ukraine participated in a meeting of the Scientific Council.

Meetings of the sections of the Scientific Council, nomely «Polymeric materials», «Titanium-based materials», «Materials on basis of copper and heavy nonferrous metals» and «Structural and functional nanomaterials for medicine», were held in the first day of the Scientific Council in May 24. More than 40 presentations were made and discussed in the sections. Results of the investigations related with obtaining of nanoparticles, study of their interaction with medium, formation of structures, investigation of their properties and development on this basis of nanotechnologies allowing obtaining of the materials with unique characteristics were represented.

Plenary meeting of the Scientific Council, opened by chairman — Prof. B.E. Paton, President of the IAAS, President of the NAS of Ukraine, Director of the E.O. Paton Electric Welding Institute, took place in May 25. In particular, he indicated that the main attention of the Council was paid to the metallic materials in the first years of its activity, and then ceramic materials and artificial polymers were included in sphere of its work. New section of the Council «Structural and functional nanomaterials for medicine», headed by I.S. Chekman, Corresponding Member of the NASU, was created in 2011. Also a decision was made about holding a session of the Scientific Council on the subject «Structural and functional materials for medicine».

Further Prof. B.E. Paton announced to the participants a program and schedule of work of the 17th plenary meeting, during which 12 presentations dedicated to wide range of the problems in the filed of materials science for medicine were listened.

Academician of the RAS V.M. Ivlev (Voronezh State University) made a presentation «Synthesis, structure and properties of thin bioactive coatings based on hydroxylapatite». He indicated that a plasma jet spraying remains the main commercial method due to its high efficiency regardless a wide range of approaches to synthesis of bioactive coatings of metallic implants. At the same time, these coatings are the less studied ones in aspect of structure. Representations about structure of metal–ceramics interface, as well as structure of grains and interphases boundaries in the ceramic coating at microscopic level, are to be developed for solving these issues. System investigations on increase of adhesion strength, control of morphology of coatings formed by physical methods are also necessary to be carried out. The representations about microscopic mechanism of plasticity, being observed in a process of indentation of various structure coatings, will be developed at sufficient data about mechanisms of coating deformation.

Academician of the NASU B.A. Movchan (E.O. Paton Electric Welding Institute) familiarized the participants with the schemes and some parameters of electron beam technologies used for development of nanostructured medicinal polymer–metal substances. Presented results of experimental investigations showed the possibility of efficient application of physical processes of evaporation and condensation of various substances in vacuum for investigation and development of the nanostructured solid- and liquid-phase medicinal substances and some medicinal drugs. Created in the recent years medicinal powder-like substances and drugs with surface modified by copper, silver and iron nanoparticles were delivered to the customers for further investigations.

Then, the presentation «Nanomaterials for noninvasive diagnostics of single living cells» was made by E.A. Gudilin, Corresponding Member of the RAS (M.V. Lomonosov Moscow State University). Nanomaterials allow making express-diagnostics using minimum quantity of analyzed biological material and preserving its structural and «chemical» information. It is determined that silver nanoparticles of various morphology (threads, rods, cut particles) are perspective material for living cell diagnostics. Investigations performed allow obtaining nanostructured materials based on silver or gold, which preserve their structure in contact with physiological liquids and cells. Such substrates can be used for investigation of red corpuscles by optical method, i.e. method of giant combination scattering.

S.A. Firstov, academician of the NASU (I.M. Frantsevich Institute of Problems of Materials Science, Kiev) gave the presentation on the subject «New materials for medical application». Research works of biomedical designation, performed in the Institute, are concentrated in development of osteotrophic materials and products from them for orthopedics, stomatology and oncology needs; development of bioadditives, drug carriers and new biocompatible alloys of titanium and tantalum. In particular, ceramics based on zirconium dioxide for application in the implants and scalpels and granular technology for obtaining of high-porous coatings for implants and bone implants have been already developed.

Problems and main results of investigation in the field of biomechanics of high achievement sport were considered in the presentation of Yu.M. Pleskachevsky, Corresponding Member of the NAS of Belarus. The biomechanics, from point of view of author, promotes development of concepts of human vital activity, innovations in all without exception technical areas, starting with the means of prosthetics and ending by global systems of control and manufacture. Also the biomechanics is a scientific basis of the high achievement sport. Analysis of muscle activity and hemodynamics allows selecting of atraumatic and maximum effective address training load for each individual case.

Presentation «Nanopharmacology: scientific-and-practical aspect» was made by I.S. Chekman, Corresponding Member of the NASU (O. Bohomolets National Medical University, Kiev). Nanopharmacology studies the properties of nanodrug and investigates the possibilities of their application in medical practice for prevention, diagnostics and curing of various diseases with control of biological activity, pharmacological and toxicological effect of obtained products or drugs. Studies on pharmacology of organic and nonorganic nanomaterials are intensively performed virtually at all countries of the world at present time. The dosage forms (ointments, gels, powders, capsules, syraps and mixtures) of nanodrugs of metals and their composites with organic substances (antibiotics, ascorbic acids, isoniazids) were developed. They make a basis for future investigation and implementation in the medicine practice.

V.N. Voevodin, Corresponding Member of the NASU (Institute for Solid-State Physics, Materials Science and Technologies, Kharkiv) told about a development of functional materials and devices from them used for solving of cardiology and oncology issues. Stainless steel 316 LVM, Co–Cr alloys (L605), Ni–Ti alloys, Co-alloys, tantalum, platinum are the most widespread materials for manufacture of permanent metallic stents for dilatation of blood vessels. Investigations of dependency of physico-mechanical and corrosion properties and bi-compatibility of new grade of magnesium alloys (Mg–Y–Sc–Re) on composition of alloys, modes of their deformation and heat treatment were carried out in the institute. Six new magnesium alloys, that can be used for materials of vessel stents and suture material for endosurgery, were created on the basis of investigations performed and super-pure alloying components. A laboratory technology was developed for manufacture of capillary high-accuracy tubes and long-length mono- and bimetal wire from several metallic materials. More than ten types of devices of cardio and oncology designation and technologies of manufacture of their pilot batches were developed.

Nanostructured materials for medicine based on functional-gradient coatings were considered in the presentation of Dr. B.V. Formakovsky (RSI of Structural Materials «Prometey», Saint-Petersburg). The Institute has sufficient instrumental and methodological support for investigation of physico-mechanical properties of nanostructures, i.e scanning hardness gauge SuperNanoScan, X-ray diffractometer Bruker, laser particle analyzer Malvern etc. This allows performing successful investigations in the filed of nanomaterial creation and nanotechnology development. Magnetron and ion-plasma spraying are used in the Institute for deposition of antibacterial corrosion-resistant protective coatings on the instruments for general and field surgery. Nanostructured coatings from tantalum were also developed for surgery operations on brain vessels without craniotomy.

Prof. Z.R. Ulberg (F.D. Ovcharenko Institute of Biocolloidal Chemistry, Kiev) made the presentation «Scientific basis of application of biocolloidal systems in nanopharmacology». Passive localizing due to electrostatic, coordination and other types of bonds and metabolism, which is a dependent accumulation character only to actively metabolizing cells, are the main mechanisms determining an interaction of biologic cells with metal nanoparticles from point of view of the author. A series of safe metal nanoparticles, i.e. silver, gold, iron, copper, bismuth as well as nanoparticles of iron with ascorbic acid, was obtained using the colloidal-chemical methods in the institute. Tests on animal verified biosafety of all nanoparticles.

Presentation of Prof. V.M. Nadutov (G.V. Kurdyumov Institute for Metal Physics, Kiev) was

dedicated to new metallic materials for medicine needs. Titanium alloys obtained on hydride technology; magnetically soft amorphous nanocrystalline alloy; bio-mechanical compatible β(Zr–Ti) alloy and half-finished materials for medical application (implants); magnetic powder nanomaterials for medical purposes and functional materials based on nano-dispersed calcium hydroxyapatite became widespread among them.

Corresponding Member of the RAS S.S. Ivanchev (Branch of G.K. Boreskov Institute of Catalysis of RAS SB, Saint-Petersburg) dedicated his presentation to polymer hydrogels and drug systems on their basis. Polymer hydrogel is the hydrophile macromolecular systems capable of holding a significant amount of water with preservation of properties character to the solids (shape, mechanical modules, characterizing material in tensile and shear strain) at that. Wide range of fields of application is typical for these systems, i.e. absorbents, membranes of various type — gas distributing, ion-exchanging and structure forming system-carriers of drug substances, substitutes of biological tissues, materials for soft contact lens, membranes for fuel elements.

Prof. B.E. Paton made a speech at the end of session work. He thanked the speakers and participants for fruitful work.

Participants of the session had the possibility to exchange the opinions about made presentations and level of works in the field of development of the new materials in their countries, evaluate work of the Scientific Council on New Materials, express the ideas of its improvement in a course of discussions. Annual sessions of the Scientific Council on new Materials of the IAAS allows preserving and developing creative bonds between the scientists of various countries, promoting intensification of information exchange.

The next session of the Scientific Council on New Materials of the IAAS is planned to be held at the E.O. Paton Electric Welding Institute in May 2013.

Prof. I.A. Ryabtsev, PWI

MODIFICATION OF WELD METAL ON STEELS 14KHN3A AND 20KHN3A TO IMPROVE SERVICE PROPERTIES OF DRILL BITS

The research work on the above subject was completed in 2011 at the E.O. Paton Electric Welding Institute (supervisor – Prof. O.K. Nazarenko)

Conventional steels 14KhN3A and 20KhN3A used in structures of rolling drill bits have limited weldability, and properties of metal of the welded joints on these steels in a number of cases do not meet the high-speed drilling conditions. If design of the diamond bits requires a combination of steels 40KhN and 14KhN3A, this makes the process of manufacture of the bits much more complicated. Increase in sizes of the bits and, at the same time, thicknesses welded raises the probability of formation of fine cracks in the welded joints, thus leading to violation of their hydraulic tightness and decrease in service life.

Technologies were developed for electron beam welding with modification of metal of the welded joints to improve their performance. Offered was the design of insert modifiers which does not violate the quality of assembly of bit components, has no effect on accuracy of operation of the seam tracking system and, at the same time, provides formation of the welds containing no solidification cracks. The most optimal material for modification of the welds on the rolling drill bits was stainless austenitic steel 10Kh18N10T with a thickness of 0.2 mm, and for the welds on the diamond bits — zirconium foil inserts, also 0.2 mm thick. Width and length of the plate modifiers depends on the type of the bits welded and may vary from 15 to 20 mm in width and from 45 to 70 mm in length.

The research and development work was performed to design the specialised fixture to fit the units for EBW of drill bits in accordance with the developed technologies. Software for EBW of the bits with modification of the welds was worked out.

Comprehensive investigations of the quality and properties of the EB welded joints on the drill bits, including the use of modification elements, were conducted to improve strength and prevent solidification cracking of the joints, tensile strength of the joints being 95–98 % of that of the base metal. All technological and design developments were verified in manufacture of an experimental batch of the full-scale parts, which were passed to tests to be conducted in real service environment of the drill bits.

Developed at PWI

TECHNOLOGY FOR RECOVERY OF CARRYING CAPACITY OF DIFFERENT-PURPOSE PIPELINES AND WELDING OF BRANCH PIPES TO THEM UNDER SERVICE CONDITIONS

The pipeline transport of the CIS countries is in a difficult situation now because of progressing ageing of oil and gas pipelines. Half of the main oil pipelines have been in operation for 20–30 years or longer. More than 5 % of the gas pipelines have exhausted their specified life (33 years), 25 % of the gas pipelines have been in service for over 25 years, and 38 % of the total length of the gas pipelines has been in operation from 10 to 20 years. As shown by statistics, ageing of pipeline systems is accompanied by increase in the number of failures caused, first of all, by corrosion processes and mechanical damages. This makes the problem of ensuring the efficient and failure-free operation of the pipeline transport increasingly pressing. The key role in addressing it belongs to improvement of the existing methods and development of the new, more reliable and safe ones for performing repair and maintenance on main pipelines.

Operation of main pipelines very often involves the need to connect new consumers or new small and medium oil and gas fields, as well as the need to perform repair-and-renewal operations by replacing defective regions of a linear part of pipelines without interruption of transportation of a product. Keeping a pipeline in the active state while performing such repair operations is economically attractive, but it must be combined with the environmental safety.

Assembly of overlap-butt joints on active pipeline

We developed and apply the safe technologies for welding of branch pipes and welding repair of active pipelines by the arc method without interruption of transportation of a product. On the one hand, these technologies provide the high quality and reliability of welded joints in building-in of additional structural elements into the active pipelines, and, on the other hand, they allow maintaining a failure-free operation of the transportation system and environmental safety.

The developed technologies are oriented to manual arc welding, as it allows performing welding and repair operations on the active pipeline in any spatial position. These operations should be performed simultaneously and at a high quality. Therefore, it is necessary to carefully select the type of welding electrodes for each particular case, depending on the pipeline steel grade, real state of the pipeline and its service conditions.

Whereas the problem of recovery of the carrying capacity of structures made from low-carbon and low-alloy steels with a comparatively low level of strength, which operate under extreme conditions of intensive cooling, can be considered solved in general, this is not the case of steels of an increased strength (σ_t — up to 450 MPa). Primarily, it concerns welding of pipe steels on active main ground-surface pipelines. Special reinforcing overlap elements were developed to ensure the appropriate operating reliability of the butt joints, and recommendations were worked out to transfer to the overlap-butt joints and the corresponding welding technology providing the required thermal cycle. The use of the overlap-butt joints allows the transverse stresses in welding to be decreased 2 times, compared with the fillet welds.

New process flow diagrams for joining structural components (sleeves, branch pipes, patches) to the pressurised pipelines make it possible to substantially improve safety of the welding operations and reliability of the welded joints in operation, as well as protect the environment from pollution.

TECHNOLOGICAL MODULE UD-690 FOR REPAIR OF MAIN ESCALATOR SHAFT SEATS

Mobile, multiple-function technological module UD-690 is designed to repair rolling bearing seats for main shafts of escalator drives directly under conditions of the city subway machine hall.

Technological module UD-690 provides a 3.5 times reduction of the time and costs of repair of the above parts, as there is no need to perform repair operations at specialised enterprises and unavoidably transport the main shafts to the above enterprises and back, to preheat the shafts for repair welding and perform postweld heat treatment, and, finally, as all the repair operations can be performed in site, i.e. in the city subway machine hall, with a shaft just once placed on stand-alone supports.

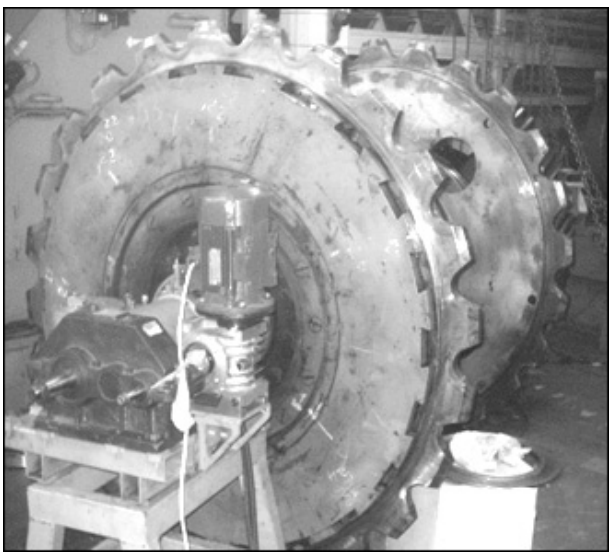

The weight of the main shaft of the escalator drive (including structural elements of the drive mounted on it) is about 6 t. Therefore, even minor violations in the procedure of assembly operations performed with the main shaft of the escalator drive lead to formation of axial loads on it, which may be accompanied by slipping of the main shaft relative to the inner races of rolling bearings. In turn, because of a very intensive operation of city subway escalators, this leads to a considerable wear of the bearing seats in the main shaft of the escalator drive. In the pre-repair state, the average area of wear of the bearing seats of the main shaft of the escalator drive is 1.5–2.0 mm at a diameter of the seats equal to 280 and 300 mm, respectively.

The process of repair of seats of the main shaft of the escalator drive implemented by using module UD-690 includes four operations performed at one setting:

- machining of worn-out seats on the main shaft to form cylindrical surfaces required to repair the shaft, their axial symmetry and zone of a defect-free structural material, the latter being identified by the dye penetrant inspection;
- deposition of the sub-layer, having the required ductile characteristics and contributing both to decrease in the sensitivity to cracking of the main deposited layer and to reduction of residual stresses within the zone of repair of the bearing seats of the main shaft of the escalator drive;
- deposition of the main layer, having the required combination of strength (hardness) and ductility, with hardness of metal of the main deposited layer being controlled, without fail, by using a portable hardness meter;
- grinding of the main deposited layer up to achieving the required alignment of the bearing seats, specified sizes of the seats and necessary roughness of their surfaces;
- comprehensive testing of the quality of all the operations performed.

The module provides accuracy of repair of the seats within 0.05 mm.

Technological module UD-690 was successfully tested under real subway conditions.

AUTOMATED SYSTEM AND TECHNOLOGY FOR REPAIR CLADDING OF WORN-OUT GIRDER TRAM RAILS WITHOUT THEIR DISMANTLING

When side surfaces of the «head» and «lip» reach their ultimate wear state, girder rails in curvilinear sections of tram ways are subject to replacement or cladding repair of their worn-out surfaces.

Replacement of worn-out rails by new ones is an expensive operation, first of all because of their high metal intensity and cost. Municipal services bear even higher losses because of the need to destroy and then restore road coverings, and stop traffic of all types of vehicles for a long time in a given section.

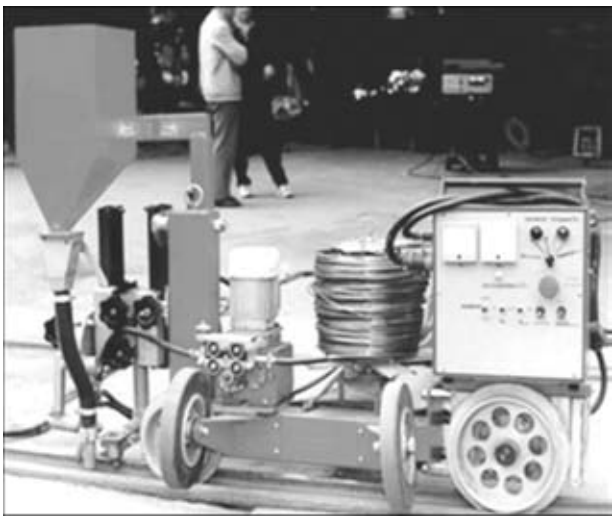

Self-propelled cladding device UD-654

The E.O. Paton Electric Welding Institute developed the equipment and technology for cladding repair of worn-out surfaces of girder rails Tv65 without preheating them under field conditions. The cladding flux-cored wire is covered by Ukraine patent 39646A of 15.06.2001, and manufacture of the wire is regulated by specifications TUU 28.7.05416923.066–2002. Self-propelled cladding device UD-654 was developed to implement the technology. It is based on a new principle of control of the mechanised arc cladding process (USSR author's cert. 1771903–92; favourable decision on Ukraine patent application 99041892 of 05.04.1999, Ukraine declaratory patent applications 2020860 of 16.02.2000 and 2020863 of 16.02.2000).

Experimental-industrial tests of the device were carried out at Company «Kievpastrans» (Kiev), the equipment and technology for automated cladding of side surfaces of the tram rails were optimised, and a 25 m long test section with an intensive traffic was treated. The deposited metal provided hardness *HRC* 45–50 after cold working. Four years' observations of the treated section showed that its wear was twice as low compared to untreated sections under the identical service conditions.

The new system of the equipment and cladding consumables developed by the E.O. Paton Electric Welding Institute are not inferior in their technical characteristics to West-European analogues. The cladding technology is implemented by using one type of the wire, whereas the West-European companies use two types of the wire for cladding, which extends the time of the cladding cycle. Moreover, the new cladding technology provides a smoother surface. This allows reducing the costs and time of subsequent grinding, or even avoiding it in some cases. The price of the new cladding system and consumables is lower than that of the West-European analogues.

SUBSCRIPTION
FOR «THE PATON WELDING JOURNAL»

If You are interested in making subscription directly via Editorial Board, fill, please, the coupon and send application by fax or e-mail.

The cost of annual subscription via Editorial Board is $324.

Telephones and faxes of Editorial Board of «The Paton Welding Journal»:

Tel.: (38044) 200 82 77, 200 81 45

Fax: (38044) 200 82 77, 200 81 45.

«The Paton Welding Journal» can be also subscribed worldwide from catalogues of subscription agency EBSO.

SUBSCRIPTION COUPON

Address for journal delivery _____

Term of subscription since _____ **20** **till** **20**

Name, initials _____

Affiliation _____

Position _____

Tel., Fax, E-mail

Subscription to the electronic version of «The Paton Welding Journal» can be done at site: *www: rucont.ru*

РУКОНТ НАЦИОНАЛЬНЫЙ ЦИФРОВОЙ РЕСУРС

We offer for the subscription all issues of the Journal in pdf format, starting from 2009. You can subscribe to individual issues or to the entire archive including all issues over a period of 2009–2011. The subscription is available for natural persons and legal entities.

ADVERTISEMENT
IN «THE PATON WELDING JOURNAL»

External cover, fully-colored:
First page of cover (190×190 mm) – $700
Second page of cover (200×290 mm) – $550
Third page of cover (200×290 mm) – $500
Fourth page of cover (200×290 mm) – $600

Internal cover, fully-colored:
First page of cover (200×290 mm) – $350
Second page of cover (200×290 mm) – $350
Third page of cover (200×290 mm) – $350
Fourth page of cover (200×290 mm) – $350

Internal insert:
Fully-colored (200×290 mm) – $300
Fully-colored (double page A3) (400×290 mm) – $500
Fully-colored (200×145 mm) – $150
Black-and-white (170×250 mm) – $80
Black-and-white (170×125 mm) – $50
Black-and-white (80×80 mm) – $15

- Article in the form of advertising is 50 % of the cost of advertising area
- When the sum of advertising contracts exceeds $1000, a flexible system of discounts is envisaged

Technical requirement for the advertising materials:
- Size of journal after cutting is 200×290 mm
- In advertising layouts, the texts, logotypes and other elements should be located 5 mm from the module edge to prevent the loss of a part of information

All files in format IBM PC:
- Corell Draw, version up to 10.0
- Adobe Photoshop, version up to 7.0
- Quark, version up to 5.0
- Representations in format TIFF, color model CMYK, resolution 300 dpi
- Files should be added with a printed copy (makeups in WORD for are not accepted)